Palaeoecology of ungulates in northern Iberia during the Late Pleistocene through isotopic analysis of teeth

~~Evolutionary ecology of ungulates in northern Iberia during the Late Pleistocene through isotopic analysis on teeth~~

Mónica Fernández-García[1,2,3] (*), Sarah Pederzani[4], Kate Britton[5], Lucía Agudo-Pérez[1], Andrea Cicero[1], Jeanne Marie Geiling[1], Joan Daura[6], Montserrat Sanz[6], Ana B. Marín-Arroyo[1] (*)

1 Grupo de I+D+i EVOADAPTA (Evolución Humana y Adaptaciones durante la Prehistoria), Departamento de Ciencias Históricas, Universidad de Cantabria, 44. 39005 Santander, Spain

2 Departament de Prehistòria, Arqueologia i Història Antiga, Universitat de València, Av. Blasco Ibañez 28, 46010 Valencia, Spain.

3 Institut Català de Paleoecologia Humana i Evolució Social (IPHES-CERCA), zona Educacional 4 Edifici W3, Campus Sescelades URV, 43007 Tarragona, Spain.

4 Spatio-Temporal Isotope Analytics Lab. Department of Geology & Geophysics. University of Utah. ~~Archaeological Micromorphology and Biomarkers Laboratory (AMBI Lab), Instituto Universitario de Bio-Orgánica "Antonio González", Universidad de La Laguna, 38206 San Cristóbal de La Laguna, Tenerife, Spain~~

5 Department of Archaeology, University of Aberdeen, Aberdeen AB24 3UF, United Kingdom

6 Grup de Recerca del Quaternari (GRQ-SERP), Department of History and Archaeology, Universitat de Barcelona, C/Montalegre 6-8, 08001 Barcelona, Spain.

(*) Corresponding authors: anabelen.marin@unican.es, monica.fegar@gmail.com

Abstract

During the Late Pleistocene, stadial and interstadial fluctuations affected vegetation, fauna, and human groups that were forced to cope with these pronounced spatial-temporal climatic and environmental changes. These changes were especially abrupt during the Marine Isotopic Stage (MIS) 3. Here, we reconstruct the climatic trends in northern Iberia considering the stable isotopic composition of ungulate skeletal tissues found in archaeological deposits dated between 80 to 15 ka cal BP. The carbon and oxygen isotopic composition preserved in the carbonate fraction of tooth enamel provides a reliable and high-resolution proxy of the food and water consumed by these animals, which is indirectly related to the local vegetation, environment, and climate, allowing us to estimate paleotemperatures and rainfall intensity. This study presents new isotope data from 44 bovine, equid, and cervid teeth from five archaeological sites in the Vasco-Cantabrian region (El Castillo, Axlor, Labeko Koba, Aitzbitarte III interior and El Otero,) and one in northeastern Iberia (Canyars), where human evidence is attested from the Mousterian to the Magdalenian. The carbon isotope values reflect animals feeding on diverse C3 plants in open environments, and point to differentiated ecological niches for equids and bovines, especially during the Aurignacian in the Vasco-Cantabrian region. Temperature estimations based on oxygen isotopic compositions and rainfall obtained from carbon isotopic compositions indicate colder and more arid conditions than nowadays for the human occupations from the Late Mousterian to the Aurignacian. The contemporary northeastern Iberia site shows slightly lower temperatures related to an arid period when animals mainly graze in open landscapes. In the Vasco-Cantabrian region, during the MIS2, the Gravettian data reflect a landscape opening, whereas the Magdalenian points to warmer (but still arid) conditions.

Keywords: Middle and Upper Palaeolithic; Neanderthal; Homo sapiens, palaeoecology; geochemistry

1. Introduction

44 Understanding local and regional climatic variability during the Late Pleistocene in southern Europe is crucial
45 for assessing the potential impact of climate on the adaptation and decline of Neanderthals and the
46 subsequent expansion and resilience of Anatomically Modern Humans during the Upper Paleolithic (e.g.,
47 D'Errico and Sánchez Goñi, 2003; Finlayson and Carrión, 2007; Sepulchre et al., 2007; Staubwasser et al.,
48 2018). During the Late Pleistocene, the climatic records demonstrate stadial and interstadial continuous
49 fluctuations during the Marine Isotope Stage 3 (MIS 3, ca. 60-27 ka) and MIS 2 (ca. 27-11 ka). Human
50 groups had to face those episodes, which affected vegetation and fauna to different extents, depending on
51 the region. Northern Iberia is a key study area due to the abundance of well-preserved archaeological caves
52 and rock shelters where, in the last decade, an updated and multidisciplinary approach has been applied to
53 disentangle how changing environmental conditions affected the subsistence dynamics of Middle and Upper
54 Paleolithic hominins. Recent chronological, technological, subsistence studies and ecological
55 reconstructions are revealing a more complex regional panorama than previously known (e.g., Sánchez
56 Goñi, 2020; Vidal-Cordasco et al., 2022; 2023; Timmermann, 2020; Klein et al., 2023).

57 The Vasco-Cantabrian region, located in northwestern Iberia, is subject to the influence of Atlantic climatic
58 conditions, where recently has been evaluated the impact of the glacial-interglacial oscillations during MIS3
59 (Vidal-Cordasco et al., 2022). Modelling of traditional environmental proxies (small vertebrates and pollen)
60 associated to archaeo-paleontological deposits show a progressive shift in the climatic conditions with
61 decreasing temperatures and rainfall levels detected during the late Mousterian (Fernández-García et al.,
62 2023). Ecological alterations have been observed in large mammals, such as niche partitioning between
63 horses and cervids (Jones et al., 2018), a decrease in the available biomass for secondary consumers, and
64 consequently, a reduction in the ungulate carrying capacity ((Jones et al., 2018; Vidal-Cordasco et al., 2022).
65 Cold and arid conditions are observed during the Aurignacian and the Gravettian until the onset of MIS2.
66 Afterwards, during the Last Glacial Maximum (LGM, 23-19 ka), the global climatic deterioration associated
67 with this glacial phase results in colder and more arid conditions in the region, with a predominance of open
68 landscapes. However, this region still provided resources for human survival acting as a refugia with more
69 humid conditions in comparison to the Mediterranean area (Cascalheira et al., 2021; Fagoaga, 2014;
70 Fernández-García et al., 2023; Garcia-Ibaibarriaga et al., 2019a; Lécuyer et al., 2021; Posth et al., 2023).
71 By the end of the LGM, a climate amelioration and a moderate expansion of the deciduous forest are
72 documented from the late Solutrean through the Magdalenian (Garcia-Ibaibarriaga et al., 2019a; Jones et
73 al., 2021).

74 In contrast, northeastern Iberia is influenced by the Mediterranean climate. The MIS 3 human settlement in
75 this region have been linked to cooler temperatures and with higher rainfall, compared to the present, but
76 with climatic fluctuations less pronounced compared to the Vasco-Cantabrian region (López-García et al.,
77 2014; Fernández-García et al., 2020; Vidal-Cordasco et al., 2022). Archaeobotanical and small vertebrate
78 evidence indicate relatively stable climatic conditions, but also suggest the persistence of open forests
79 during the Middle to Upper Paleolithic transition, as found in northwestern Iberia (Allué et al., 2018; Ochando
80 et al., 2021). However, certain archaeological records indicate specific climatic episodes, such as increased
81 aridity and landscape opening during Heinrich ~~Events~~ Stadials 4 and 5 (e.g., Álvarez-Lao et al., 2017; Daura
82 et al., 2013; López-García et al., 2022; Rufí et al., 2018).

83 These multi-proxy studies have significantly expanded our understanding of the environmental evolution in
84 Iberia, alongside proxies derived from marine core records in Iberia margins (Fourcade et al., 2022; Martrat
85 et al., 2004; Naughton et al., 2007; Roucoux et al., 2001; Sánchez-Goñi et al., 1999, 2009) and other regional
86 paleoclimatic records sourced from local natural deposits (e.g., Pérez-Mejías et al., 2019; Moreno et al.,
87 2010, 2012; González-Sampériz et al., 2020; Ballesteros et al., 2020). However, the availability of proxies
88 enabling the direct connections between these environmental shifts and human activities remains limited.

89 In this study, we investigate the palaeoecological and palaeoenvironmental dynamics in northern Iberia
90 during the late Middle and Upper Paleolithic by measuring the carbon and oxygen isotopic composition of
91 bioapatite carbonates ($\delta^{13}C_{carb}$/$\delta^{18}O_{carb}$) preserved in archaeological mammal teeth. These analyses provide
92 high-resolution snapshots of ecological information from animals accumulated during human occupations at

93 the caves. Tooth enamel forms incrementally and does not biologically remodel (Kohn, 2004; Passey and
94 Cerling, 2002), in contrast to other bodily tissues such as bone, which implies that the isotope values
95 measured on them reflect the animal diet and water sources consumed during its mineralisation, around
96 one to two years of life for the species included in our study (bovids, equids, cervids)(e.g., Hoppe et al.,
97 2004; Pederzani and Britton, 2019; Ambrose and Norr, 1993; Luz et al., 1984). The preserved carbon
98 isotope composition relies on animal dietary choices reflecting mainly the type of plant consumed (C3/C4),
99 exposition to light and humidity levels. Otherwise, the oxygen isotope composition reflects mainly the
100 environmental water consumed by animals, directly by drinking or through diet, which reflects isotopic
101 information derived from water sources as well as changes in climatic conditions. Both indirectly provide
102 information on the vegetation and climate that allows estimating past temperatures, rainfall, and moisture
103 on a sub-annual scale, returning isotopic data of the foraging areas where animals were feeding during teeth
104 formation.

105 By analysing the stable isotopic composition of 44 ungulate teeth obtained from 15 archaeological levels
106 directly associated with human occupation, including El Castillo, Axlor, Labeko Koba, Aitzbitarte III interior
107 and El Otero in northwestern Iberia, and Terrasses de la Riera dels Canyars in northeastern Iberia, this
108 study presents novel insights into local and regional environmental and climatic trends associated to human
109 presence during the Late Pleistocene (Fig.1; Fig.2; Appendix A). Specifically, it focuses on the Middle to
110 Upper Paleolithic transition in both areas and the post-LGM period in the Vasco-Cantabrian region.

111 The main objectives of this work are: 1) to assess how regional environmental conditions, including changes
112 in moisture and vegetation cover, but also temperatures and rainfall, are recorded in the stable isotopic
113 composition of tooth enamel; 2) to characterize animal diet and their ecological niches; 3) to obtain
114 quantitative temperature data to compare with available proxies; 4) to characterise seasonal patterns of
115 animals found in the archaeological sites by identifying winter and summer fluctuations.
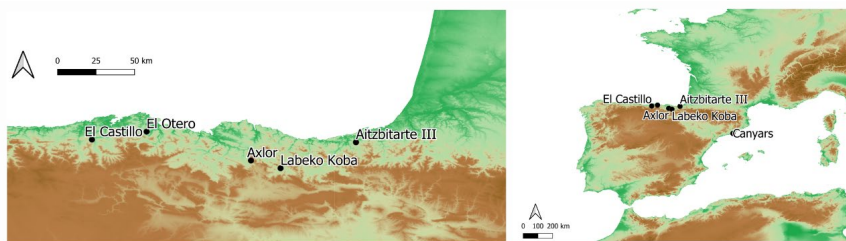
116

117 **Figure 1.** Location of the archaeological sites included in this study. From west to east, in the autonomous community of
118 Cantabria, El Castillo, and El Otero; in the Basque Country, Axlor and Aitzbitarte III interior; in Catalonia, Canyars.

119 **2. Archaeological sites and sampled material**

120 This study selected a total of 44 ungulate teeth including 25 bovines (*Bos primigenius, Bison priscus,*
121 *Bos/Bison* sp.), 14 equids (*Equus* sp. and *Equus ferus*), and five cervids (*Cervus elaphus*) originating from
122 five archaeological sites in the Vasco-Cantabrian region (El Castillo, El Otero, Axlor, Labeko Koba,
123 Aitzbitarte III interior) and one in the northeastern area (Terrasses de la Riera dels Canyars, henceforth
124 Canyars). These teeth were recovered from 15 archaeological levels attributed to the following
125 technocomplexes: Mousterian (n=14), Transitional Aurignacian (n=10), Châtelperronian (n=2), Aurignacian
126 (n=12), Gravettian (n=1) and Magdalenian (n=5) (Table 1 and 2). Archaeozoological studies of the
127 archaeological sites are available (synthesis in Marín-Arroyo and Sanz-Royo, 2022; Daura et al., 2013) and
128 most prove that faunal remains were accumulated by human acquisition during the different cultural phases.
129 The isotopic results of equids teeth and other ungulates bone collagen from El Castillo were previously
130 published by Jones et al. (2019) in combination with the stable isotopes of ungulates from the site, as well
131 as the combined bioapatite carbonate and phosphate analyses of bovines from Axlor (Pederzani et al.,
132 2023). A comprehensive description of each archaeological site is provided in Appendix A.
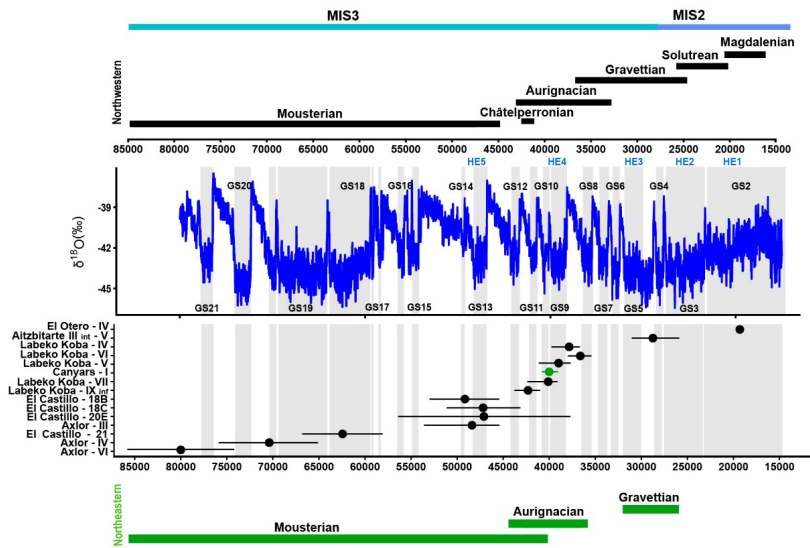
133 **Figure 2.** Representation of the duration each archaeological level (dots represent the median values, bars represent 95%
134 confidence intervals for ~14C dates and 68% for ESR and OSL dates) related to techno-complexes in both northwestern (in black)
135 and northeastern Iberia (in green) and the δ18O record from the NGRIP (North Greenland Ice Core Project members, 2004;
136 Rasmussen et al., 2014). Grey bands indicate Greenland Stadials (GS). Dates from EL Castillo (C14 UF, ESR), El Otero (C14
137 UF), Axlor (C14 UF, OSL), Labeko Koba (C14 UF), Aitzbitarte III-interior (C14 AMS) and Canyars (C14 UF, ABA, ABOx-SC) are
138 shown in Appendix B and C.

145 **3. Methods**

146 **3.1 Methods: Dating methods**

147 Individual Bayesian age models were built for Canyars, El Castillo, Labeko Koba and Aitzbitarte III interior
148 based on radiocarbon dates (AMS UF and non-UF, ABOx-SC and ABA pretreatments on bones and
149 charcoal remains) using OxCal4.4 software (Ramsey, 2009), considering the INTCAL20 calibration curve
150 (Reimer et al., 2020) (Appendix C). The Bayesian model enables the modification of the calibrated
151 Probability Distribution Function (PDF) of individual dates based on the existing relative stratigraphic and
152 other relative age information. A resolution of 20 years was assumed, being a reasonable balance between
153 required accuracy and computational costs. An order function in the OxCal was used to calculate the
154 probability that one PDF predated another, providing information to assess synchronicity and temporal
155 overlap of individual archaeological levels and cultural phases in each of the four separate sites modelled.
156 Dates were organised into a 'Sequence,' and chronological information for each level was grouped into a
157 single 'Phase' with start and end 'boundaries' to bracket each archaeological level. The interval between the
158 start of each level and its end provided the duration of each level. In all cases, convergence was greater
159 than 95%. CQL codes, individual Bayesian models and modelled dates per site are reported in Appendix C.

No chronological models were built for El Otero because only a single date was obtained for level IV and El Castillo levels 20E and 21 (ESR dated) and Axlor levels III, IV and VI (OSL dated) because dates go beyond the limit of the radiocarbon. To show the duration of these levels in combination with the other sites and levels, each of these dates was estimated by adding and subtracting the sigma (68% Confidence Interval) from the uncalibrated date. In this way, we estimated the duration of these levels to be beyond 55 ka cal BP.

3.2 Tooth sampling

All teeth included were sequentially sampled to reconstruct the complete $\delta^{18}O_{carb}$ and $\delta^{13}C_{carb}$ intratooth profiles based on enamel carbonate bioapatite. Intratooth sequential sampling was applied to the second and third molars and third and fourth premolars. Bovine and horse teeth sampled exceeded 3-4 cm of crown height to ensure that at least a one-year isotopic record of animal life was obtained (Britton et al., 2019; Hoppe et al., 2004). Samples were taken perpendicular to the growth axis on the tooth where the enamel was best preserved, avoiding, whenever possible taphonomic alterations such as cracks or postdepositional damages. Samples were performed in the buccal face for the lower teeth and the lingual part for the upper ones. The outermost enamel surface was abraded to remove the superficial enamel, calculus, cementum, or concretions adhering to the surface to avoid contaminations. The sequential sampling consisted of straight strips (ca. 8 x 1.5 x 1 mm) covering the width of the selected lobe, approximately every 2-3 mm, from the crown to the Enamel-Root-Junction (ERJ). The sample depth covered around 75% of the enamel depth, and dentine inclusion was avoided. A low-revolution variable-speed manual drill was used, equipped with 1 mm diamond-coated drill bits of conical and cylindrical shape. About 10-15mg of enamel powder was collected in each subsample, generating 693 subsamples for IRMS measurements (see complete intratooth profiles in Appendix D).

Site	Level - Cultural period	Bovines	Horses	Red deer	Teeth	Subsamples
Axlor	VI - Mousterian	2			2	32
	IV - Mousterian	1			1	12
	III - Mousterian	4			4	62
El Castillo	21A - Mousterian	2	1		3	47
	20E - Mousterian	2	2		4	56
	18C - Trans. Aurignacian	4			4	66
	18B - Trans. Aurignacian	3	2	1	6	93
Labeko Koba	IX inf - Châtelperronian		1	1	2	24
	VII - ProtoAurignacian	3			3	68
	VI - Aurignacian		1		1	16
	V - Aurignacian	1	1		2	39
	IV - Aurignacian		1		1	16
Canyars	I - Aurignacian	2	3		5	76
Aitzbitarte III interior	V - Gravettian	1			1	18
El Otero	IV - Magdalenian		2	3	5	68
TOTAL		**25**	**14**	**5**	**44**	**693**

Table 1. Number of teeth sampled by species, archaeological sites and cultural periods.

3.3 Sample treatment and stable isotope mass spectrometry

Several authors have debated the necessity of chemical pre-treatments to remove organic matter and secondary carbonates from bioapatite carbonates before stable isotopic analysis. Some chemical treatments can introduce secondary carbonates, increase carbonate content, and alter the original isotopic

190 signal (Pellegrini and Snoeck, 2016; Snoeck and Pellegrini, 2015). For this reason, in this work, most of the
191 samples were not pretreated except for the equids and cervids samples from Labeko Koba, El Otero and El
192 Castillo that were sampled and pretreated in an earlier phase of the project. The absence of pretreatment
193 can elevate the risk of secondary carbonates (Chesson et al., 2021; France et al., 2020). Nonetheless, any
194 pretreatment method cannot guarantee their complete removal, and the 'side effects' may compromise the
195 final isotopic signal to a greater extent. While variations in pretreatment methods exist among samples in
196 this study, the lack of a universally accepted protocol necessitates careful consideration of any potential
197 isotopic effects resulting from these differences.

198 Pretreatment was followed for above-mentioned samples from fourteen teeth, where around 7 mg of
199 powdered enamel was prepared and pretreated with 3% of sodium hypochlorite (NaOCl) at room
200 temperature for 24 h (0.1 ml/mg sample) and thoroughly rinsed with deionised water, before a reaction with
201 0.1M acetic acid for 4 h (0.1 ml/mg sample) (Balasse et al., 2002; equivalent protocol in Jones et al., 2019).
202 Samples were then thoroughly rinsed, frozen, and freeze-dried. NaOCl is one of the most common agents
203 used for pretreating carbonates and works as a base that removes organic matter by oxidation. Although it
204 is considered one of the most efficient agents for removing organic matter, it can induce the absorption of
205 exogenous carbonates, such as atmospheric CO_2 and secondary carbonates (Pellegrini and Snoeck, 2016;
206 Snoeck and Pellegrini, 2015). It is argued that acetic acid after NaOCl pretreatment can remove exogenous
207 carbonates absorbed during NaOCl application. However, it is unclear if all newly introduced carbonates are
208 finally released and which effect they produce on the original isotopic composition. These samples were
209 analysed in the Godwin Laboratory (Department of Earth Sciences, University of Cambridge). Enamel
210 powder samples were reacted with 100% orthophosphoric acid for 2 h at 70°C in individual vessels in an
211 automated Gasbench interfaced with a Thermo Finnigan MAT253 isotope ratio mass spectrometer. Results
212 were reported in reference to the international standard VPDB and calibrated using the NBS-19 standard
213 (limestone, $\delta^{13}C$ = +1.95‰ and $\delta^{18}O$ = -2.2‰; Coplen, 2011) for which the precision is better than 0.08‰
214 for $\delta^{13}C$ and 0.11‰ for $\delta^{18}O$.

215 For the non-pre-treated samples, carbon and oxygen stable isotopic ratios were measured using continuous
216 flow-isotope ratio mass spectrometry, specifically a Europa Scientific 20-20 IRMS coupled to a
217 chromatograph, at the Iso-Analytical laboratory in Cheshire, UK. The samples were weighed into clean
218 exetainer tubes after being flushed with 99.995% helium. Phosphoric acid was then added to the samples,
219 and they were allowed to react overnight to ensure the complete conversion of carbonate to CO_2, following
220 the method outlined by Coplen et al. (1983). The reference materials used for VPDB calibration and quality
221 control of the analysis included IA-R022 (calcium carbonate, $\delta^{13}C$ = -28.63‰, $\delta^{18}O$ = -22.69‰), NBS-18
222 (carbonatite, $\delta^{13}C$ = -5.01‰, $\delta^{18}O$ = -23.2‰), IA-R066 (chalk, $\delta^{13}C$ = +2.33‰; $\delta^{18}O$ = -1.52). The accepted
223 values of the in-house standards IA-R022 and IA-R066 were obtained by calibrating against IAEA
224 international reference materials, NBS-18 and NBS-19, and NBS-18 and IAEA-CO-1 (Carrara marble, $\delta^{13}C$
225 = 2.5‰, and $\delta^{18}O$ = -2.4‰), respectively. Additionally, in-house standards long-term measured were used:
226 ILC1 (calcite, $\delta^{13}C$ = 2.13, $\delta^{18}O$ = -3.99‰), and Y-02 (calcite, $\delta^{13}C$ = 1.48, $\delta^{18}O$ = -9.59‰). The analytical
227 precision of quality control standard replicates was better than 0.09‰ for $\delta^{13}C$ and better than 0.12‰ for
228 $\delta^{18}O$. The calcium carbonate content test of these samples, ranging between 3.9% and 8.9%, does not
229 indicate a substantial presence of secondary carbonates, considering Chesson et al. (2021). Additionally,
230 phosphate results on samples from Axlor showed $\delta^{18}O_{carb}$-$\delta^{18}O_{phos}$ offsets within the expected range for well-
231 preserved samples (Pederzani et al., 2023).

232 **3.4 Carbon stable isotopic compositions as environmental and ecological tracers**

233 To unravel animal diet and compare the different species, in standardised terms, it is necessary to consider
234 the enrichment factor (ε*) between $\delta^{13}C$ obtained by the animal on its diet ($\delta^{13}C_{diet}$) and $\delta^{13}C$ recorded on

enamel carbonates ($\delta^{13}C_{carb}$) (Bocherens, 2003; Cerling and Harris, 1999). The ε* estimated for large ruminant mammals results in an offset of around 14.1‰ between diet and dental enamel, commonly applied to medium-sized herbivores. However, it is well-known that this offset varies between species, considering animals' different physiological parameters. Recently, a formal model to predict species-specific diet-consumer isotopic offsets has been proposed, which uses body mass (BM) and digestive physiology as the main factors that regulate the ε* (Tejada-Lara et al., 2018). This model proposes the following prediction equations for ruminant or foregut fermenters (Equation 1: Eq.1) and hindgut fermenters (Eq. 2):

(Eq. 1) ε* = 2.34+0.05 (BM)   [r^2=0.78; p-value=0.008]

(Eq. 2) ε* = 2.42+0.032 (BM)   [r^2=0.74; p-value=0.003]

This work compares species with different digestive physiology, ruminants for bovines and cervids, and non-ruminants for equids. The ε* value was adjusted for each animal to avoid bias from digestive physiology when comparing these species. The following enrichment factors have been used: 14.6‰ for *Bos taurus* (Passey et al., 2005a), 13.7‰ for *Equus caballus* (Cerling and Harris, 1999), and 13.2‰ for *Cervus elaphus* (Merceron et al. (2021) following (Eq. 1) for ruminants with a mean body mass of 125 kg.

In body tissues, carbon isotopic composition is considered a combination of diet (understood as consumed food), environment openness (and associated exposure to light), and the amount of precipitation. Assuming that $\delta^{13}C$ of past vegetation is close to $\delta^{13}C_{diet}$ of ungulates, Lécuyer et al. (2021) proposed to estimate Mean Annual Precipitations (MAP) from $\delta^{13}C_{carb}$, derived from diets based on C3 plants. After transforming $\delta^{13}C_{carb}$ to $\delta^{13}C_{diet}$ using the enrichment factors established above, this work suggested transforming this value to $\delta^{13}C$ from vegetation ($\delta^{13}C_{leaf}$). However, the isotopic composition of animals' diet may not directly reflect vegetation cover, but rather the food preference of the animal and this approach should be discussed alongside other environmental data.

The MAP estimation is based on least square regression developed by Rey et al. (2013) and based on Kohn (2010) dataset (Eq.4), which requires first to estimate the $\delta^{13}C_{leaf}$ (Eq. 3). The $\delta^{13}C$ values of atmospheric CO_2 ($\delta^{13}C_{atm}$) are fixed in -7‰ (Lécuyer et al., 2021; Leuenberger et al., 1992; Schmitt et al., 2012). Atmospheric CO_2 levels have varied throughout the Late Pleistocene, with $\delta^{13}C_{atm}$ range between -7 to -6.4‰ (Eggleston et al., 2016), favouring an age-specific correction approach. However, maintaining general corrections is preferred considering the chronological uncertainty of the studied levels.

(Eq.3) $\delta^{13}C_{leaf}$ (VPDB) = ($\delta^{13}C_{atm}$ - $\delta^{13}C_{diet}$) / [1+($\delta^{13}C_{diet}$ / 1000)]

(Eq.4) Log1(MAP+300) = 0.092(±0.004) x $\delta^{13}C_{leaf}$ + 1.148(±0.074)

Additionally, Lécuyer et al. (2021) equation also accounts for the pCO_2 effect on $\delta^{13}C_{leaf}$ estimation, which is expected to result in an offset of +1‰ from current levels (considering that pCO_2 was lower than that experienced after the deglaciation period). If this correction was not applied, MAP results could be underestimated by -150mm. In agreement with Lécuyer et al. (2021) appreciation, these MAP estimations are a preliminary approximation and should be cross-validated with other environmental proxies. The associated uncertainties range from ±100 to 200 mm, influencing the interpretation of the final values.

3.5 Oxygen stable isotope compositions as environmental tracers

Stable oxygen isotopes from meteoric water (mainly derived from rainfall) strongly correlate with mean air temperatures in mid to high latitudes (Dansgaard, 1964; Rozanski et al., 1992) on a regional-to-local scale. Obligate drinkers, like bovines and horses, acquire this water and record its isotopic composition in their teeth and bones with a fixed but species-specific offset (Pederzani and Britton, 2019). Considering this two-

278 step relationship, past climatic conditions can be estimated. However, most of the temperature
279 reconstructions based on $\delta^{18}O$ have considered the $\delta^{18}O$ from the phosphate fraction of bioapatite enamel
280 ($\delta^{18}O_{phos}$) to build linear correlations between tooth enamel and drinking water $\delta^{18}O$ and obtain climatic
281 information. For this reason, the $\delta^{18}O_{carb}$ values obtained in this work were converted into $\delta^{18}O_{phos}$. To do so,
282 first, to express in VSMOW notation, the $\delta^{18}O_{carb}$ was corrected using the following correlation (Brand et al.,
283 2014; Coplen et al., 1983):

284   (Eq.5) $\delta^{18}O_{carb}$ (VSMOW)= 1.0309 x $\delta^{18}O_{carb}$ (VPDB) + 30.91

285 Second, considering the relationship existent in tooth enamel between the carbonate and phosphate fraction
286 (Iacumin et al., 1996; Pellegrini et al., 2011), from a compilation of the existent bibliography of modern
287 animals measurements (Bryant et al., 1996; Pellegrini et al., 2011; Trayler and Kohn, 2017), Pederzani et
288 al. (2023) proposed the following correlation:

289   (Eq.6) $\delta^{18}O_{phos}$ (VSMOW) = 0.941 x c (VSMOW) - 7.16

290 Once the isotopic information is expressed in $\delta^{18}O_{phos}$ (VSMOW), we can estimate the $\delta^{18}O$ on meteoric
291 waters ($\delta^{18}O_{mw}$). It is known that different physiological factors will condition how oxygen isotope composition
292 is fixed in each mammalian group. Thus, the correlations are usually species-specific and developed
293 considering the physiology of each animal group. The obligate drinkers heavily rely on consuming large
294 amounts of liquid drinking water, being the relative contribution of water from plants negligible and then
295 minimizing the possible impact of isotopic enrichment through evapotranspiration in plants (Hoppe, 2006;
296 Maloiy, 1973, Pederzani and Britton, 2019). However, certain types of drinking behaviours can impact δ
297 ^{18}O, such as systematic consumption of certain highly buffered water sources (rivers or lakes), can
298 significantly attenuate the final signal recorded. The correlation employed by this work relies on recent data
299 compilations (Pederzani et al., 2021b, 2023). In the case of horses (Eq. 7), it has been considered the data
300 combination of Blumenthal et al. (2019); Chillón et al. (1994); Bryant et al., 1994; Delgado Huertas et al.,
301 1995), whereas for bovines (Eq. 8) the data from D'Angela and Longinelli (1990) and Hoppe (2006) have
302 been put together in Eq. 4. To estimate $\delta^{18}O_{mw}$ from red deer remains, we selected D'Angela and Longinelli
303 (1990) correlation (Eq. 9):

304   (Eq.7) $\delta^{18}O_{mw}$ (VSMOW)= ($\delta^{18}O_{phos}$ (VSMOW) - 22.14) / 0.62

305   (Eq.8) $\delta^{18}O_{mw}$ (VSMOW)= ($\delta^{18}O_{phos}$ (VSMOW) - 22.36) / 0.78

306   (Eq.9) $\delta^{18}O_{mw}$ (VSMOW)= ($\delta^{18}O_{phos}$ (VSMOW) - 24.39) / 0.91

307 Finally, paleotemperatures estimations from $\delta^{18}O_{mw}$ are typically approached using a geographically
308 adjusted linear regression, which can vary from precise adjustments (aimed at reducing errors) to broader
309 geographical adjustments that encompass more variability but are less precise (e.g., Pryor et al., 2014;
310 Skrzypek et al., 2011; Tütken et al., 2007). In this work, temperatures were calculated considering the linear
311 regression model relating $\delta^{18}O_{mw}$ and air temperatures proposed by Pederzani et al. (2021) based on
312 monthly climatic records (monthly mean $\delta^{18}O_{mw}$ and monthly mean air temperatures), from Western,
313 Southern and Central Europe stations from the Global Network of Isotopes in Precipitation (IAEA/ WMO,
314 2020). Considering current IAEA data sets from northern Iberia, there is a strong positive relationship
315 between $\delta^{18}O_{mw}$ and annual or monthly temperatures (Moreno et al., 2021). However, it is known that Iberia
316 is under a mixed influence between Atlantic and Mediterranean moisture sources that affects the isotopic
317 composition of rainfall (Araguas-Araguas and Diaz Teijeiro, 2005; García-Alix et al., 2021; Moreno et al.,
318 2021). Given uncertainties in past atmospheric circulation patterns and the limited availability of reference
319 stations, it was deemed most appropriate to select an equation that extends beyond the borders of Iberia

and incorporates higher variability. Different correlations were for mean annual temperature (Eq. 10), summer (Eq. 11), and winter (Eq. 12) temperatures (T):

(Eq.10) $\delta^{18}O_{mw}$ (VSMOW)= (0.50 x T) - 13.64

(Eq.11) $\delta^{18}O_{mw}$ (VSMOW) = (0.46 x T) - 14.70

(Eq.12) $\delta^{18}O_{mw}$ (VSMOW)= (0.52 x T) - 11.26

Nonetheless, oscillations between glacial and interglacial conditions in the past have influenced global ice volume and sea level fluctuations (Dansgaard, 1964; Shackleton, 1987), impacting seawater oxygen isotope composition and the surface hydrological cycle on a worldwide scale, including $\delta^{18}O_{mw}$ (Schrag et al., 2002). Prior studies have used sea level information to correct $\delta^{18}O_{mw}$ (e.g., Fernández-García et al., 2019; Schrag et al., 2002). Given the chronological uncertainty in the studied levels, a general correction was applied to $\delta^{18}O_{mw}$ before temperature estimations, following Fernández-García et al. (2020) approach. Considering the mean sea level descent for the MIS 3 period (50 meters below present-day sea level)(Chappell and Shackleton, 1986), this may have contributed to a potential increase in the global $\delta^{18}O_{mw}$ value by ≈0.5‰, inferring a bias in calculated air temperatures of ≈1°C.

Due to the uncertainties incurred from converting stable isotope measurements to palaeotemperature, the final estimations in this work should be considered exploratory and as a method of standardisation to make results comparable among different sites, species, and other non-isotopic palaeoclimatic records. In these estimations, the associated error from converting $\delta^{18}O_{phos}$ to MAT is enlarged by the uncertainty derived from the transformation of $\delta^{18}O_{carb}$ (VPDB) to $\delta^{18}O_{phos}$ (VSMOW) (see Pryor et al., 2014; Skrzypek et al., 2016 for further discussion). However, Pryor et al. (2014) and Pederzani et al. (2023) concluded that the impact of this conversion is negligible compared to the error propagation in subsequent calibrations used for temperature estimations from $\delta^{18}O_{phos}$. These associated errors were quantified following the methodology outlined by Pryor et al. (2014) (Appendix B).

3.6 Inverse modelling applied to intratooth profiles

Intratooth profiles frequently provide a time-averaged signal compared to the input isotopic signal ($\delta^{13}C$/ $\delta^{18}O_{carb}$) during enamel formation (Passey et al., 2005b). This signal attenuation is caused by time-averaging effects incurred through the extended nature of amelogenesis and tooth formation, and through the sampling strategy. During mineralisation, the maturation zone, which is time-averaged, often affects a large portion of the crown height and might affect the temporal resolution of the input signal of the sample taken. To obtain climatically informative seasonal information on the analysed teeth, the inverse modelling method proposed by (Passey et al. (2005b) is applied in this work. This method computationally estimates the time-averaging effects of sampling and tooth formation to obtain the original amplitude of the isotopic input signal more accurately, thus, to summer and winter extremes (Appendix E). This method considers parameters based on the amelogenesis trends of each species and sampling geometry, which are critical for a meaningful interpretation of intratooth isotope profiles. The model also estimates the error derived from the sampling uncertainty and the mass spectrometer measurements to evaluate the data's reproducibility and precision. This method was initially developed for continuously growing teeth, taking into account a constant growth rate within a linear maturation model, with a progressive time-average increment as sampling advances along the teeth profile. The species studied in this research exhibit non-linear tooth enamel formation, particularly in later-forming molars (Bendrey et al., 2015; Blumenthal et al., 2014; Kohn, 2004; Passey and Cerling, 2002; Zazzo et al., 2012). Although the model mentioned above is not ideal, as it does not take into account non-linear enamel formation and specific growth parameters for the species included are unknown, it is the best estimation based on the current state of the field and remains widely used (Pederzani et al., 2021a, b, 2023). Flat and less sinusoidal profiles are less suitable for the application of the model, given its

inherent assumption of an approximately sinusoidal form. Therefore, we chose not to apply this methodology in the analysis of intratooth $\delta^{13}C$ profiles, and it is recommended to approach the interpretation of model outcomes for non-sinusoidal $\delta^{18}O$ curves with caution. Further details on the application of this method can be found in Appendix E.

Following Pederzani et al. (2021b), mean annual temperatures (MAT) were deduced from the average of $\delta^{18}O_{carb}$ values between summer and winter detected in original sinusoidal intratooth profiles (Appendix D). This work shows that comparable results for annual means can be obtained before and after model application, but doing it beforehand avoids the associated errors induced by the inverse model. To maximize data, in non-sinusoidal teeth profiles, MAT was deduced from the average of all points within a tooth. However, this approach is less reliable when complete annual cycles are not recorded. When possible, summer and winter temperature estimations were derived from the obtained $\delta^{18}O_{carb}$ values after inverse modelling application, aiming to identify the corrected seasonal amplitude, which is dampened in the original $\delta^{18}O_{carb}$ signal.

3.7 Present-day isotopic and climatic data

Present-day climatic conditions surrounding each site have been considered, allowing an inter-site comparison, essential for compare this study with other regional and global data. Considering current MATs and MAPs, estimated climatic data is expressed in relative terms as MAT and MAP anomalies. Present-day summer and winter temperatures were also considered. Present-day temperatures and precipitation values were obtained from the WorldClim Dataset v2 (Fick and Hijmans, 2017) (Appendix B). This dataset includes the average of bioclimatic variables between 1970-2000 in a set of raster files with a spatial resolution every 2.5 minutes. The exact location of the selected archeo-palaeontological sites was used, using geographical coordinates in the projection on modern climatic maps with QGIS software.

Present-day $\delta^{18}O_{mw}$ values from the analysed sites' areas were obtained using the Online Isotopes in Precipitation Calculator (OIPC Version 3.1 (4/2017); Bowen, 2022) based on datasets collected by the Global Network for Isotopes in Precipitation from the IAEA/WMO (Appendix B).

Site	Level	Culture	Species	Tooth type	Code	CCE (%)	n	δ13Ccarb VPDB (‰)	min	max	SD	Range	δ18Ocarb VPDB (‰)	min	max	SD	Range
Axlor	III	Mousterian	*Bos/Bison* sp.	LRM3	AXL59	5.6	14	-8.9	-9.6	-8.2	1.4	0.4	-6.0	-7.3	-5.2	0.7	2.1
Axlor	III	Mousterian	*Bos/Bison* sp.	LRM2	AXL60	5.5	18	-9.7	-10.0	-8.9	1.1	0.3	-5.7	-6.8	-4.6	0.7	2.2
Axlor	III	Mousterian	*Bos/Bison* sp.	LRM3	AXL65	6.2	13	-8.9	-9.3	-8.1	1.2	0.4	-6.0	-7.2	-4.6	0.8	2.6
Axlor	III	Mousterian	*Bos/Bison* sp.	LRM2	AXL66	5.6	16	-8.9	-9.8	-8.3	1.5	0.5	-4.8	-6.1	-3.8	0.7	2.3
Axlor	IV	Mousterian	*Bos/Bison* sp.	LRM2	AXL70	5.7	12	-9.1	-9.4	-8.6	0.7	0.3	-5.3	-7.3	-3.9	1.2	3.4
Axlor	VI	Mousterian	*Bos/Bison* sp.	LLM3	AXL77	5.9	14	-9.7	-10.2	-9.2	1.0	0.4	-6.2	-7.9	-5.0	0.9	2.9
Axlor	VI	Mousterian	*Bos/Bison* sp.	LLM3	AXL86	5.5	18	-9.9	-10.2	-9.3	0.9	0.3	-5.4	-6.5	-3.8	0.7	2.6
El Castillo	20E	Mousterian	*Equus* sp.	LRP3/LRP4	CAS60		14	-11.9	-12.5	-11.5	1.0	0.3	-3.3	-4.1	-2.4	0.4	1.6
El Castillo	20E	Mousterian	*Equus* sp.	LRP3/LRP4	CAS61		14	-12.2	-12.4	-12.1	0.3	0.1	-4.9	-5.8	-4.3	0.4	1.5
El Castillo	20E	Mousterian	*Bos/Bison* sp.	LLM2	CAS139	6.7	16	-11.6	-12.2	-11.2	0.9	0.3	-5.6	-6.3	-4.9	0.5	1.4
El Castillo	20E	Mousterian	*Bos/Bison* sp.	LLM2	CAS140	5.7	12	-11.5	-11.9	-11.1	0.8	0.3	-5.5	-6.3	-4.6	0.6	1.7
El Castillo	21A	Mousterian	*Bos/Bison* sp.	LLM3	CAS141	5.7	15	-11.2	-11.5	-10.9	0.6	0.2	-5.4	-6.5	-4.3	0.6	2.2
El Castillo	21A	Mousterian	*Bison priscus*	LLM3	CAS142	6.1	15	-11.2	-11.7	-10.9	0.7	0.2	-5.0	-5.7	-4.4	0.4	1.3
El Castillo	21A	Mousterian	*Equus* sp.	LLM3	CAS143	6.5	17	-12.6	-12.9	-12.5	0.4	0.1	-6.2	-7.2	-5.4	0.5	1.8
El Castillo	18B	Transitional Aurignacian	*Bos/Bison* sp.	ULM2	CAS132	6.2	13	-11.3	-11.5	-10.9	0.6	0.2	-6.2	-7.4	-4.9	0.7	2.6
El Castillo	18B	Transitional Aurignacian	*Bos/Bison* sp.	ULM2	CAS133	6.8	18	-10.9	-11.6	-10.5	1.1	0.3	-5.4	-6.5	-4.2	0.7	2.2
El Castillo	18B	Transitional Aurignacian	*Bos/Bison* sp.	ULM2	CAS134	6.6	18	-12.4	-12.8	-11.6	1.2	0.3	-5.4	-6.3	-4.5	0.5	1.8
El Castillo	18C	Transitional Aurignacian	*Bos/Bison* sp.	LLM3	CAS135	6	17	-11.3	-11.5	-11.0	0.5	0.2	-6.1	-6.6	-5.5	0.3	1.1
El Castillo	18C	Transitional Aurignacian	*Bos/Bison* sp.	LLM3	CAS136	5.8	17	-12.0	-12.5	-11.7	0.9	0.2	-5.8	-6.7	-5.0	0.6	1.7
El Castillo	18C	Transitional Aurignacian	*Bos/Bison* sp.	LLM3	CAS137	6.6	14	-10.2	-10.6	-9.9	0.7	0.2	-5.8	-6.5	-4.1	0.7	2.4
El Castillo	18C	Transitional Aurignacian	*Bos/Bison* sp.	LLM3	CAS138	6.1	18	-11.6	-11.8	-11.4	0.4	0.1	-5.3	-5.9	-4.8	0.3	1.2
El Castillo	18B	Transitional Aurignacian	*Cervus elaphus*	ULM2+ULM3	CAS8		11	-13.0	-14.9	-12.1	2.8	1.0	-6.8	-10.4	-4.1	2.1	6.3
El Castillo	18B	Transitional Aurignacian	*Equus* sp.	ULP3/ULP4	CAS58		19	-11.7	-11.8	-11.5	0.3	0.1	-6.6	-7.5	-5.6	0.5	1.8
El Castillo	18B	Transitional Aurignacian	*Equus* sp.	LLP3/LLP3	CAS59		14	-11.5	-11.7	-11.0	0.7	0.2	-4.0	-4.7	-3.5	0.4	1.2
Labeko Koba	IX inf	Chatelperronian	*Equus* sp.	URM3	LAB38		17	-12.0	-12.2	-11.9	0.3	0.1	-6.6	-7.7	-5.9	0.5	1.9
Labeko Koba	IX inf	Chatelperronian	*Cervus elaphus*	LLM2	LAB02		7	-12.3	-12.4	-12.1	0.3	0.1	-4.7	-6.0	-3.7	1.0	2.3
Labeko Koba	VI	Aurignacian	*Equus* sp.	URM2	LAB20		16	-12.0	-12.2	-11.8	0.4	0.1	-5.3	-6.1	-4.4	0.6	1.7
Labeko Koba	V	Aurignacian	*Equus* sp.	LRM3	LAB42		17	-11.9	-12.3	-11.5	0.2	0.7	-5.7	-6.6	-5.0	0.5	1.6
Labeko Koba	IV	Aurignacian	*Equus* sp.	LRM2	LAB36		17	-11.6	-11.8	-11.3	0.6	0.2	-5.9	-6.2	-5.5	0.2	0.7
Canyars	I	Aurignacian	*Equus* sp.	URM3	CAN01	7.8	12	-10.0	-10.4	-9.5	0.9	0.3	-4.8	-5.3	-4.3	0.3	1.1
Canyars	I	Aurignacian	*Equus ferus*	URM3	CAN02	6.2	17	-10.5	-10.7	-10.3	0.4	0.1	-4.4	-5.0	-3.6	0.5	1.4
Canyars	I	Aurignacian	*Equus ferus*	URP3/URP4	CAN03	6.4	17	-10.7	-11.2	-10.4	0.8	0.2	-4.8	-5.3	-4.0	0.4	1.4
Labeko Koba	VII	Aurignacian	*Bos primigenius*	LRM3	LAB53	5.2	23	-9.5	-10.1	-8.7	1.4	0.3	-5.7	-7.0	-4.2	0.9	2.8
Labeko Koba	VII	Aurignacian	*Bos/Bison* sp.	LRM3	LAB55	5.6	23	-10.4	-11.5	-9.8	1.6	0.3	-5.1	-7.0	-2.7	1.2	4.3
Labeko Koba	VII	Aurignacian	*Bos/Bison* sp.	LRM3	LAB62	6.5	21	-9.7	-10.2	-9.1	1.2	0.3	-7.2	-8.1	-6.2	0.6	2.0
Labeko Koba	V	Aurignacian	*Bos primigenius*	LRM3	LAB69	5.5	21	-9.3	-10.3	-7.3	3.0	0.9	-7.2	-8.8	-5.5	0.9	3.3
Canyars	I	Aurignacian	*Bos primigenius*	ULM3	CAN04	6.8	14	-9.3	-9.8	-8.7	1.1	0.3	-3.6	-4.2	-2.6	0.5	1.6
Canyars	I	Aurignacian	Bos primigenius	ULM3	CAN05	6.6	14	-9.0	-9.5	-8.5	0.9	0.3	-5.5	-6.2	-5.0	0.4	1.2
Aitzbitarte III	V (int)	Gravettian	*Bos/Bison* sp.	LLM3	AITI10	5.5	17	-9.2	-9.6	-8.7	0.9	0.3	-5.5	-6.5	-4.3	0.5	2.2
El Otero	IV	Magdalenian	*Cervus elaphus*	LLM2+LLM3	OTE1		11	-11.4	-11.6	-11.2	0.4	0.1	-4.4	-5.8	-2.9	1.0	2.9
El Otero	IV	Magdalenian	*Cervus elaphus*	LLM2+LLM3	OTE5		10	-11.3	-11.5	-11.0	0.5	0.2	-5.1	-5.7	-3.8	0.6	1.9
El Otero	IV	Magdalenian	*Cervus elaphus*	LLM2+LLM3	OTE6		14	-11.4	-11.8	-10.6	1.2	0.3	-4.6	-5.4	-4.0	0.4	1.4
El Otero	IV	Magdalenian	*Equus* sp.	LLP3/LLP4	OTE11		17	-11.6	-11.8	-11.4	0.5	0.1	-5.0	-6.3	-3.9	0.7	2.4
El Otero	IV	Magdalenian	*Equus* sp.	LLP3/LLP4	OTE12		16	-11.3	-11.5	-10.9	0.6	0.1	-3.9	-4.9	-3.3	0.6	1.6

Table 2. Mean, maximum value (Max), minimum value (Min), and standard deviation (SD) of δ13C and δ18O values per archaeological site and level organised by cultural periods. CCE, calcium carbonate equivalent; n, number of intratooth subsamples measured. In tooth type: position (U, upper; L, lower); laterality (R, right; L, left); tooth (M, molar; P, premolar).

4. Results

In northwestern Iberia, specifically in the Vasco-Cantabrian region, the mean δ13Ccarb values range from -13‰ to -8.9‰, with a mean value of -11‰ (SD = 1.2‰) (Table 2; Table 3). Considering species' different enrichment factors, the δ13Ccarb were transformed in δ13Cdiet, resulting in mean values that extend from -27‰ to -23.5‰ (Fig. 4). It must be considered that average values may reflect slightly different periods or be affected by seasonal bias because different teeth encompass diverse periods, but it has been verified in our teeth that the variations are limited when the seasonal information of the sequential sampling is incorporated (±0.2; Appendix B). The carbon isotopic composition varies between species. The bovines have generally higher mean δ13Ccarb (from -12.4‰ to -8.9‰) than the horses (from -12.6‰ to -11.3‰), whereas the red deer fall within the horses' range (from -13‰ to -11.3‰). Average values of δ18Ocarb in all Vasco-Cantabrian individuals extend between -7.2‰ and -3.3‰ (mean = -5.5‰; SD = 0.8‰). When transformed to δ18O expected from meteoric waters (δ18Omw), with species-adapted correlations, the δ18Omw values range from -10.6‰ to -5.5‰. Less clear patterns in δ18Ocarb are observed between bovines and horses, with mean values of -5.7‰ and -5.2‰, respectively. In northeastern Iberia, the site of Canyars, both species have relatively high δ18Ocarb values that fall inside the range of variation observed in the Cantabria region, between -5.5‰ and -3.6‰ in bovines and between -4.8‰ and -4.4‰ in horses.

		Vasco-Cantabrian region (NW Iberia)				Northeastern Iberia			
		δ13Ccarb VPDB (‰)	δ13Cdiet VPDB (‰)	δ18Ocarb VPDB (‰)	δ18Omw VSMOW (‰)	δ13Ccarb VPDB (‰)	δ13Cdiet VPDB (‰)	δ18Ocarb VPDB (‰)	δ18Omw VSMOW (‰)
Total	Mean	-11.0	-25.1	-5.5	-8.0	-9.9	-24.0	-4.6	-7.1
	Max	-8.9	-23.5	-3.3	-5.5	-9.0	-23.6	-3.6	-5.0
	Min	-13.0	-27.0	-7.2	-10.6	-10.7	-24.4	-5.5	-7.9
	Range	4.1	3.5	3.9	5.1	1.7	0.8	1.9	2.9
	SD	1.2	0.9	0.8	1.2	0.8	0.3	0.7	1.2
Bovines	Mean	-10.4	-25.0	-5.7	-7.7	-9.1	-23.7	-4.5	-6.2
	Max	-8.9	-23.5	-4.8	-6.5	-9.0	-23.6	-3.6	-5.0
	Min	-12.4	-27.0	-7.2	-9.5	-9.3	-23.9	-5.5	-7.4
	Range	3.5	3.5	2.4	3.0	0.3	0.3	1.9	2.4
	SD	1.1	1.1	0.6	0.7	0.2	0.2	1.4	1.7
Horses	Mean	-11.8	-25.5	-5.2	-8.5	-10.4	-24.1	-4.7	-7.6
	Max	-11.3	-25.0	-3.3	-5.5	-10.0	-23.7	-4.4	-7.2
	Min	-12.6	-26.3	-6.6	-10.6	-10.7	-24.4	-4.8	-7.9
	Range	1.4	1.4	3.3	5.1	0.7	0.7	0.5	0.7
	SD	0.4	0.4	1.1	1.8	0.3	0.3	0.3	0.4

Table 3. Mean δ13C from enamel carbonate (δ13Ccarb) and diet (δ13Cdiet), and δ18O from enamel carbonate (δ18Ocarb) and meteoric waters (δ18Omw), by species on the Vasco-Cantabrian and northeastern Iberia areas. Max: maximum value; Min: minimum value; SD: standard deviation.

4.1 Axlor (Mousterian, ca. 80 ka BP - 50 ka cal BP)

A total of seven bovine teeth were included from levels III (n = 4), IV (n = 1), and VI (n = 2) of Axlor cave (Pederzani et al., 2023). The mean δ13Ccarb range from -9.9‰ to -8.9‰ (δ13Cdiet= -24.5‰ to -23.5‰); whereas mean δ18Ocarb values are between -6.2‰ and -4.8‰ (δ18Omw = -8.3‰ and -6.5‰), indicating a range of variation around 1‰ and 1.4‰, respectively (Fig. 3; 4). Considering isotopic compositions by levels, mean δ13Ccarb decreases from level III to level IV, whereas mean δ18Ocarb remains stable through the sequence (Table 2; Appendix B). A range between 0.3‰ and 0.5‰ is observed in δ13Ccarb variation within tooth profiles. Individuals show clear δ18O sinusoidal profiles, with peaks and troughs and intratooth ranges from 2.1‰ to 3.4‰. The δ18Omw after inverse modelling intratooth profiles range from -9.1‰ to -7.35‰ (Appendix D; E). Mean Annual Temperatures (MATs) oscillated between 9.1ºC and 12.6ºC (MATAs = -3.1/+0.4ºC) (Table 4). From sinusoidal profiles, summer temperatures were extracted from peaks, resulting from 15.4ºC to 23.7ºC, and winter temperatures from troughs provided values ranging from -7ºC to 10.8ºC. Mean Annual Precipitation (MAPs), extracted from δ13Ccarb, extend between 204mm and 326mm (MAPAs = -843/-721mm). Based on these estimations, a non-clear climatic trend is observed through these levels.

4.2 El Castillo (Mousterian and Transitional Aurignacian, 62.5 ka BP – 46.4 ka cal BP)

From El Castillo, this work includes bovines (n = 11), horses (n = 5), and red deer (n = 1) teeth from the Mousterian (21 and 20E) and the Transitional Aurignacian levels (18B and 18C). The mean δ13Ccarb values are lower for horses, bovines, and red deer (-13‰ to -10.2‰) than other sites. Between -12.4‰ and -10.2‰ for bovines (δ13Cdiet = -24.6‰ to -25.8‰) and between -12.6‰ and -11.5‰ for horses (δ13Cdiet = -26.3‰ to -25.2‰) (Fig. 3). The mean δ18Ocarb values extend from -6.8‰ and -3.3‰. Horses and bovines overlap in their isotopic niche (Fig. 4), mainly due to the notably lower δ13Ccarb reported by bovines. The mean δ13Ccarb (-13‰) of the single red deer tooth is inside the variation range of bovines and horses but with a lower δ18Ocarb mean value (-6.8‰). Considering these isotopic compositions by levels, bovine mean δ13Cdiet values highly increase the variation range from Mousterian levels (20E and 21A) to Transitional Aurignacian levels (18C and 18B). In contrast, horses increase mean δ13Cdiet values (Fig. 5). Bovine mean δ18Omw values decrease from level 21A to level 18B, while horses from 18B have a large intra-level amplitude.

The mean δ18Ocarb values from horses have a more significant variation (range = 3.3‰) than bovines (range = 2.2‰). All individuals show flat δ13Ccarb intratooth profiles (<0.4‰), except for red deer (1‰) (Appendix D). Intratooth δ18Ocarb ranges of individuals are around 1-2‰ for horses and 1-3‰ for bovines. Some of the individuals analyzed do not show non-complete annual cycles. No precise δ18Ocarb sinusoidal profiles are

445   detected in three teeth; the other six have particularly unclear profiles. After modelling, individual $\delta^{18}O_{carb}$
446   ranges oscillated between 2.7‰ and 7.4‰ (Appendix E). MATs oscillated between 4.6ºC and 12.6ºC
447   (MATAs = -8.8ºC/-0.9ºC), with mean summer temperatures from around 20.5ºC and mean winter
448   temperatures around -1.1ºC. MAPs extend between 376mm and 784mm (MAPAs = -656/-248mm) (Table
449   4). Non-important differences in rainfall estimations based on bovines and equids are noticed, probably
450   because they feed on similar ecological resources. Diachronic trends are unclear along the sequence but
451   mean annual and winter temperatures from levels 18C and 18C seem slightly lower. MAPs estimations
452   oscillated more in the upper levels.
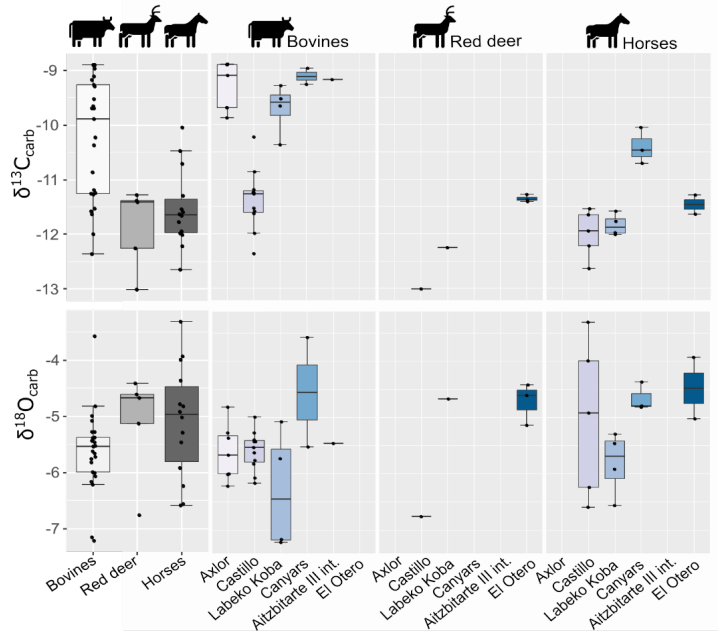
453

454   **Figure 3.** Distribution of mean carbon ($\delta^{13}C_{carb}$) and oxygen ($\delta^{18}O_{carb}$) isotopic values of enamel carbonate by species and
455   archaeological site.
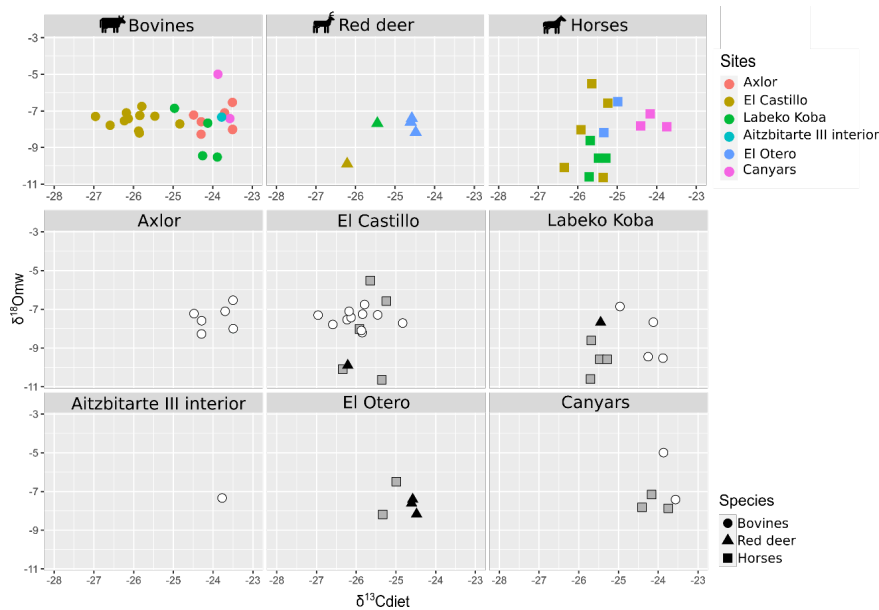
456
457   **Figure 4.** Biplot crossing δ13C from diet (δ13Cdiet) and δ18O from meteoric waters (δ18Omw) by species and archaeological site.

4.3 Labeko Koba (Châtelperronian and Aurignacian, 45.1-36.3 ka cal BP)

459   This work includes bovines (n = 4), horses (n = 4), and red deer (n = 1) teeth from levels related to
460   Châtelperronian (IXb inf), ProtoAurignacian (VII), and Aurignacian (VI, V, and IV). Significant differentiation
461   in mean δ13Ccarb between bovines and horses is observed, with higher values between -9.3‰ and -10.4‰
462   in bovines (δ13Cdiet = -25‰ to -23.8‰) than equids, whose values extend from -12‰ to -11.6‰ (δ13Cdiet = -
463   25.8‰ to -25.2‰) (Fig. 3;). These horses' values are within the ranges observed from this species in the
464   region. Red deer have similar δ13Ccarb values to those of horses (δ13Ccarb = -12.3‰; δ13Cdiet = -25.5‰). Mean
465   δ18Ocarb values are similar between species from -7.2‰ to -4.7‰ (δ18Omw = -8.5‰ to -6.1‰). However,
466   bovines have a very high variation within mean δ18Ocarb values (2.1‰), also reflected in the intratooth
467   profiles. These δ18O values are lower than in other Vasco-Cantabrian sites, especially for two individuals in
468   levels VII and V (Table 3). Differences in δ13Cdiet values between bovines and horses result in isotopic niche
469   differentiation between both species (Fig. 4). The red deer niche is placed within the horses' niche. The
470   evolution of niche over time cannot be evaluated by levels due to the limited sample. Considering the isotopic
471   compositions by levels (Fig. 5), both bovines and horses experienced a slight increase in mean δ13Cdiet from
472   levels IX inf to IV, from Châtelperronian to Aurignacian. Mean δ18Omw values of bovines decrease from VII
473   to V, whereas horses increase from IXb inf to VI to decrease from VI to IV.

474   Variability of δ13Ccarb values in intratooth profiles is slightly higher (0.1-0.7‰), especially in bovines (0.3-
475   0.9‰), with more oscillating profiles than generally flat profiles observed in horses and red deer (Appendix
476   D; E). Intratooth profiles ranges of δ18Ocarb are also larger within bovines (2-4‰) than in horses (1-2‰).
477   Inverse-modelled individual δ18Ocarb ranges oscillated between 5-8‰ and 2-4‰, respectively. Sinusoidal
478   curves are observed in horses and bovines, but bovine profiles are noisier. The red deer has an extensive
479   δ18Ocarb range (6.3‰) from summer peak to an incomplete winter thought. We detect an inverse relation
480   between δ13Ccarb and δ18Ocarb in some points of these individual profiles. MATs oscillated between 5.2ºC and
481   11.4ºC (MATAs = -5.6/+1.1ºC), with summer temperatures from 14.5ºC to 27.3ºC and winter temperatures
482   from 1.9ºC to -4.9ºC. MAPs extend between 248mm and 521mm, notably drier than nowadays (MAPAs = -

483 798/-525mm) (Table 4). Lower rainfall levels and higher seasonal amplitudes are recorded along the
484 sequence, especially in samples from the ProtoAurignacian level VII. Relevant differences are noticed
485 between MAPs estimated from bovines and equids, the first providing more arid conditions.

4.4 Aitzbitarte III interior (Gravettian, 27.9 ka cal BP)

487 A single bovine individual was analysed from Gravettian level V located in the inner part of the cave. It has
488 a high mean $\delta^{13}C_{carb}$ (-9.2‰) considering the observed range in bovines from the Vasco-Cantabrian region,
489 whereas the $\delta^{18}O_{carb}$ mean value (-5.5‰) is inside the common $\delta^{18}O_{carb}$ variation observed (Fig. 3). The
490 mean $\delta^{13}C_{diet}$ value of -23.8‰ is comparable with Canyars and some individuals from Axlor but different
491 from Labeko Koba and El Castillo individuals. The individual $\delta^{13}Ccarb$ fluctuation is slight (0.3‰) (Appendix
492 D; E). These teeth show not quite sinusoidal profile shape in $\delta^{18}O_{carb}$, with an intratooth range of around
493 2.2‰. Climatic information is extracted but may be considered cautiously due to the profile shape and the
494 limited sample size. From the inverse modelled mean $\delta^{18}O_{mw}$ value (-5.4‰), we estimate a MAT of 13ºC
495 (MATA = -0.4ºC) with a summer temperature of 19.7ºC and winter temperature of -2.9ºC. The MAP
496 estimation reached 235mm (-1127mm to nowadays) (Table 4).

4.5 El Otero (Magdalenian, ca. 17.3 ka cal BP)

498 Two equids and three cervids are included from level IV from El Otero, recently redate and chronologically
499 related to the Magdalenian (Marín-Arroyo et al., 2018). The mean $\delta^{13}C_{carb}$ values are close, between -11.4‰
500 and -11.3‰ for red deer ($\delta^{13}C_{diet}$ = -24.4‰ and -24.6‰) and -11.6‰ and -11.3‰ for horse ($\delta^{13}C_{diet}$ = -25.3‰
501 and -25.3‰) (Fig. 3). These $\delta^{13}C$ values for both species are relatively high concerning other studied
502 samples, especially for cervids (around +1-2‰). Both species have higher $\delta^{18}O_{carb}$ values concerning the
503 common range of variation observed in the Vasco-Cantabria region, between -5‰ and -3.9‰ for horses
504 and between -5.1‰ and -4.4‰ for red deer. When values are transformed to $\delta^{13}C_{diet}$ and $\delta^{18}O_{mw}$, equids
505 and cervids isotopic niches are separated (Fig. 4). All individuals show low amplitude $\delta^{13}C_{carb}$ intratooth
506 profiles (<0.3‰), but especially equids with an intratooth variation around 0.1‰ (Appendix D; E). Equids
507 and cervids show $\delta^{18}O_{carb}$ sinusoidal profiles, with intratooth ranges between 1.4‰ and 2.4‰. Climatic
508 estimations are proposed only for equids, providing MATs estimations from 8.8ºC to 12.6ºC (MATAs = -4.9/-
509 1ºC) and MAP between 400mm and 456mm (MAPAs = -755/-699mm) (Table 4). A high-temperature
510 seasonality can be seen, with summer temperatures between 19.7ºC and 23.8ºC and winter temperatures
511 from -10.4ºC to -3.1ºC.
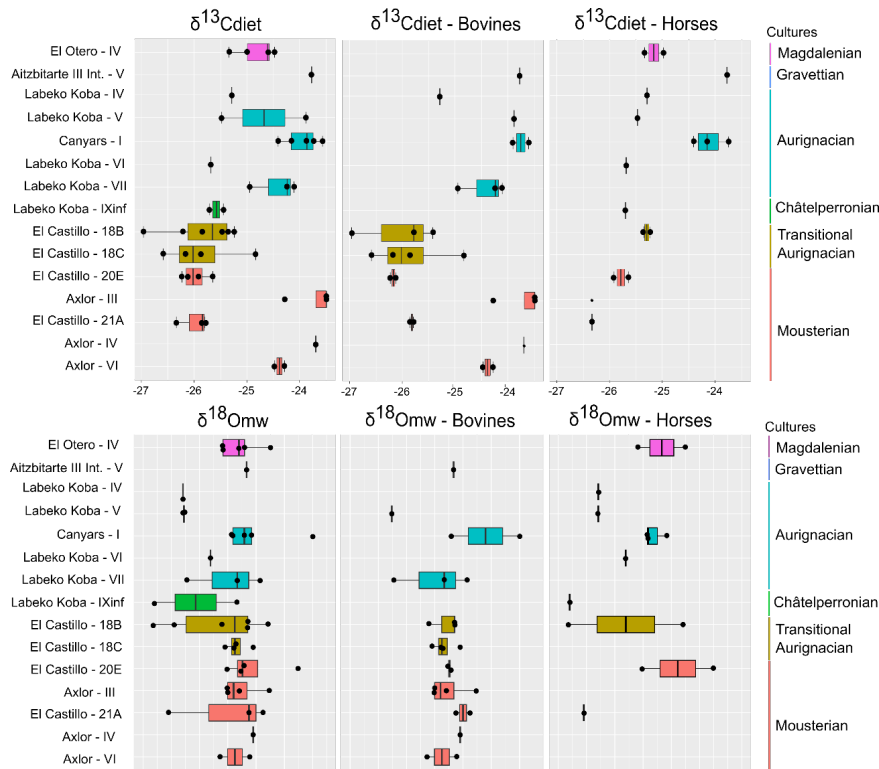
512
513 **Figure 5.** Evolution of δ13C in diet (δ13Cdiet) and δ18O in meteoric waters (δ18Omw) by archaeological levels in a diachronic order.
514 From right to left: all species, including cervids, bovines and horses. Colours correspond to different chrono-cultures.

4.6 Canyars (Aurignacian, 39.7 ka cal BP)

From the archaeological level I at Canyars, corresponding to the Aurignacian, this work includes bovines (n = 2) and equids (n = 3) teeth. The mean δ13Ccarb values for bovines are between -9‰ to -9.3‰ (δ13Cdiet = -23.6‰ and -23.8‰), and for horses between -10‰ and -10.7‰ (δ13Cdiet = -23.7‰ and -24.4‰) (Fig.3). In this site, the δ13Ccarb values for horses are notably higher than in the Vasco-Cantabrian region (around +1-2‰) (Table 3). Both species have relatively high δ18Ocarb values, but they fall inside the range of variation observed in the Vasco-Cantabrian region, between -5.5‰ and -3.6‰ in bovines and between -4.8‰ and -4.4‰ in horses. Bovine and equid isotopic niches overlap (Fig. 4), but different responses are seen in mean δ18Omw values between the two bovines, with one high mean value but close δ13Cdiet mean values.

All individuals show flat δ13Ccarb intratooth profiles (<0.3‰ variation). Some individuals analysed do not show δ18Ocarb sinusoidal profiles, with intratooth profiles moderately flat and ranging from 1.1‰ to 1.6‰. We detect an inverse relation between δ13Ccarb and δ18Ocarb in some points of bovine individual isotopic profiles. MATs oscillated between 9.8ºC and 11.9ºC (MATAs = -5.4ºC/-3.3ºC), with summer temperatures from 16.3ºC to 27.5ºC and winter temperatures from -0.5ºC to 1.8ºC (Table 4). MAPs extend between 211mm and 316mm (MAPAs = -431/-326mm). No substantial differences are noticed in the estimations based on bovines and equids because mean δ13C diet values differed relatively little.

Site	Sample	Level	Species	MAT (°C)		Summer (°C)		Winter (°C)		Seasonality (°C)	MAP (mm)	
				Estimated	Relative	Estimated	Relative	Estimated	Relative		Estimated	Relative
Axlor	AXL59	III	*Bos/Bison* sp.	9.4	-2.8	17.6	-0.3	-3.9	-11.0	21.5	204	-843
	AXL60	III	*Bos/Bison* sp.	10.8	-1.4	22.7	4.7	4.8	-2.3	17.9	300	-747
	AXL65	III	*Bos/Bison* sp.	9.7	-2.5	22.7	4.8	-2.5	-9.6	25.2	204	-843
	AXL66	III	*Bos/Bison* sp.	12.6	0.4	22.8	4.8	-3.2	-10.3	26.0	204	-843
	AXL70	IV	*Bos/Bison* sp.	11.1	-1.1	21.9	3.9	-8.0	-15.1	29.9	227	-820
	AXL77	VI	*Bos/Bison* sp.	9.1	-3.1	20.4	2.5	-10.9	-17.9	31.3	300	-747
	AXL86	VI	*Bos/Bison* sp.	11.1	-1.1	25.9	8.0	3.1	-4.0	22.8	326	-721
El Castillo	CAS141	21A	*Bos/Bison* sp.	11.7	-1.7	24.2	5.6	-0.8	-9.9	25.1	546	-486
	CAS142	21A	*Bison priscus*	12.6	-0.9	19.6	1.0	3.1	-5.9	16.5	536	-496
	CAS143	21A	*Equus* sp.	5.7	-7.8	20.7	2.1	-5.6	-14.7	26.3	645	-387
	CAS60	20E	*Equus* sp.					1.6	-7.5		510	-522
	CAS61	20E	*Equus* sp.	9.7	-3.8	25.9	7.3	-4.1	-13.2	30.1	561	-471
	CAS139	20E	*Bos/Bison* sp.	11.2	-2.3	18.8	0.2	1.8	-7.3	17.0	622	-410
	CAS140	20E	*Bos/Bison* sp.	*11.3*	*-2.1*						602	-430
	CAS135	18C	*Bos/Bison* sp.			17.0	-1.6				551	-481
	CAS136	18C	*Bos/Bison* sp.	*10.6*	*-2.9*						699	-333
	CAS137	18C	*Bos/Bison* sp.					0.0	-9.1		376	-656
	CAS138	18C	*Bos/Bison* sp.	11.8	-1.7	18.3	-0.3	3.1	-6.0	15.3	612	-420
	CAS132	18B	*Bos/Bison* sp.	9.8	-3.6	26.3	7.6	-1.2	-10.3	27.5	548	-484
	CAS133	18B	*Bos/Bison* sp.					-0.1	-9.2		477	-555
	CAS134	18B	*Bos/Bison* sp.					0.8	-8.3		784	-248
	CAS58	18B	*Equus* sp.	4.6	-8.8	13.5	-5.1	-11.2	-20.3	24.7	460	-572
	CAS59	18B	*Equus* sp.	*13.0*	*-0.5*						440	-592
Labeko Koba	LAB38	IX inf	*Equus* sp.	5.2	-7.4	14.5	-4.1	-1.8	-9.1	16.2	521	-526
	LAB36	IV	*Equus* sp.	7.0	-5.6	16.3	-2.3	-2.4	-9.7	18.7	448	-599
	LAB42	V	*Equus* sp.	*7.6*	*-5.0*				-7.3		501	-546
	LAB69	V	*Bos primigenius*	6.3	-6.3	17.3	-1.2	-4.9	-12.2	22.2	248	-799
	LAB20	VI	*Equus* sp.	9.1	-3.5	15.7	-2.9	-0.9	-8.2	16.6	517	-530
	LAB53	VII	*Bos primigenius*	11.3	-1.3	27.3	8.7	-2.4	-9.7	29.7	278	-769
	LAB55	VII	*Bos primigenius*	11.4	-1.2	26.3	7.8	1.9	-5.4	24.4	397	-650
	LAB62	VII	*Bos/Bison* sp.	7.2	-5.4	20.6	2.1	-2.9	-10.2	23.5	295	-752
Canyars	CAN01	I	*Equus* sp.	9.8	-5.4	16.3	-5.9	1.7	-7.5	14.6	232	-410
	CAN02	I	*Equus ferus*	*11.9*	*-3.3*						284	-358
	CAN03	I	*Equus ferus*	10.4	-4.7	18.6	-3.6	-0.5	-9.7	19.1	316	-326
	CAN04	I	*Bos primigenius*	17.2	2.1	27.5	5.3				247	-395
	CAN05	I	*Bos primigenius*	11.3	-3.9	17.5	-4.7	1.8	-7.4	15.7	211	-431
Aitzbitarte III int	AITI10	V	*Bos/Bison* sp.	*13.0*	*-0.4*	19.7	0.7	-2.9	-11.4	22.6	235	-1127
Otero	OTE11	IV	*Equus* sp.	8.8	-4.9	19.7	0.9	-10.4	-19.8	30.1	456	-699
	OTE12	IV	*Equus* sp.	12.6	-1.0	23.8	5.0	-3.1	-12.5	26.8	400	-755

Table 4. Summary of paleoclimatic estimations, based on δ^{18}O for temperatures (Mean Annual Temperatures, MAT; summer; winter) and in δ^{13}C for precipitation (Mean Annual Precipitations, MAP). Summer and winter temperature estimations were obtained from teeth with clear seasonal profiles after modelling, while MAT was averaged between summer and winter before modelling. In profiles with an unclear seasonal shape, MAT was deduced from the original average of all teeth points (values marked in italics). Mean error associated to temperature estimations is 5.1±0.6 (see details in Appendix B). Seasonality is calculated as the temperature difference between summer and winter.

5. Discussion

5.1 Diet and ecological niches: carbon ratios

Carbon isotopic ratios are valuable indicators for discerning past animal diets, partially influenced by the physiology of the animal. Considering species trends in the studied sites, bovines have generally higher mean δ^{13}C$_{carb}$ values (from -12.4‰ to-8.9‰) than horses (from -12.6‰ to -11.3‰), whereas the red deer fall within the horses' range (from -13‰ to 11.3‰). In the notheastern site of Canyars, bovines also show higher mean δ^{13}C$_{carb}$ values (-9‰ to -9.3‰) compared to horses (-10.7‰ to -10‰). These differentiated isotopic ranges for equids and bovines can be potentially linked to feeding behaviour. Still, these species are expected to present different basal δ^{13}C$_{carb}$ driven by their feeding behaviour and distinct physiological characteristics. Bovines, being ruminants, have been suggested in previous studies to exhibit higher δ^{13}C$_{carb}$ values due to increased methane production (Cerling and Harris, 1999; Tejada-Lara et al., 2018). Therefore, transforming δ^{13}C$_{carb}$ to δ^{13}C$_{diet}$ values using species-specific equations is crucial to mitigate the species-specific impact, particularly when comparing ruminants and non-ruminants. Bovines report δ^{13}C$_{diet}$ values between -27.5‰ and -23.5‰ and horses between -26‰ and -25‰. These carbon compositions are typical of animals feeding on C3 plants (commonly accepted range between -34‰ and -23‰), as can be expected

554 from high-latitude ecosystems during the Pleistocene (Bocherens, 2003; Cerling and Harris, 1999; Drucker,
555 2022).

556 Environmental factors such as light exposure, water stress, temperature fluctuations, salinity, and
557 atmospheric CO_2 changes can influence variations in $\delta^{13}C$ values in a diet primarily based on C3 plants
558 (Bocherens, 2003; Kohn, 2010). Typically, $\delta^{13}C_{diet}$ values below -27‰ ($\delta^{13}C_{carb}$ = -13‰) are associated with
559 animals feeding on C3 vegetation found in closed forested environments, whereas $\delta^{13}C_{diet}$ values between
560 -27‰ and -23‰ are linked to C3 open landscapes, which could include grasslands and steppe areas
561 (Bocherens, 2003). The relatively high $\delta^{13}C_{diet}$ observed here points to animals predominantly feeding in
562 open environments. The canopy effect, characterised by a depletion in ^{13}C isotopes due to dense tree cover,
563 seems unlikely among the analysed samples since none of the individuals reported $\delta^{13}C_{diet}$ below the
564 standard cut-off of -27‰ (Drucker et al., 2008; Kohn, 2010; van der Merwe, 1991). Therefore, in general
565 terms, open mosaic landscapes, ranging from light forests to meadows and grasslands, can be inferred for
566 northwestern Iberia. Given the generally higher $\delta^{13}C_{diet}$ values reported by bovines, it is likely that they were
567 foraging in more open environments than horses and can be considered predominantly grazers. Particularly,
568 bovines from El Castillo exhibit distinct feeding behaviour compared to other Vasco-Cantabrian sites, as
569 evidenced by their lower $\delta^{13}C_{diet}$ values, indicating a potential preference for browsing and feeding in closer
570 environments, possibly in lightly forested areas. Both extinct aurochs (*Bos primigenius*) and steppe bison
571 (*Bison priscus*) are usually classified as grass-dominant mix-feeders during the Pleistocene, although it
572 should be noted that modern European bison (*Bison bonasus*) could include browsing in their diet (Rivals
573 et al., 2022). For aurochs, a browse-dominated mixed feeding behaviour is also frequently described.

574 The $\delta^{13}C_{diet}$ range in equids also indicates feeding in open environments, suggesting a general mixed-
575 feeding pattern for the Vasco-Cantabrian region. However, individuals from northeastern Iberia are likely
576 grazing in more open environments, as evidenced by their notably higher $\delta^{13}C_{diet}$ values compared to the
577 Vasco-Cantabrian region (+1-2‰). Evaluating if other factors contribute to lower $\delta^{13}C_{diet}$ values in horses is
578 critical. In the case of equid from the Vasco-Cantabrian region, it should be considered that they have been
579 pretreated with a combination of NaClO and acetic acid, which could potentially affect the isotopic values.
580 Samples after organic removal pretreatment can potentially show either higher or lower $\delta^{13}C$ values and
581 higher $\delta^{18}O$ values based on previous experiments (Pellegrini and Snoeck, 2016; Snoeck and Pellegrini,
582 2015), with $\delta^{13}C$ values generally varying below 0.3‰. Based on the observation that horses in the Vasco-
583 Cantabrian region present lower $\delta^{13}C_{carb}$ values compared to bovines but similar mean $\delta^{18}O_{carb}$ value ranges,
584 the influence of the pre-treatment on our samples is deemed to be limited.

585 Furthermore, the high variability in $\delta^{18}O_{carb}$ values at El Castillo and Labeko Koba does not correlate with a
586 significant variation in $\delta^{13}C_{carb}$ values. Based on dental wear and stable isotopes analysis, Middle and Late
587 Pleistocene horses (*Equus ferus*) were primarily grazers, although some rare cases have been reported as
588 mixed feeders or browsers, such as at Igue des Rameaux and Schöningen (Kuitems et al., 2015; Rivals et
589 al., 2009, 2015; Uzunidis, 2020). Horse populations from northern and eastern Europe were found to be
590 browsers or mixed feeders, while those from the Mediterranean region tend to be grazers (Rivals et al.,
591 2022).

592 Finally, the few cervids included in this study exhibit $\delta^{13}C_{diet}$ values that frequently overlap with horses,
593 indicating a mixed feeding behaviour that varies from more closed environments in El Castillo to more open
594 habitats in El Otero. During the Pleistocene, the red deer (*Cervus elaphus*) exhibit a flexible, mixed-feeding
595 behaviour, consuming leaves, shrubs, forbs, grass, and sedges, similar to their present-day counterparts
596 (Merceron et al., 2021; Rivals et al., 2022). Today, this species inhabits diverse habitats ranging from
597 steppes to closed temperate forests.

598 **5.2 Seasonality, mobility and water acquisition: oxygen ratios and intratooth profiles**

599 Average values of $\delta^{18}O_{carb}$ in Vasco-Cantabrian individuals extend between -7.2‰ and -3.3‰ (Table 3).
600 Even if no clear species patterns in $\delta^{18}O_{carb}$ are observed, in general, bovines present slightly lower $\delta^{18}O_{carb}$
601 values from -7.2‰- to 4.8‰ than other species; horses have a significant variation from -6.6‰ to -3.3‰ and
602 red deer from -6.8‰ to -4.4‰. In Canyars, both species have relatively high $\delta^{18}O_{carb}$ values that fall inside
603 the variation range observed in the Vasco-Cantabrian region, between -5.5‰ and -3.6‰ in bovines and
604 between -4.8‰ and -4.4‰ in horses. Each species shows different $\delta^{18}O_{carb}$ intratooth ranges, with bovines
605 between 1‰ and 3‰, horses mostly around 1.5%, and red deer from 1‰ to 6‰ presenting the higher
606 ranges (Table 3; Appendix D). After applying inverse modelling to correct the dampening effect (Passey et
607 al., 2005b), the majority of teeth increase the $\delta^{18}O_{carb}$ intratooth range, between 3‰ and 8‰ for bovines and
608 2‰ and 7‰ for horses (Appendix E). Most bovines from Axlor and Labeko Koba and horses from El Castillo
609 and El Otero exhibit well-defined sinusoidal profiles in their $\delta^{18}O_{carb}$ and large intratooth individual ranges,
610 related to the predominant consumption of water sources that reflect seasonal fluctuations between summer
611 and winter. Although not all samples consistently follow this pattern, specific intratooth profiles, particularly
612 those from bovines in El Castillo and Canyars, exhibit sharp profiles with narrow ranges (<1.5‰). This
613 phenomenon was previously reported in the region in preliminary studies conducted at the sites of El Castillo
614 (Jones et al., 2019) and in the Magdalenian levels of El Mirón cave (Geiling, 2020).

615 Non-sinusoidal profiles observed in the data can be attributed to various factors, including sample
616 techniques and preservation issues and the inherent variability in the original isotopic signal. Factors related
617 to sampling and methods can be connected to 1) the sampling process (e.g. too deep or too distant sampling
618 grooves); 2) the imprecision of the mass spectrometer measurements; 3) uncontrolled effects of samples
619 pretreatments; 4) diagenetic alterations affecting the carbonate fraction. However, it must be noted that
620 technical reasons, whether related to sampling or pretreatment, do not appear to impact the obtained results
621 significantly. First, this study reproduces the same intratooth sampling methods that previously yielded
622 reliable results in similar research (e.g., Pederzani et al., 2023, 2021a). Second, non-significant alterations
623 in intratooth profiles of pretreated horse samples (El Castillo, Labeko Koba, Otero) are noticed in comparison
624 to untreated bovid samples (Appendix D). Some bovid samples show these non-sinusoidal profiles equally.
625 In sites where both species are analysed, no correlation is observed between $\delta^{18}O_{carb}$ and $\delta^{13}C_{carb}$. In tooth
626 enamel, diagenetic alterations are generally less pronounced than in bone due to its higher mineral content.
627 However, carbonates within tooth enamel can be more susceptible to diagenesis and recrystallisation
628 compared to the phosphate fraction, which contains a more extensive reservoir of oxygen and stronger
629 oxygen bonds (Zazzo et al., 2004; Chenery et al., 2012; Bryant et al., 1996). The carbonate content in our
630 samples, ranging from 3.9% to 8.9%, is similar to the proportion found in modern tooth enamel, suggesting
631 no immediate indication of diagenetic alteration. Diagenesis can also be evaluated by comparing the isotopic
632 values of the carbonate and phosphate fractions in a sample, as there is a predictable difference between
633 them. However, phosphate fraction measurements were still unavailable in our study, except at Axlor
634 (Pederzani et al., 2023) where good preservation was attested. Additionally, in the case of diagenetic
635 alteration, we would expect specimens from the same archaeological levels to be affected similarly, which
636 is not the case.

637 Based on these arguments, it is suggested that the non-sinusoidal $\delta^{18}O_{carb}$ signal observed in some
638 individuals may not be attributed to poor preservation; instead, it likely reflects the original isotopic signature
639 from water input, which appears to be non-seasonal. Several factors can explain why some teeth do not
640 reflect an evident seasonal fluctuation, which could be related to animals' mobility, the isotopic composition
641 of the water sources, and seasonal buffering within those water sources (Pederzani and Britton, 2019). The
642 main factors considered in our study are 1) the high mobility of the animals analysed among ecosystems
643 with different isotopic baselines due to large migrations; 2) the inland-coastal or short altitudinal movements
644 through the region, which lead to the acquisition of water from sources with different isotopic signal; and 3)
645 the acquisition of water from sources with no clear seasonal signal, such as large bodies of water, rivers,

646 groundwaters, or meltwaters. At mid-latitudes, the temperature effect is currently the dominant
647 factor. However, it is crucial to note that past changes in rainfall density (as the "amount effect"; Dansgaard,
648 1964) cannot be dismissed from having a more significant role then, particularly during glacial and arid
649 periods. These effects, with their potential to mask temperature oscillations, underscore the urgency and
650 importance of our research in understanding and predicting climate patterns. Furthermore, variability
651 between species and within the same species, even within populations living in the same habitat, is also
652 possible. This can be attributed to multiple factors, from minor differences in foraging and drinking behaviour
653 to slight metabolic and physiological variations, including body size, metabolic rate, breathing rate, moisture
654 content of food, and faeces, among others (Hoppe et al., 2004; Kohn, 1996; Magozzi et al., 2019).

655 Analyses of nitrogen and sulphur stable isotopes on ungulate bone collagen from Axlor, El Castillo and
656 Labeko Koba (Jones et al., 2018, 2019; Pederzani et al., 2023) have already revealed large variation ranges
657 linked to the existence of several microenvironments just in a few kilometres within the Vasco-Cantabria
658 region. Long migrations and long hunting distances cannot solely explain these diverse values because of
659 the range of species involved and their likely small-scale movements. In our study, the minimal $\delta^{13}C_{carb}$
660 intratooth variation within individuals (<1‰) indicates limited seasonal changes in their feeding behaviour
661 that influenced the carbon isotopic composition (Appendix D). Therefore, considering the diverse topography
662 of the Vasco-Cantabrian, characterized by steep valleys connecting the Cantabrian Cordillera with the
663 Atlantic Ocean through rivers over short distances (30-50 km), the availability in the past of a wide range of
664 water sources in small areas seems highly likely. Certain drinking behaviours can influence $\delta^{18}O$, as animals
665 may acquire water from various sources, with small streams better reflecting seasonal isotopic oscillations
666 than large lakes or evaporating ponds (see synthesis in Pederzani and Britton, 2019). Systematic
667 consumption of highly buffered water sources can significantly attenuate the final recorded signal.
668 Furthermore, rivers in the region frequently contain meltwater from snow during the winter-spring months
669 and water springs.

5.3 Regional trends and ecological niches

671 This study provides valuable insights despite the limited sample size at each archaeological level. It
672 establishes a baseline of isotopic values for northern Iberia, allowing for the evaluation of regional trends.
673 In the northwest, in the Vasco-Cantabrian region, the $\delta^{13}C_{carb}$ values obtained oscillated between -13‰ and
674 -8.9‰ and between -7.2‰ and -3.3‰ in the case of $\delta^{18}O_{carb}$ values. These values are within the range
675 expected, considering previous regional studies in ungulates (Carvalho et al., 2022; Jones et al., 2019;
676 Lécuyer et al., 2021; Pederzani et al., 2023). Although oxygen variability trends are less precise, the main
677 factor distinguishing the observed changes over time is the variation of carbon isotopic composition among
678 species and regions. The combination of mean $\delta^{13}C_{diet}$ and $\delta^{18}O_{mw}$ values (Fig. 4; 5) accentuates disparities
679 in ecological niche overlap between horses and bovines, whereas cervids and horses frequently exhibit
680 shared ecological niches. The dissimilarities between bovines and horses could be attributed to shifts in
681 feeding behaviour, which may be accompanied by ecological and environmental changes, either
682 independently or in parallel.

683 Comparing the entire dataset and across all sites, the consistently lower $\delta^{13}C_{diet}$ values in horses compared
684 to bovids throughout time suggest both animals inhabited open landscapes, with bovines exhibiting a grazer
685 preference while horses show a mix-feeding diet. Only in the Middle-to-Upper Paleolithic transition 18B and
686 18C levels of El Castillo, an exception is observed with lower $\delta^{13}C_{diet}$ values in bovines, linked to a higher
687 browser input due to a higher habitat in closer environments, such as open forests, similar to those inhabited
688 by the horses. This generates a niche overlapping between horses and bovines, most likely reflecting stable
689 conditions that could support both species in similar ecosystems. Contrarily, in the Châtelperronian and
690 early Aurignacian levels from Labeko Koba, a clear differentiation between horses and bovines is observed,
691 mainly in $\delta^{13}C_{diet}$ values, highlighting the occupation of different parts of the landscape by both species. This

spatially-driven niche separation between species could result from resource competition derived from an unstable climatic period, where species needed to specialise to adapt to the changing conditions. Notable changes are also observed in the $\delta^{18}O_{carb}$ values from Labeko Koba compared to the older El Castillo and Axlor sites, with bovines exhibiting a higher fluctuation range and the lowest values in the region. These trends are consistent with values observed on bone collagen from previous studies in these sites. During the Middle-to-Upper Paleolithic transition in the region, by comparing horses and red deer, a decrease in mean $\delta^{13}C$ (from -21‰ to -20‰) and $\delta^{15}N$ values (from 2.5‰ to 6‰) in bone collagen was observed in contrast to stable red deer mean $\delta^{13}C$ (Fernández-García et al., 2023; Jones et al., 2018, 2019). This decrease was previously interpreted as niche fractionation, derived from an opening landscape, that drove equids into low-quality pastures compared to cervids. Pollen evidence in the region suggests a prevalence of steppe vegetation and low tree cover for the Châtelperronian and Aurignacian (Iriarte-Chiapusso, 2000).

In the same period, Canyars in the northeastern area, higher mean $\delta^{13}C_{diet}$ are observed in both species (between -23.6‰ and -24.4‰), indicating a preference for more open landscapes by bovines and equids. The indication of open areas could be linked to the arid climatic conditions associated with the Heinrich ~~Event~~ Stadial 4, which coincides with the formation of the studied level. This predominance of open areas coincides with the presence of typical steppe herbivore species, such as *Equus hydruntinus* and *Coelodonta antiquitatis*, the microfauna and pollen taxa, and the data offered by the use-wear analysis on ungulate remains identified at the site (Daura et al., 2013; López-García et al., 2022; Rivals et al., 2017).

Aridity is a plausible explanation for the higher niche partitioning observed in Labeko Koba and the higher $\delta^{13}C_{diet}$ values found in Canyars for both species during the Aurignacian. The $\delta^{13}C_{diet}$ results of bovines from Aitzbitarte III interior during the Gravettian are consistent with the trend observed in Labeko Koba, where previous studies have already suggested this time to be notably arid and cold (Arrizabalaga et al., 2010). Finally, in the Magdalenian level of El Otero, higher $\delta^{13}C_{diet}$ values resemble those observed in Canyars. However, this time, carbon values are related to niche partitioning between horses and red deer. In contrast, higher $\delta^{18}O_{mw}$ values might indicate warmer conditions but are still associated with open landscapes in the Vasco-Cantabrian area.

5.4 Late Pleistocene climatic evolution in Northern Iberia

Carbon and oxygen isotopes were used to estimate quantitative parameters related to past temperatures and precipitation. In the case of oxygen isotopic compositions, an evaluation of environmental water composition can be addressed before approaching temperature estimations. When transformed to $\delta^{18}O_{mw}$ using species-adapted correlations and correcting bias in sea water $\delta^{18}O_{mw}$, the summer $\delta^{18}O_{mw}$ values obtained from the modelled teeth range from -8.9‰ to -2.2‰, while the winter values range from -17.1‰ to -8.9‰. These values can be tentatively compared with the current trends observed in $\delta^{18}O_{mw}$ range recorded by the IAEA station (IAEA/ WMO, 2022) in Santander (from -3.5‰ in summer to -6.6‰ in winter) and in Barcelona (from -2.2‰ in summer to -6.3‰ in winter) and the OIPC (Bowen, 2022) estimations for studied locations (from -1‰ to -9‰) (Appendix B). As observed in the present, Canyars exhibit mean annual $\delta^{18}O_{mw}$ values around -8.2‰, which is lower than the current $\delta^{18}O_{mw}$ estimated for this location (-5.4‰) but higher than Labeko Koba mean annual $\delta^{18}O_{mw}$ (-9.5‰). This raises the question of whether the baseline $\delta^{18}O_{mw}$ differences between Canyars and the other sites can be attributed to Mediterranean influence rather than the Atlantic, assuming equivalent air circulation patterns and moisture sources experienced in the past as in the present (Araguas-Araguas and Diaz Teijeiro, 2005; García-Alix et al., 2021; Moreno et al., 2021). However, it's important to note that these comparisons must be approached thoughtfully, considering that moisture fluxes and precipitation trends may have varied significantly during the Pleistocene and the Holocene (Dansgaard, 1964; Shackleton, 1987).

As indicated by the climate reconstructed here, temperatures were colder, and precipitation levels were notably lower in the Late Pleistocene period in this region than they are nowadays (Table 4; Appendix B). From 80 to 50 ka BP, in the Mousterian levels of Axlor, temperatures were slightly colder than today, but older levels showed higher differences between summer and winter temperatures. Rainfall estimations exhibit an unusual arid pattern, possibly affected by bovines predominantly feeding in open areas at that time. This aligns with the impact of basal feeding behaviour on rainfall estimations, as previously advised by Lécuyer et al. (2021). In this case, it is not possible to isolate the effect of diet from environmental interference, but previous studies have highlighted stable climatic conditions at the site (Pederzani et al., 2023). Climatic reconstruction, relying on a compilation of lake sediments from northern Iberia (Moreno et al., 2012) suggests that from late MIS4 to 60 ka cal BP, cold but relatively humid conditions predominated, with drier conditions emerging later. Additionally, stalagmites from the Ejulve cave in the Iberian range indicate a dry climate until 65.5 ka BP, preceding HE6, followed by more humid conditions afterwards (Pérez-Mejías et al., 2019).

During the late Middle Paleolithic and early Aurignacian occupations, the observed shift in the niche configuration of species suggests potential climatic perturbations. There is a decreasing trend in temperatures from the Transitional Aurignacian levels in El Castillo (18C and 18B; ca. 47-46 ka cal BP) to the Châtelperronian (Xinf; 45.1 ka cal BP) and Early Aurignacian (VII-V; from 40.7 to 36.3 ka cal BP) levels in Labeko Koba. Lower mean annual and winter temperatures are particularly notable at El Castillo and Labeko Koba. Labeko Koba levels exhibit high seasonal amplitude, especially at level VII. Additionally, there is a slight decrease in rainfall and increased fluctuations from the Transitional Aurignacian levels from El Castillo (18B-18C) to the Aurignacian levels in Labeko Koba (VII-V). Previous studies in the northern Iberian region underlined an environmental and ecological shift after GS13/HE5, from 48 to 44 ka cal BP, based on a progressive trend to colder temperatures, aridity increase, and open environmental conditions, matching with the late Neanderthal occupations, followed by a population hiatus before the arrival of Anatomically Modern Humans (Fernández-García et al., 2023; Vidal-Cordasco et al., 2022). This episode coincides with the maximum extent of glaciers in this region, as recorded in Lake Enol and Vega Comeya and an significant decrease in plant biomass and herbivore abundance around 44 to 38 ka BP (Ballesteros et al., 2020; Jiménez-Sánchez et al., 2013; Ruiz-Fernández et al., 2022). Moreover, previous isotopic analyses in the region pointed to some ecological alterations considering perturbations observed in the δ^{13}C and δ^{15}N of bone collagen (Jones et al., 2018, 2019). This tendency of increased aridity aligns with observations made in regional lake sediments from northern Iberia between 60 and 23.5 ka cal BP, marked by abrupt climate changes associated with HE (Moreno et al., 2012). Supporting this, the marine core MD04-2845 in the northern margin of Iberia reveals a decline in the Atlantic forest and an expansion of steppe and cold grasses from 47 to 40 ka BP (Fourcade et al., 2022).

When comparing the environmental reconstruction of the Aurignacian period between the Vasco-Cantabrian (levels V-IV from Labeko Koba) and the northeastern region (Layer I from Canyars), which are synchronous to HE4 (39 ka BP), this study reveals notably lower rainfall levels for the latter. This is due to the feeding behaviour observed in animals, mainly in open areas. However, these drier conditions align with the specific climatic conditions expected for this period and support previous findings revealing aridity and the predominance of open landscapes (Daura et al., 2013; Rivals et al., 2017). The temperature data indicates that, at Canyars, colder conditions were experienced, especially during the winter season, compared to the present. However, in comparison to Labeko Koba, Canyars experienced warmer conditions. As explained earlier, the Mediterranean basin had consistently higher temperatures, even during colder periods. This is consistent with the persistence of Mediterranean open forests in the surroundings, as indicated by other studies (López-García et al., 2013; Rivals et al., 2017). Continuous natural records are lacking in the northeastern Iberian margin. However, the inland stalagmite record from Ejulve Cave (Pérez-Mejías et al., 2019) and the sedimentary lacustrine sequence of Cañizar de Villarquemado (González-Sampériz et al.,

2020) have identified the most arid intervals during HE5 and HE4. These periods were characterized by steppe vegetation expansions, followed by deciduous woodland expansion. To the south, the Padul sequence agrees with cold and dry conditions alternating with forest recovery (Camuera et al., 2019), as documented in the Alborean Sea (Martrat et al., 2004).

Finally, the sites Aitzbitarte III interior (27.9 ka cal BP) and El Otero (17.3 ka cal BP) provided valuable climatic insights into the Vasco-Cantabrian region during the Upper Paleolithic, specifically during the Gravettian and Magdalenian, respectively. Considering previous research in the region, the climatic trend reported for the Aurignacian, characterised by colder and more arid conditions, was expected to continue or even intensify during the Gravettian (Fernández-García et al., 2023; Garcia-Ibaibarriaga et al., 2019b; Lécuyer et al., 2021). Both sites indicate lower precipitation than today in this area, indicating significant aridity, with ungulates feeding predominantly in open landscapes. However, El Otero's higher mean annual temperatures recorded in the Magdalenian horses respect to other sites within the Vasco-Cantabrian, are consistent with a climatic amelioration following the Last Glacial Maximum (Jones et al., 2021). MIS 2 is marked by the most extreme glacial conditions, as indicated by NGRIP and marine cores in Iberian margins (Martrat et al., 2004; Sánchez Goñi et al., 2002). However, other regional proxies, such as lake sediment and the stalagmite sequence in Pindal Cave (Moreno et al., 2010), suggest a complex and highly variable climate during MIS 2. These proxies identify the coldest and most arid period within MIS 2 as the interval from 18 to 14 ka cal BP rather than the global Last Glacial Maximum (23 to 19 ka cal BP).

5. Conclusions

This study provides a detailed analysis of the temporal evolution of the environment and climatic conditions in northern Iberia, spanning from the Middle Paleolithic to the late Upper Paleolithic, this is from the GS21 to the GS2, ranging from 80 ka BP to 17 ka cal BP. In the Vasco-Cantabrian region, the results reveal a heterogeneous open mosaic landscape, ranging from light forest to meadows and grasslands. This landscape reconstruction is primarily inferred by the feeding locations of the studied animals and, consequently, related to the ecosystems where hominins captured them. Despite shifts in niche configuration observed between equids and bovines, both species typically foraging in open areas, with bovines showing a higher preference for grazing. Only in El Castillo, during the late Mousterian and the Transitional Aurignacian levels, bovines show unusually low $\delta^{13}C_{diet}$ related to higher browsing and overlapping with horse isotopic niche. This might indicate a slightly closed mosaic landscape that could sustain both species. In contrast, only horses from Canyars exhibit a preference for grazing behaviour.

Stable climatic conditions are described for Mousterian in Axlor and El Castillo levels from 80 to 50 ka cal BP. However, some elements indicate environmental perturbations initiated during the Transitional Aurignacian levels of El Castillo, around 48-45 ka BP and after HE5/GS13. After GS12 (44.2-43.3 ka BP), horses and bovines are potentially occupying different ecological niches during the Châtelperronian and early Aurignacian levels of Labeko Koba, pointing to a species' environmental specialisation, which can be a consequence of competition for food resources during an unstable ecological period. The climatic estimations indicate a temperature shift during this period, with a slight decrease in temperatures and evidence of fluctuations in rainfall. Previous environmental studies on the region have underlined ecological stress and increasing aridity from around 42.5 ka cal BP, which may relate to a broader ecosystem decline. When comparing the environmental conditions during the Aurignacian period in the northeast (Canyars) and the northwest (Labeko Koba), the first had higher baseline temperatures but also experienced higher aridity. Animals continued to feed on open landscapes during the Gravettian and Magdalenian levels in the Vasco-Cantabrian region, represented by Aitzbitarte III interior and El Otero. However, there is evidence of a temperature recovery after the LGM at the El Otero.

827 The results presented here, derived from the first extensive sampling in the Vasco-Cantabrian, establish the
828 basis of future stable isotopic studies on faunal tooth enamel in Iberia. Despite the uncertainties inherent in
829 this work, both $\delta^{18}O$ and $\delta^{13}C$ contributed to the regional climatic characterisation, including the estimation
830 of temperatures and precipitations, as well as the seasonality range between summer and winter. The
831 potential influence of pretreatment effects and uncontrolled diagenetic alterations on the enamel carbonate
832 fraction has been assessed. However, complementary diagenetic tests, using new techniques like $\delta^{18}O_{phos}$
833 and FTIR analyses are advised in further works to gain more insights into sample preservation. Ongoing
834 sulphur, hydrogen and strontium studies will provide additional information on the mobility patterns of
835 animals hunted by Late Pleistocene hominins and, therefore, will help better understand the ecological and
836 environmental context occupied by Neanderthal and modern humans and their landscape use in this
837 particular region. Finally, a more comprehensive characterisation of the baseline oxygen values would also
838 enhance the environmental interpretation of the existing data.

Appendices

840 Appendices A, C, D and E are presented after bibliography. Raw data is presented in Appendix B, available
841 at https://github.com/ERC-Subsilience/Ungulate_enamel-carbonate

Code availability

843 R code used to perform plots, temperature and error calculations, Bayesian models code and inverse
844 models in this manuscript can be accessed at GitHub (https://github.com/ERC-
845 Subsilience/Ungulate_enamel-carbonate).

Data availability

847 The available datasets used for this article are provided in the supplementary materials (Appendix A-E).

Author contribution

849 A.B.M.-A. got the funding and designed the research. A.B.M.-A and M.F.-G. get the permissions for sampling
850 in the regional museums. M.F.-G., K.B, and S.P. defined the analysis strategy. M.F.-G. analysed the data
851 and wrote the manuscript with critical inputs from A.B.M.-A., K.B, and S.P. J.M.G., L.A., M.F.-G., and A.C.
852 M.F.-G., L.A., J.M.G., and A.C. achieved the teeth sampling and lab sample preparation. J.D. and M.S. are
853 responsible for the excavations in Canyars and contribute to the discussion. All the authors revised and
854 commented on the manuscript.

Competing interests

856 The contact author has declared that none of the authors has any competing interests.

Acknowledgements

858 We acknowledge the Museo de Arqueología y Prehistoria de Cantabria (MUPAC), the Consejería de
859 Educación, Cultura y Deporte del Gobierno de Cantabria, the Museo de Arqueología de Bizkaia (Arkeologi
860 Museoa) and the Centro de Colecciones Patrimoniales de la Diputación Foral de Gipuzkoa (Gordailua) –
861 Provincial Government of Guipuzkoa's Heritage Collection Centre for the access to the archaeological
862 collections. We do appreciate the work achieved by H. Reade during the initial sampling, pretreatment and
863 analyses of samples undertaken at the University of Cantabria and Cambridge. We want to thank the two
864 anonymous referees for their valuable comments, which significantly improved the quality of the paper.

Financial support

Field Code Changed

Field Code Changed

Funding for Vasco-Cantabria research was obtained from the Spanish Ministry of Science and Innovation (PID2021-125818NB-I00, HAR2017-84997-P and HAR2012-33956), the European Research Council under the European Union's Horizon 2020 Research and Innovation Programme (grant agreement number 818299; SUBSILIENCE project) and Proyecto Puente by Consejería de Educación, Cultura y Deporte del Gobierno de Cantabria. Research for Canyars was funded by the Spanish Ministry of Science and Innovation (PID2020-113960GB-100), Departament de Cultura de la Generalitat de Catalunya (CLT/2022/ARQ001SOLC/128) and AGAUR (SGR2021-00337). M.F.-G. is supported by the APOSTD postdoctoral fellowship (CIAPOS/2022/081/AEI/10.13039/501100011033), funded by the Generalitat Valenciana and the European Social Fund. S.P. was supported by a German Academy of Sciences Leopoldina postdoctoral fellowship (LPDS 2021-13) during this project. M.S. benefited from financial support from a Ramon y Cajal postdoctoral grant (RYC2021-032999-I) funded by the Spanish Ministry of Science and Innovation and the European Union-NextGenerationEU.

References

Allué, E., Martínez-Moreno, J., Roy, M., Benito-Calvo, A., and Mora, R.: Montane pine forests in NE Iberia during MIS 3 and MIS 2. A study based on new anthracological evidence from Cova Gran (Santa Linya, Iberian Pre-Pyrenees), Review of Palaeobotany and Palynology, 258, 62–72, https://doi.org/10.1016/j.revpalbo.2018.06.012, 2018.

Álvarez-Lao, D. J., Rivals, F., Sánchez-Hernández, C., Blasco, R., and Rosell, J.: Ungulates from Teixoneres Cave (Moià, Barcelona, Spain): Presence of cold-adapted elements in NE Iberia during the MIS 3, Palaeogeography, Palaeoclimatology, Palaeoecology, 466, 287–302, https://doi.org/10.1016/j.palaeo.2016.11.040, 2017.

Ambrose, S. H. and Norr, L.: Experimental Evidence for the Relationship of the Carbon Isotope Ratios of Whole Diet and Dietary Protein to Those of Bone Collagen and Carbonate, in: Prehistoric Human Bone, Springer Berlin Heidelberg, Berlin, Heidelberg, 1–37, https://doi.org/10.1007/978-3-662-02894-0_1, 1993.

Araguas-Araguas, L. J. and Diaz Teijeiro, M. F.: Isotope composition of precipitation and water vapour in the Iberian Peninsula. First results of the Spanish Network of Isotopes in Precipitation, in: Isotopic Composition of Precipitation in the Mediterranean Basin in Relation to Air Circulation Patterns and Climate. IAEA-TECDOC-1453, Vienna, 173–190, 2005.

Balasse, M., Ambrose, S. H., Smith, A. B., and Price, T. D.: The Seasonal Mobility Model for Prehistoric Herders in the South-western Cape of South Africa Assessed by Isotopic Analysis of Sheep Tooth Enamel, Journal of Archaeological Science, 29, 917–932, https://doi.org/10.1006/jasc.2001.0787, 2002.

Ballesteros, D., Álvarez-Vena, A., Monod-Del Dago, M., Rodríguez-Rodríguez, L., Sanjurjo-Sánchez, J., Álvarez-Lao, D., Pérez-Mejías, C., Valenzuela, P., DeFelipe, I., Laplana, C., Cheng, H., and Jiménez-Sánchez, M.: Paleoenvironmental evolution of Picos de Europa (Spain) during marine isotopic stages 5c to 3 combining glacial reconstruction, cave sedimentology and paleontological findings, Quaternary Science Reviews, 248, 106581, https://doi.org/10.1016/j.quascirev.2020.106581, 2020.

Bendrey, R., Vella, D., Zazzo, A., Balasse, M., and Lepetz, S.: Exponentially decreasing tooth growth rate in horse teeth: implications for isotopic analyses, Archaeometry, 57, 1104–1124, https://doi.org/10.1111/arcm.12151, 2015.

Blumenthal, S. A., Cerling, T. E., Chritz, K. L., Bromage, T. G., Kozdon, R., and Valley, J. W.: Stable isotope time-series in mammalian teeth: In situ δ18O from the innermost enamel layer, Geochimica et Cosmochimica Acta, 124, 223–236, https://doi.org/10.1016/j.gca.2013.09.032, 2014.

Blumenthal, S. A., Cerling, T. E., Smiley, T. M., Badgley, C. E., and Plummer, T. W.: Isotopic records of climate seasonality in equid teeth, Geochimica et Cosmochimica Acta, 260, 329–348, https://doi.org/10.1016/j.gca.2019.06.037, 2019.

Bocherens, H.: Isotopic biogeochemistry and the paleoecology of the mammoth steppe fauna, Deinsea, 91, 57–76, 2003.

Brand, W. A., Coplen, T. B., Vogl, J., Rosner, M., and Prohaska, T.: Assessment of international reference materials for isotope-ratio analysis (IUPAC Technical Report), Pure and Applied Chemistry, 86, 425–467, https://doi.org/10.1515/pac-2013-1023, 2014.

Britton, K., Pederzani, S., Kindler, L., Roebroeks, W., Gaudzinski-Windheuser, S., Richards, M. P., and Tütken, T.: Oxygen isotope analysis of Equus teeth evidences early Eemian and early Weichselian palaeotemperatures at the Middle Palaeolithic site of Neumark-Nord 2, Saxony-Anhalt, Germany, Quaternary Science Reviews, 226, 106029, https://doi.org/10.1016/j.quascirev.2019.106029, 2019.

Bryant, J. D., Luz, B., and Froelich, P. N.: Oxygen isotopic composition of fossil horse tooth phosphate as a record of continental paleoclimate, Palaeogeography, Palaeoclimatology, Palaeoecology, 107, 303–316, https://doi.org/10.1016/0031-0182(94)90102-3, 1994.

Bryant, J. D., Koch, P. L., Froelich, P. N., Showers, W. J., and Genna, B. J.: Oxygen isotope partitioning between phosphate and carbonate in mammalian apatite, Geochimica et Cosmochimica Acta, 60, 5145–5148, https://doi.org/10.1016/S0016-7037(96)00308-0, 1996.

Camuera, J., Jiménez-Moreno, G., Ramos-Román, M. J., García-Alix, A., Toney, J. L., Anderson, R. S., Jiménez-Espejo, F., Bright, J., Webster, C., Yanes, Y., and Carrión, J. S.: Vegetation and climate changes during the last two glacial-interglacial cycles in the western Mediterranean: A new long pollen record from Padul (southern Iberian Peninsula), Quaternary Science Reviews, 205, 86–105, https://doi.org/10.1016/j.quascirev.2018.12.013, 2019.

Carvalho, M., Jones, E. L., Ellis, M. G., Cascalheira, J., Bicho, N., Meiggs, D., Benedetti, M., Friedl, L., and Haws, J.: Neanderthal palaeoecology in the late Middle Palaeolithic of western Iberia: a stable isotope analysis of ungulate teeth from Lapa do

926   Picareiro (Portugal), Journal of Quaternary Science, 37, 300–319, https://doi.org/10.1002/jqs.3363, 2022.

927 Cascalheira, J., Alcaraz-Castaño, M., Alcolea-González, J., de Andrés-Herrero, M., Arrizabalaga, A., Aura Tortosa, J. E., Garcia-
928   Ibaibarriaga, N., and Iriarte-Chiapusso, M.-J.: Paleoenvironments and human adaptations during the Last Glacial
929   Maximum in the Iberian Peninsula: A review, Quaternary International, 581–582, 28–51,
930   https://doi.org/10.1016/j.quaint.2020.08.005, 2021.

931 Cerling, T. E. and Harris, J. M.: Carbon isotope fractionation between diet and bioapatite in ungulate mammals and implications for
932   ecological and paleoecological studies, Oecologia, 120, 347–363, https://doi.org/10.1007/s004420050868, 1999.

933 Chappell, J. and Shackleton, N. J.: Oxygen isotopes and sea level, Nature, 324, 137–140, https://doi.org/10.1038/324137a0, 1986.

934 Chesson, L. A., Beasley, M. M., Bartelink, E. J., Jans, M. M. E., and Berg, G. E.: Using bone bioapatite yield for quality control in
935   stable isotope analysis applications, Journal of Archaeological Science: Reports, 35, 102749,
936   https://doi.org/10.1016/j.jasrep.2020.102749, 2021.

937 Chillón, B. S., Alberdi, M. T., Leone, G., Bonadonna, F. P., Stenni, B., and Longinelli, A.: Oxygen isotopic composition of fossil equid
938   tooth and bone phosphate: an archive of difficult interpretation, Palaeogeography, Palaeoclimatology, Palaeoecology,
939   107, 317–328, https://doi.org/10.1016/0031-0182(94)90103-1, 1994.

940 Coplen, T. B.: Guidelines and recommended terms for expression of stable-isotope-ratio and gas-ratio measurement results, Rapid
941   Communications in Mass Spectrometry, 25, 2538–2560, https://doi.org/10.1002/rcm.5129, 2011.

942 Coplen, T. B., Kendall, C., and Hopple, J.: Comparison of stable isotope reference samples, Nature, 302, 236–238,
943   https://doi.org/10.1038/302236a0, 1983.

944 D'Angela, D. and Longinelli, A.: Oxygen isotopes in living mammal's bone phosphate: Further results, Chemical Geology, 86, 75–
945   82, 1990.

946 D'Errico, F. and Sánchez Goñi, M. F.: Neandertal extinction and the millennial scale climatic variability of OIS 3, Quaternary Science
947   Reviews, 22, 769–788, https://doi.org/10.1016/S0277-3791(03)00009-X, 2003.

948 Dansgaard, W.: Stable isotopes in precipitation, Tellus, XVI, 436–468, 1964.

949 Daura, J., Sanz, M., García, N., Allué, E., Vaquero, M., Fierro, E., Carrión, J. S., López-García, J. M., Blain, H. a., Sánchez-Marco,
950   a., Valls, C., Albert, R. M., Fornós, J. J., Julià, R., Fullola, J. M., and Zilhão, J.: Terrasses de la Riera dels Canyars (Gavà,
951   Barcelona): The landscape of Heinrich Stadial 4 north of the " Ebro frontier" and implications for modern human dispersal
952   into Iberia, Quaternary Science Reviews, 60, 26–48, https://doi.org/10.1016/j.quascirev.2012.10.042, 2013.

953 Delgado Huertas, A., Iacumin, P., Stenni, B., Sánchez Chillón, B., and Longinelli, A.: Oxygen isotope variations of phosphate in
954   mammalian bone and tooth enamel, Geochimica et Cosmochimica Acta, 59, 4299–4305, https://doi.org/10.1016/0016-
955   7037(95)00286-9, 1995.

956 Drucker, D. G.: The Isotopic Ecology of the Mammoth Steppe, Annual Review of Earth and Planetary Sciences, 50, 395–418,
957   https://doi.org/10.1146/annurev-earth-100821-081832, 2022.

958 Drucker, D. G., Bridault, A., Hobson, K. A., Szuma, E., and Bocherens, H.: Can carbon-13 in large herbivores reflect the canopy
959   effect in temperate and boreal ecosystems? Evidence from modern and ancient ungulates, Palaeogeography,
960   Palaeoclimatology, Palaeoecology, 266, 69–82, https://doi.org/10.1016/j.palaeo.2008.03.020, 2008.

961 Eggleston, S., Schmitt, J., Bereiter, B., Schneider, R., and Fischer, H.: Evolution of the stable carbon isotope composition of
962   atmospheric CO_2 over the last glacial cycle, Paleoceanography and Paleoclimatology, 31, 434–452,
963   https://doi.org/10.1002/2015PA002874, 2016.

964 Fagoaga, A.: 26iomineraliz paleoclimática y paisajística durante el MIS3 a partir del estudio de los micromamíferos del yacimiento
965   de El Salt (Alcoi, Alicante)., Universidad de Burgos, 34 pp., 2014.

966 Fernández-García, M., Royer, A., López-García, J. M., Bennàsar, M., Goedert, J., Fourel, F., Julien, M.-A., Bañuls-Cardona, S.,
967   Rodríguez-Hidalgo, A., Vallverdú, J., and Lécuyer, C.: Unravelling the oxygen isotope signal (δ18O) of rodent teeth from
968   northeastern Iberia, and implications for past climate reconstructions, Quaternary Science Reviews, 218, 107–121,
969   https://doi.org/10.1016/j.quascirev.2019.04.035, 2019.

970 Fernández-García, M., López-García, J. M., Royer, A., Lécuyer, C., Allué, E., Burjachs, F., Chacón, M. G., Saladié, P., Vallverdú,
971   J., and Carbonell, E.: Combined palaeoecological methods using small-mammal assemblages to decipher environmental
972   context of a long-term Neanderthal settlement in northeastern Iberia, Quaternary Science Reviews, 228, 106072,
973   https://doi.org/10.1016/j.quascirev.2019.106072, 2020.

974 Fernández-García, M., Vidal-Cordasco, M., Jones, J. R., and Marín-Arroyo, A. B.: Reassessing palaeoenvironmental conditions
975   during the Middle to Upper Palaeolithic transition in the Cantabrian region (Southwestern Europe), Quaternary Science
976   Reviews, 301, 107928, https://doi.org/10.1016/j.quascirev.2022.107928, 2023.

977 Fick, S. E. and Hijmans, R. J.: WorldClim 2: new 1-km spatial resolution climate surfaces for global land areas, International Journal
978   of Climatology, 37, 4302–4315, https://doi.org/10.1002/joc.5086, 2017.

979 Finlayson, C. and Carrión, J. S.: Rapid ecological turnover and its impact on Neanderthal and other human populations, Trends in
980   Ecology and Evolution, 22, 213–222, https://doi.org/10.1016/j.tree.2007.02.001, 2007.

981 Fourcade, T., Sánchez Goñi, M. F., Lahaye, C., Rossignol, L., and Philippe, A.: Environmental changes in SW France during the
982   Middle to Upper Paleolithic transition from the pollen analysis of an eastern North Atlantic deep-sea core, Quaternary
983   Research, 1–18, https://doi.org/10.1017/qua.2022.21, 2022.

984 France, C. A. M., Sugiyama, N., and Aguayo, E.: Establishing a preservation index for bone, dentin, and enamel bioapatite mineral
985   using ATR-FTIR, Journal of Archaeological Science: Reports, 33, 102551, https://doi.org/10.1016/j.jasrep.2020.102551,
986   2020.

987 García-Alix, A., Camuera, J., Ramos-Román, M. J., Toney, J. L., Sachse, D., Schefuß, E., Jiménez-Moreno, G., Jiménez-Espejo,
988   F. J., López-Avilés, A., Anderson, R. S., and Yanes, Y.: Paleohydrological dynamics in the Western Mediterranean during
989   the last glacial cycle, Global and Planetary Change, 202, 103527, https://doi.org/10.1016/j.gloplacha.2021.103527, 2021.

990 Garcia-Ibaibarriaga, N., Suárez-Bilbao, A., Iriarte-Chiapusso, M. J., Arrizabalaga, A., and Murelaga, X.: Palaeoenvironmental
991   dynamics in the Cantabrian Region during Greenland stadial 2 approached through pollen and micromammal records:
992   State of the art, Quaternary International, 506, 14–24, https://doi.org/10.1016/j.quaint.2018.12.004, 2019a.

993 Garcia-Ibaibarriaga, N., Suárez-Bilbao, A., Iriarte-Chiapusso, M. J., Arrizabalaga, A., and Murelaga, X.: Palaeoenvironmental
994   dynamics in the Cantabrian Region during Greenland stadial 2 approached through pollen and micromammal records:
995   State of the art, Quaternary International, 506, 14–24, https://doi.org/10.1016/j.quaint.2018.12.004, 2019b.
996 Geiling, J. M.: Human Ecodynamics in the Late Upper Pleistocene of Northern Spain: An Archeozoological Study of Ungulate
997   Remains from the Lower Magdalenian and other Periods in El Mirón Cave (Cantabria), Universidad de Cantabria, 734
998   pp., 2020.
999 González-Sampériz, P., Gil-Romera, G., García-Prieto, E., Aranbarri, J., Moreno, A., Morellón, M., Sevilla-Callejo, M., Leunda, M.,
1000   Santos, L., Franco-Múgica, F., Andrade, A., Carrión, J. S., and Valero-Garcés, B. L.: Strong continentality and effective
1001   moisture drove unforeseen vegetation dynamics since the last interglacial at inland Mediterranean areas: The
1002   Villarquemado   sequence   in   NE   Iberia,   Quaternary   Science   Reviews,   242,
1003   https://doi.org/10.1016/j.quascirev.2020.106425, 2020.
1004 Hoppe, K. A.: Correlation between the oxygen isotope ratio of North American bison teeth and local waters: Implication for
1005   paleoclimatic   reconstructions,   Earth   and   Planetary   Science   Letters,   244,   408–417,
1006   https://doi.org/10.1016/j.epsl.2006.01.062, 2006.
1007 Hoppe, K. A., Stover, S. M., Pascoe, J. R., and Amundson, R.: Tooth enamel biomineralization in extant horses: implications for
1008   isotopic   microsampling,   Palaeogeography,   Palaeoclimatology,   Palaeoecology,   206,   355–365,
1009   https://doi.org/10.1016/j.palaeo.2004.01.012, 2004.
1010 Iacumin, P., Bocherens, H., Mariotti, A., and Longinelli, A.: Oxygen isotope analyses of co-existing carbonate and phosphate in
1011   biogenic apatite: a way to monitor diagenetic alteration of bone phosphate?, Earth and Planetary Science Letters, 142,
1012   1–6, https://doi.org/10.1016/0012-821X(96)00093-3, 1996.
1013 Iriarte-Chiapusso, M. J.: El entorno vegetal del yacimiento paleolítico de Labeko Koba (Arrasate, País Vasco): análisis polínico.,
1014   Labeko Koba (País Vasco). Hienas y humanos en los albores del Paleolítico superior., Munibe, 89–106, 2000.
1015 Jiménez-Sánchez, M., Rodríguez-Rodríguez, L., García-Ruiz, J. M., Domínguez-Cuesta, M. J., Farias, P., Valero-Garcés, B.,
1016   Moreno, A., Rico, M., and Valcárcel, M.: A review of glacial geomorphology and chronology in northern Spain: Timing
1017   and   regional   variability   during   the   last   glacial   cycle,   Geomorphology,   196,   50–64,
1018   https://doi.org/10.1016/j.geomorph.2012.06.009, 2013.
1019 Jones, J. R., Richards, M. P., Straus, L. G., Reade, H., Altuna, J., Mariezkurrena, K., and Marín-Arroyo, A. B.: Changing
1020   environments during the Middle-Upper Palaeolithic transition in the eastern Cantabrian Region (Spain): direct evidence
1021   from stable isotope studies on ungulate bones, Scientific Reports, 8, 14842, https://doi.org/10.1038/s41598-018-32493-
1022   0, 2018.
1023 Jones, J. R., Richards, M. P., Reade, H., Bernaldo de Quirós, F., and Marín-Arroyo, A. B.: Multi-Isotope investigations of ungulate
1024   bones and teeth from El Castillo and Covalejos caves (Cantabria, Spain): Implications for paleoenvironment
1025   reconstructions across the Middle-Upper Palaeolithic transition, Journal of Archaeological Science: Reports, 23, 1029–
1026   1042, https://doi.org/10.1016/j.jasrep.2018.04.014, 2019.
1027 Jones, J. R., Marín-Arroyo, A. B., Corchón Rodríguez, M. S., and Richards, M. P.: After the Last Glacial Maximum in the refugium
1028   of northern Iberia: Environmental shifts, demographic pressure and changing economic strategies at Las Caldas Cave
1029   (Asturias, Spain), Quaternary Science Reviews, 262, 106931, https://doi.org/10.1016/j.quascirev.2021.106931, 2021.
1030 Klein, K., Weniger, G.-C., Ludwig, P., Stepanek, C., Zhang, X., Wegener, C., and Shao, Y.: Assessing climatic impact on transition
1031   from Neanderthal to anatomically modern human population on Iberian Peninsula: a macroscopic perspective, Science
1032   Bulletin, 68, 1176–1186, https://doi.org/10.1016/j.scib.2023.04.025, 2023.
1033 Kohn, M. J.: Predicting animal δ18O: Accounting for diet and physiological adaptation, Geochimica et Cosmochimica Acta, 60,
1034   4811–4829, https://doi.org/10.1016/S0016-7037(96)00240-2, 1996.
1035 Kohn, M. J.: Comment: Tooth Enamel Mineralization in Ungulates: Implications for Recovering a Primary Isotopic Time-Series, by
1036   B. H. Passey and T. E. Cerling (2002), Geochimica et Cosmochimica Acta, 68, 403–405, https://doi.org/10.1016/S0016-
1037   7037(03)00443-5, 2004.
1038 Kohn, M. J.: Carbon isotope compositions of terrestrial C3 plants as indicators of (paleo)ecology and (paleo)climate, Proceedings
1039   of the National Academy of Sciences, 107, 19691–19695, https://doi.org/10.1073/pnas.1004933107, 2010.
1040 Lécuyer, C., Hillaire-Marcel, C., Burke, A., Julien, M.-A., and Hélie, J.-F.: Temperature and precipitation regime in LGM human
1041   refugia of southwestern Europe inferred from δ13C and δ18O of large mammal remains, Quaternary Science Reviews,
1042   255, 106796, https://doi.org/10.1016/j.quascirev.2021.106796, 2021.
1043 Leuenberger, M., Siegenthaler, U., and Langway, C.: Carbon isotope composition of atmospheric CO2 during the last ice age from
1044   an Antarctic ice core, Nature, 357, 488–490, https://doi.org/10.1038/357488a0, 1992.
1045 López-García, J. M., Blain, H.-A., Bennàsar, M., Sanz, M., and Daura, J.: Heinrich event 4 characterized by terrestrial proxies in
1046   southwestern Europe, Climate of the Past, 9, 1053–1064, https://doi.org/10.5194/cp-9-1053-2013, 2013.
1047 López-García, J. M., Blain, H.-A., Bennàsar, M., and Fernández-García, M.: Environmental and climatic context of Neanderthal
1048   occupation in southwestern Europe during MIS3 inferred from the small-vertebrate assemblages, Quaternary
1049   International, 326–327, 319–328, https://doi.org/10.1016/j.quaint.2013.09.010, 2014.
1050 López-García, J. M., Blain, H. A., Fagoaga, A., Bandera, C. S., Sanz, M., and Daura, J.: Environment and climate during the
1051   Neanderthal-AMH presence in the Garraf Massif mountain range (northeastern Iberia) from the late Middle Pleistocene
1052   to Late Pleistocene inferred from small-vertebrate assemblages, Quaternary Science Reviews, 288,
1053   https://doi.org/10.1016/j.quascirev.2022.107595, 2022.
1054 Luz, B., Kolodny, Y., and Horowitz, M.: Fractionation of oxygen isotopes between mammalian, Geochimica et Cosmochimica Acta,
1055   48, 1689–1693, 1984.
1056 Magozzi, S., Vander Zanden, H. B., Wunder, M. B., and Bowen, G. J.: Mechanistic model predicts tissue–environment relationships
1057   and   trophic   shifts   in   animal   hydrogen   and   oxygen   isotope   ratios,   Oecologia,   191,   777–789,
1058   https://doi.org/10.1007/s00442-019-04532-8, 2019.
1059 Marín-Arroyo, A. B. and Sanz-Royo, A.: What Neanderthals and AMH ate: reassessment of the subsistence across the Middle–

1060   Upper Palaeolithic transition in the Vasco-Cantabrian region of SW Europe, Journal of Quaternary Science, 37, 320–
1061   334, https://doi.org/10.1002/jqs.3291, 2022.
1062 Martrat, B., Grimalt, J. O., Lopez-Martinez, C., Cacho, I., Sierro, F. J., Flores, J. A., Zahn, R., Canals, M., Curtis, J. H., and Hodell,
1063   D. A.: Abrupt Temperature Changes in the Western Mediterranean over the Past 250,000 Years, Science, 306, 1762–
1064   1765, https://doi.org/10.1126/science.1101706, 2004.
1065 Merceron, G., Berlioz, E., Vonhof, H., Green, D., Garel, M., and Tütken, T.: Tooth tales told by dental diet proxies: An alpine
1066   community of sympatric ruminants as a model to decipher the ecology of fossil fauna, Palaeogeography,
1067   Palaeoclimatology, Palaeoecology, 562, 110077, https://doi.org/10.1016/j.palaeo.2020.110077, 2021.
1068 Van der Merwe, N. J.: Light Stable Isotopes and the Reconstruction of Prehistoric Diets, Proceedings of the British Academy, 77,
1069   247–264, 1991.
1070 Moreno, A., Stoll, H., Jiménez-Sánchez, M., Cacho, I., Valero-Garcés, B., Ito, E., and Edwards, R. L.: A speleothem record of glacial
1071   (25–11.6 kyr BP) rapid climatic changes from northern Iberian Peninsula, Global and Planetary Change, 71, 218–231,
1072   https://doi.org/10.1016/j.gloplacha.2009.10.002, 2010.
1073 Moreno, A., González-Sampériz, P., Morellón, M., Valero-Garcés, B. L., and Fletcher, W. J.: Northern Iberian abrupt climate change
1074   dynamics during the last glacial cycle: A view from lacustrine sediments, Quaternary Science Reviews, 36, 139–153,
1075   https://doi.org/10.1016/j.quascirev.2010.06.031, 2012.
1076 Moreno, A., Iglesias, M., Azorin-Molina, C., Pérez-Mejías, C., Bartolomé, M., Sancho, C., Stoll, H., Cacho, I., Frigola, J., Osácar,
1077   C., Muñoz, A., Delgado-Huertas, A., Bladé, I., and Vimeux, F.: Measurement report: Spatial variability of northern Iberian
1078   rainfall stable isotope values – investigating atmospheric controls on daily and monthly timescales, Atmospheric
1079   Chemistry and Physics, 21, 10159–10177, https://doi.org/10.5194/acp-21-10159-2021, 2021.
1080 Naughton, F., Sánchez-Goñi, M. F., Desprat, S., Turon, J.-L., and Duprat, J.: Present-day and past (last 25 000 years) marine pollen
1081   signal off western Iberia, Marine micropaleontology, 62, 91–114, https://doi.org/10.1016/j.marmicro.2006.07.006, 2007.
1082 North Greenland Ice Core Project members: High-resolution record of Northern Hemisphere climate extending into the last
1083   interglacial period, Nature, 431, 147–151, https://doi.org/10.1038/nature02805, 2004.
1084 Ochando, J., Amorós, G., Carrión, J. S., Fernández, S., Munuera, M., Camuera, J., Jiménez-Moreno, G., González-Sampériz, P.,
1085   Burjachs, F., Marín-Arroyo, A. B., Roksandic, M., and Finlayson, C.: Iberian Neanderthals in forests and savannahs,
1086   Journal of Quaternary Science, 1–28, https://doi.org/10.1002/jqs.3339, 2021.
1087 Passey, B. H. and Cerling, T. E.: Tooth enamel mineralization in ungulates: implications for recovering a primary isotopic time-
1088   series, Geochimica et Cosmochimica Acta, 66, 3225–3234, https://doi.org/10.1016/S0016-7037(02)00933-X, 2002.
1089 Passey, B. H., Robinson, T. F., Ayliffe, L. K., Cerling, T. E., Sponheimer, M., Dearing, M. D., Roeder, B. L., and Ehleringer, J. R.:
1090   Carbon isotope fractionation between diet, breath CO_2, and bioapatite in different mammals, Journal of Archaeological
1091   Science, 32, 1459–1470, https://doi.org/10.1016/j.jas.2005.03.015, 2005a.
1092 Passey, B. H., Cerling, T. E., Schuster, G. T., Robinson, T. F., Roeder, B. L., and Krueger, S. K.: Inverse methods for estimating
1093   primary input signals from time-averaged isotope profiles, Geochimica et Cosmochimica Acta, 69, 4101–4116,
1094   https://doi.org/10.1016/j.gca.2004.12.002, 2005b.
1095 Pederzani, S. and Britton, K.: Oxygen isotopes in bioarchaeology: Principles and applications, challenges and opportunities, Earth-
1096   Science Reviews, 188, 77–107, https://doi.org/10.1016/j.earscirev.2018.11.005, 2019.
1097 Pederzani, S., Aldeias, V., Dibble, H. L., Goldberg, P., Hublin, J. J., Madelaine, S., McPherron, S. P., Sandgathe, D., Steele, T. E.,
1098   Turq, A., and Britton, K.: Reconstructing Late Pleistocene paleoclimate at the scale of human behaviour: an example
1099   from the Neandertal occupation of La Ferrassie (France), Scientific Reports, 11, 1–10, https://doi.org/10.1038/s41598-
1100   020-80777-1, 2021a.
1101 Pederzani, S., Britton, K., Aldeias, V., Bourgon, N., Fewlass, H., Lauer, T., McPherron, S. P., Rezek, Z., Sirakov, N., Smith, G. M.,
1102   Spasov, R., Tran, N. H., Tsanova, T., and Hublin, J. J.: Subarctic climate for the earliest Homo sapiens in Europe, Science
1103   Advances, 7, 1–11, https://doi.org/10.1126/sciadv.abi4642, 2021b.
1104 Pederzani, S., Britton, K., Jones, J. R., Agudo Pérez, L., Geiling, J. M., and Marín-Arroyo, A. B.: Late Pleistocene Neanderthal
1105   exploitation of stable and mosaic ecosystems in northern Iberia shown by multi-isotope evidence, Quaternary Research,
1106   1–25, https://doi.org/10.1017/qua.2023.32, 2023.
1107 Pellegrini, M. and Snoeck, C.: Comparing bioapatite carbonate pre-treatments for isotopic measurements: Part 2 — Impact on
1108   carbon   and   oxygen   isotope   compositions,   Chemical   Geology,   420,   88–96,
1109   https://doi.org/10.1016/j.chemgeo.2015.10.038, 2016.
1110 Pellegrini, M., Lee-Thorp, J. A., and Donahue, R. E.: Exploring the variation of the $\delta^{18}O_p$ and $\delta^{18}O_c$ relationship in enamel
1111   increments,   Palaeogeography,   Palaeoclimatology,   Palaeoecology,   310,   71–83,
1112   https://doi.org/10.1016/j.palaeo.2011.02.023, 2011.
1113 Pérez-Mejías, C., Moreno, A., Sancho, C., Martín-García, R., Spötl, C., Cacho, I., Cheng, H., and Edwards, R. L.: Orbital-to-
1114   millennial scale climate variability during Marine Isotope Stages 5 to 3 in northeast Iberia, Quaternary Science Reviews,
1115   224, https://doi.org/10.1016/j.quascirev.2019.105946, 2019.
1116 Posth, C., Yu, H., Ghalichi, A., Rougier, H., Crevecoeur, I., Huang, Y., Ringbauer, H., Rohrlach, A. B., Nägele, K., Villalba-Mouco,
1117   V., Radzeviciute, R., Ferraz, T., Stoessel, A., Tukhbatova, R., Drucker, D. G., Lari, M., Modi, A., Vai, S., Saupe, T.,
1118   Scheib, C. L., Catalano, G., Pagani, L., Talamo, S., Fewlass, H., Klaric, L., Morala, A., Rué, M., Madelaine, S., Crépin,
1119   L., Caverne, J.-B., Bocaege, E., Ricci, S., Boschin, F., Bayle, P., Maureille, B., Le Brun-Ricalens, F., Bordes, J.-G., Oxilia,
1120   G., Bortolini, E., Bignon-Lau, O., Debout, G., Orliac, M., Zazzo, A., Sparacello, V., Starnini, E., Sineo, L., van der Plicht,
1121   J., Pecqueur, L., Merceron, G., Garcia, G., Leuvrey, J.-M., Garcia, C. B., Gómez-Olivencia, A., Połtowicz-Bobak, M.,
1122   Bobak, D., Le Luyer, M., Storm, P., Hoffmann, C., Kabaciński, J., Filimonova, T., Shnaider, S., Berezina, N., González-
1123   Rabanal, B., González Morales, M. R., Marín-Arroyo, A. B., López, B., Alonso-Llamazares, C., Ronchitelli, A., Polet, C.,
1124   Jadin, I., Cauwe, N., Soler, J., Coromina, N., Rufí, I., Cottiaux, R., Clark, G., Straus, L. G., Julien, M.-A., Renhart, S.,
1125   Talaa, D., Benazzi, S., Romandini, M., Amkreutz, L., Bocherens, H., Wißing, C., Villotte, S., de Pablo, J. F.-L., Gómez-
1126   Puche, M., Esquembre-Bebia, M. A., Bodu, P., Smits, L., Souffi, B., Jankauskas, R., Kozakaitė, J., Cupillard, C., Benthien,

H., Wehrberger, K., Schmitz, R. W., Feine, S. C., et al.: Palaeogenomics of Upper Palaeolithic to Neolithic European hunter-gatherers, Nature, 615, 117–126, https://doi.org/10.1038/s41586-023-05726-0, 2023.

Pryor, A. J. E., Stevens, R. E., Connell, T. C. O., and Lister, J. R.: Quantification and propagation of errors when converting vertebrate biomineral oxygen isotope data to temperature for palaeoclimate reconstruction, Palaeogeography, Palaeoclimatology, Palaeoecology, 412, 99–107, https://doi.org/10.1016/j.palaeo.2014.07.003, 2014.

Ramsey, C. B.: Bayesian Analysis of Radiocarbon Dates, Radiocarbon, 51, 337–360, https://doi.org/10.1017/S0033822200033865, 2009.

Rasmussen, S. O., Bigler, M., Blockley, S. P., Blunier, T., Buchardt, S. L., Clausen, H. B., Cvijanovic, I., Dahl-Jensen, D., Johnsen, S. J., Fischer, H., Gkinis, V., Guillevic, M., Hoek, W. Z., Lowe, J. J., Pedro, J. B., Popp, T., Seierstad, I. K., Steffensen, J. P., Svensson, A. M., Vallelonga, P., Vinther, B. M., Walker, M. J. C., Wheatley, J. J., and Winstrup, M.: A stratigraphic framework for abrupt climatic changes during the Last Glacial period based on three synchronized Greenland ice-core records: Refining and extending the INTIMATE event stratigraphy, Quaternary Science Reviews, 106, 14–28, https://doi.org/10.1016/j.quascirev.2014.09.007, 2014.

Reimer, P. J., Austin, W. E. N., Bard, E., Bayliss, A., Blackwell, P. G., Bronk Ramsey, C., Butzin, M., Cheng, H., Edwards, R. L., Friedrich, M., Grootes, P. M., Guilderson, T. P., Hajdas, I., Heaton, T. J., Hogg, A. G., Hughen, K. A., Kromer, B., Manning, S. W., Muscheler, R., Palmer, J. G., Pearson, C., van der Plicht, J., Reimer, R. W., Richards, D. A., Scott, E. M., Southon, J. R., Turney, C. S. M., Wacker, L., Adolphi, F., Büntgen, U., Capano, M., Fahrni, S. M., Fogtmann-Schulz, A., Friedrich, R., Köhler, P., Kudsk, S., Miyake, F., Olsen, J., Reinig, F., Sakamoto, M., Sookdeo, A., and Talamo, S.: The IntCal20 Northern Hemisphere Radiocarbon Age Calibration Curve (0–55 cal kBP), Radiocarbon, 62, 725–757, https://doi.org/10.1017/RDC.2020.41, 2020.

Rey, K., Amiot, R., Lécuyer, C., Koufos, G. D., Martineau, F., Fourel, F., Kostopoulos, D. S., and Merceron, G.: Late Miocene climatic and environmental variations in northern Greece inferred from stable isotope compositions (δ18O, δ13C) of equid teeth apatite, Palaeogeography, Palaeoclimatology, Palaeoecology, 388, 48–57, https://doi.org/10.1016/j.palaeo.2013.07.021, 2013.

Rivals, F., Uzunidis, A., Sanz, M., and Daura, J.: Faunal dietary response to the Heinrich Event 4 in southwestern Europe, Palaeogeography, Palaeoclimatology, Palaeoecology, 473, 123–130, https://doi.org/10.1016/j.palaeo.2017.02.033, 2017.

Rivals, F., Bocherens, H., Camarós, E., and Rosell, J.: Diet and ecological interactions in the Middle and Late Pleistocene, in: Updating Neanderthals. Understanding Behavioural Complexity in the Late Middle Palaeolithic, 39–54, 2022.

Roucoux, K. H., Shackleton, N. J., Abreu, L. De, Schönfeld, J., and Tzedakis, P. C.: Combined marine proxy and pollen analyses reveal rapid Iberian vegetation response to North Atlantic millennial-scale climate oscillations, Quaternary Research, 56, 128–132, https://doi.org/10.1006/qres.2001.2218, 2001.

Rozanski, K., Araguás-Araguás, L., and Gonfiantini, R.: Relation Between Long-Term Trends of Oxygen-18 Isotope Composition of Precipitation and Climate, Science, 258, 981–985, 1992.

Rufí, I., Solés, A., Soler, J., and Soler, N.: A mammoth (Mammuthus primigenius Blumenbach 1799, Proboscidea) calf tooth from the Mousterian of Arbreda Cave (Serinyà, NE Iberian Peninsula), Estudios Geológicos, 74, e079, https://doi.org/10.3989/egeol.43130.478, 2018.

Ruiz-Fernández, J., García-Hernández, C., and Gallinar Cañedo, D.: The glaciers of the Picos de Europa, in: Iberia, Land of Glaciers, Elsevier, 237–263, https://doi.org/10.1016/B978-0-12-821941-6.00012-8, 2022.

Sánchez-Goñi, M. F., Eynaud, F., Turon, J.-L., and Shackleton, N. J.: High resolution palynological record off the Iberian margin: direct land-sea correlation for the Last Interglacial complex, Earth and Planetary Science Letters, 171, 123–137, 1999.

Sánchez-Goñi, M. F., Landais, A., Cacho, I., Duprat, J., and Rossignol, L.: Contrasting intrainterstadial climatic evolution between high and middle North Atlantic latitudes: A close-up of Greenland Interstadials 8 and 12, Geochemistry, Geophysics, Geosystems, 10, 1–16, https://doi.org/10.1029/2008GC002369, 2009.

Sánchez Goñi, M., Cacho, I., Turon, J., Guiot, J., Sierro, F., Peypouquet, J., Grimalt, J., and Shackleton, N.: Synchroneity between marine and terrestrial responses to millennial scale climatic variability during the last glacial period in the Mediterranean region, Climate Dynamics, 19, 95–105, https://doi.org/10.1007/s00382-001-0212-x, 2002.

Sánchez Goñi, M. F.: Regional impacts of climate change and its relevance to human evolution, Evolutionary Human Sciences, 2, e55, https://doi.org/10.1017/ehs.2020.56, 2020.

Schmitt, J., Schneider, R., Elsig, J., Leuenberger, D., Lourantou, A., Chappellaz, J., Köhler, P., Joos, F., Stocker, T. F., Leuenberger, M., and Fischer, H.: Carbon Isotope Constraints on the Deglacial CO 2 Rise from Ice Cores, Science, 336, 711–714, https://doi.org/10.1126/science.1217161, 2012.

Schrag, D. P., Adkins, J. F., Mcintyre, K., Alexander, J. L., Hodell, A., Charles, C. D., and Mcmanus, J. F.: The oxygen isotopic composition of seawater during the Last Glacial Maximum, Quaternary Science Reviews, 21, 331–342, 2002.

Sepulchre, P., Ramstein, G., Kageyama, M., Vanhaeren, M., Krinner, G., Sánchez-Goñi, M. F., and d'Errico, F.: H4 abrupt event and late Neanderthal presence in Iberia, Earth and Planetary Science Letters, 258, 283–292, https://doi.org/10.1016/j.epsl.2007.03.041, 2007.

Shackleton, N. J.: Oxygen isotopes, ice volume and sea level, Quaternary Science Reviews, 6, 183–190, https://doi.org/10.1016/0277-3791(87)90003-5, 1987.

Skrzypek, G., Wiśniewski, A., and Grierson, P. F.: How cold was it for Neanderthals moving to Central Europe during warm phases of the last glaciation?, Quaternary Science Reviews, 30, 481–487, https://doi.org/10.1016/j.quascirev.2010.12.018, 2011.

Skrzypek, G., Sadler, R., and Wi, A.: Reassessment of recommendations for processing mammal phosphate δ18O data for paleotemperature reconstruction, Palaeogeography, Palaeoclimatology, Palaeoecology, 446, 162–167, https://doi.org/10.1016/j.palaeo.2016.01.032, 2016.

Snoeck, C. and Pellegrini, M.: Comparing bioapatite carbonate pre-treatments for isotopic measurements: Part 1—Impact on structure and chemical composition, Chemical Geology, 417, 394–403, https://doi.org/10.1016/j.chemgeo.2015.10.004, 2015.

1194 Staubwasser, M., Drăgușin, V., Onac, B. P., Assonov, S., Ersek, V., Hoffmann, D. L., and Veres, D.: Impact of climate change on
1195   the transition of Neanderthals to modern humans in Europe, Proceedings of the National Academy of Sciences, 115,
1196   9116–9121, https://doi.org/10.1073/pnas.1808647115, 2018.
1197 Tejada-Lara, J. V., MacFadden, B. J., Bermudez, L., Rojas, G., Salas-Gismondi, R., and Flynn, J. J.: Body mass predicts isotope
1198   enrichment in herbivorous mammals, Proceedings of the Royal Society B: Biological Sciences, 285, 20181020,
1199   https://doi.org/10.1098/rspb.2018.1020, 2018.
1200 Timmermann, A.: Quantifying the potential causes of Neanderthal extinction: Abrupt climate change versus competition and
1201   interbreeding, Quaternary Science Reviews, 238, 106331, https://doi.org/10.1016/j.quascirev.2020.106331, 2020.
1202 Trayler, R. B. and Kohn, M. J.: Tooth enamel maturation reequilibrates oxygen isotope compositions and supports simple sampling
1203   methods, Geochimica et Cosmochimica Acta, 198, 32–47, https://doi.org/10.1016/j.gca.2016.10.023, 2017.
1204 Tütken, T., Furrer, H., and Vennemann, T. W.: Stable isotope compositions of mammoth teeth from Niederweningen, Switzerland:
1205   Implications for the Late Pleistocene climate, environment, and diet, Quaternary International, 164–165, 139–150,
1206   https://doi.org/10.1016/j.quaint.2006.09.004, 2007.
1207 Vidal-Cordasco, M., Ocio, D., Hickler, T., and Marín-Arroyo, A. B.: Ecosystem productivity affected the spatiotemporal
1208   disappearance of Neanderthals in Iberia, Nature Ecology & Evolution, 6, 1644–1657, https://doi.org/10.1038/s41559-
1209   022-01861-5, 2022.
1210 Vidal-Cordasco, Terlaro, G., M., Ocio, D., T., Marín-Arroyo, A.B., 2023. Neanderthal coexistence with Homo sapiens in Europe was
1211   affected by herbivore carrying capacity. Science Advances 9 (38), https://www.science.org/doi/10.1126/sciadv.adi4099
1212 Zazzo, A., Bendrey, R., Vella, D., Moloney, A. P., Monahan, F. J., and Schmidt, O.: A refined sampling strategy for intra-tooth stable
1213   isotope analysis of mammalian enamel, Geochimica et Cosmochimica Acta, 84, 1–13,
1214   https://doi.org/10.1016/j.gca.2012.01.012, 2012.
1215
1216 '"'"30iomin30iomineralization

Appendix A. Sites description

A1. Vasco-Cantabrian sites

Axlor (Dima, Vizcaya, País Vasco)

Axlor is a rock-shelter located in Dima (43.2706; -1.8905), with a continuous Middle Paleolithic sequence from the MIS5 to the MIS3 (DeMuro et al., 2023; Pederzani et al., 2023; Marín-Arroyo et al., 2018). It is placed on the southwestern slope of the Dima Valley, with an elevation of approximately 320 m above sea level (a.s.l.), at 33 km straight from the present-day coastline, next to one of the lowest mountain passes linking the Cantabrian basins and the Alavese Plateau. The site was discovered in 1932 and initial excavations were performed by Barandiarán (1967-1974). J. M. Barandiarán undertook the excavations between 1967 and 1974, identifying eight Mousterian levels (I-VIII) (Barandiarán, 1980).

From 2000 to 2008, new excavations by González-Urquijo, Ibáñez-Estévez and Rios-Garaizar were achieved and, since 2019, these are ongoing by González-Urquijo and Lazuén. Due to the lack of chronology during Barandiarán excavations, among other aspects, work was focused on obtaining a detailed stratigraphy on the new excavation areas to correlate it with Barandiarán's levels (González-Urquijo & Ibáñez-Estévez, 2021; González Urquijo et al., 2005). The new stratigraphic sequence is roughly equivalent to the previous one, but with additional levels not previously identified or excavated by Barandiarán. Some of these levels were deposited before Level VIII (Gómez-Olivencia et al., 2018; 2020). The Middle Paleolithic sequence extends from layers VIII to III (or from N to B-C). Levallois production is predominant in the lower levels (VI to VIII), while Quina Mousterian technocomplex does in the upper ones (from III to V) (Rios-Garaizar, 2012, 2017). Recent chronological data by radiocarbon (Pederzani et al., 2023; Marín-Arroyo et al., 2018) and OSL (Demuro et al., 2023) methods confirm that a sequence Axlor levels VI, VIII, and VIII probably accumulated during MIS5d–a (109–82 ka), while levels D to B probably were formed during the period encompassing the start of MIS 4 (71–57 ka) through to the beginning or middle of MIS 3 (57–29 ka) and upper Level III to 46,200 ±3,000 BP, which calibrates between 45,350 cal BP and beyond the calibration curve at > 55,000 cal BP.

The archaeozoological study indicates an anthropic origin of the faunal assemblage with scarce carnivore activity documented (Altuna, 1989; Castaños, 2005; Gómez-Olivencia et al., 2018). In lower layers, the most abundant taxa are *Cervus elaphus* (VIII) and *Capra pyrenaica* (VII), while in upper layers III-V, *Cervus elaphus* is substituted by *Bos primigenious/Bison priscus* and *Equus sp*. The material included in this work comes from the faunal collection of the Barandiarán excavation currently curated at the Bizkaia Museum of Archaeology (Bilbao), where teeth were sampled, and the stable isotope analyses on enamel phosphate were included in Pederzani et al. (2023).

El Castillo (Puente Viesgo, Cantabria)

El Castillo cave is located in Puente Viesgo (43.2924; -3.9656), with an elevation of approximately 195m a.s.l., at 17 km straight from the present-day coastline. The cave belongs to the karstic system that was formed in the Monte Castillo, which dominates the Pas Valley. The site was discovered in 1903 by H. Alcalde del Río. H. Obermaier carried out the first excavation seasons between 1910 and 1914 when many of the archaeological remains were recovered, mainly from the cave hall. These interventions were done under the supervision of the "Institut de Paléontologie Humaine" (IPH) and Prince Albert I of Monaco. From 1980 to 2011, V. Cabrera and F. Bernaldo de Quirós underwent new excavations focusing on the cave entrance, on the Middle to Upper Paleolithic transitional levels, mainly 16, 18 and 20 (Cabrera-Valdes, 1984). The site has yielded an important stratigraphic sequence, composed by 26 sedimentological units (1-26) related to

different anthropic occupational units, often separated by archaeologically sterile units: Eneolithic (2), Azilian (4), Magdalenian (6 and 8), Solutrean (10), Aurignacian (12, 14, 16 and 18), Mousterian (20, 21 and 22) and Acheulean (24) (Cabrera-Valdés, 1984).

Unit 21 is mostly sterile (Cabrera Valdés, 1984; Martín-Perea et al., 2023), and ESR dated it, yielding a mean date of 69,000 ± 9,200 years BP (Rink et al., 1997). However, Martín-Perea et al. (2023) suggested some dating uncertainty from interpreting the initial stratigraphic nomenclature. They suggest that the ESR dates provided for level 21 by Rink et al. (1997) were erroneously attributed to this unit and it might correspond to 20E, indicating that below that subunit, the chronology is older than 70,000 years BP (Martín-Perea et al., 2023). The Mousterian Unit 20 cave is divided into several subunits (Martín-Perea et al., 2023). In Unit 20, a cave roof collapse took place, transforming the cave system into an open rock shelter. This unit contains abundant archaeological and paleontological remains. Lithic industry consists of sidescrapers, denticulates, notches and cleavers, the majority on quartzite and presents both unifacial, bifacial discoid debitage and Levallois debitage. Unit 20E was attributed to Quina Mousterian by Sánchez-Fernández and Bernaldo De Quiros (2009) and contains a Neanderthal tooth (Garralda, 2005). Considering the geochronological uncertainties for dates on 20E related to Rink et al. (1997), we have decided to rely solely on ESR date of 47,000 ± 9400 BP provided by Liberda et al. (2010) for this level. Unit 20C presents clear evidence of the Mousterian lithic industry and radiocarbon dates of 48,700±3,400 uncal BP (OxA-22204) and 49,400±3,700 uncal BP (OxA-22205) (Wood et al., 2018) and mean ESR date of 42,700 ±9900 BP (Liberda et al., 2010). Level 19 is archaeologically sterile and separates Unit 20 from Unit 18 (Wood et al., 2018).

Unit 18 is divided into 18A (archaeologically sterile), 18B, and 18C. Levels 18B and 18C were classified as Transitional Aurignacian, representing a gradual transformation from the Mousterian to the Aurignacian, which is unique to El Castillo cave (Cabrera et al., 2001; Maíllo and Bernaldo de Quirós, 2010; Wood et al., 2018). These levels' dates and cultural attribution have been the subject of much debate (e.g. Zilhao and D'Errico, 2003; Wood et al., 2018). According to Wood et al. (2018), the last dates of these levels range between 42,000±1,500 uncal BP (OxA-22203) and 46,000±2,400 uncal BP (OxA-21973), which is much earlier than the start of the Aurignacian period in the Cantabrian region (Marín-Arroyo et al., 2018; Vidal-Cordasco et al., 2022). The lithic assemblage of Unit 18 appears to be dominated by Discoid/Levallois technology (Bernaldo de Quirós and Maíllo-Fernández, 2009) but with a high percentage of "Upper Paleolithic" pieces. Additionally, punctual bone industry and pieces with incisions and engravings were discovered in Unit 18 (Cabrera-Valdés et al., 2001). Three deciduous tooth crowns attributed to Neanderthals were found in Unit 18B (Garralda et al., 2022). Above, Unit 17 is sterile but contains scarce lithic and faunal materials, while Level 16 was attributed to the Proto-Aurignacian, with dates of 38,600±1,000 uncal BP (OxA-22200) (Wood et al., 2018).

According to Luret et al. (2020), there was a shift in hunting practices between the Late Mousterian (unit 20) and the Transitional Aurignacian (unit 18). During the Late Mousterian, hunting strategies were less specialized, and the species hunted included red deer, horses, and bovines. However, in Unit 18, a specialization in red deer hunting is observed. However, the explanation of this shift has been proposed as a response to a cultural choice or induced by climatic changes. However, recent taphonomic studies by Sanz-Royo et al. (2023) on the old collections of Aurignacian Delta level reveal a more significant role of carnivores than shown by Luret et al. (2020). The material included in this work comes from the faunal collection recovered during the Cabrera-Valdés and Bernaldo de Quirós excavations curated at Museo de Prehistoria y Arqueología de Cantabria (MUPAC, Santander).

Labeko Koba (Arrastre, Guipúzcoa, País Vasco)

Labeko Koba is a cave in the Kurtzetxiki Hill (43.0619; -2.4833), at 246 m a.s.l. and 29 km straight from the present-day Atlantic coast. In 1987 and 1988, the site was discovered due to the construction of the Arrasate ring road, and a savage excavation was carried out (Arrizabalaga, 2000a). Unfortunately, the site was destroyed after that. The stratigraphic sequence identified nine different levels. The lower Level IX was attributed to the Châtelperronian, based on the presence of three Châtelperron points. Although there is a lack of human remains in few Cantabrian Châtelperronian sites, recent research has suggested that this techno-complex was produced by Neanderthals (Maroto et al., 2012; Rios-Garaizar et al., 2022). Level VII marks the beginning of the Aurignacian sequence, likely Proto-Aurignacian, with a lithic assemblage dominated by Dufour bladelets (Arrizabalaga, 2000a). Levels VI, V, and IV contain lithic assemblages that suggested an Early Aurignacian attribution (Arrizabalaga, 2000b; Arrizabalaga et al., 2009). This site is significant because it is one of the few sites with Châtelperronian assemblages and with both Proto-Aurignacian and Early Aurignacian separated (Arrizabalaga et al., 2009).

Initial radiocarbon dates were inconsistent with the stratigraphy of the site and much more recent than expected for the Early Upper Paleolithic (Arrizabalaga, 2000a). This incoherence was determined to be affected by taphonomic alterations (Wood et al., 2014). Later radiocarbon dates undertaken with an ultrafiltration pre-treatment provided a new regional framework for the regional Early Upper Paleolithic (Wood et al., 2014). The Châtelperronian layer IX inf is dated to 38,100±900 uncal BP (OxA-22562) and 37,400±800 uncal BP (OxA-22560). The Proto-Aurignacian levels cover a period from 36,850±800 uncal BP (OxA-21766) to 35,250±650 uncal BP (OxA-21793). The three Early Aurignacian levels are dated to 35,100±600 uncal BP (OxA-21778) for level VI, ~ 34,000 uncal BP (OxA-21767 and OxA-21779) for level V, and ~ 33,000 BP (OxA-21768 and OxA-21780) for level IV (Arrizabalaga et al., 2009).

Taphonomic studies indicate an alternation in the use of the cave between carnivores and humans, the latter during short occupation periods (Villaluenda et al., 2012; Ríos-Garaizar et al., 2012; Arrizabalaga et al., 2010). Labeko Koba is considered to have functioned as a natural trap where carnivores, mainly hyenas, access animal carcasses. At least in the base of Labeko Koba IX, carnivore activity was higher, and they would have consumed the same prey as humans (Villaluenga et al., 2012). The presence of humans is linked to strategic use as a campsite associated with a small assemblage of lithic artifacts. The most consumed species by Châtelperronian groups were red deer, followed by the consumption of large bovids, equids, and woolly rhinoceros. During the Aurignacian period, there was some stability in human occupations, although they still alternated with carnivore occupations (Arrizabalaga et al., 2010). Cold-adapted fauna such as reindeer and woolly rhinoceros were identified in association with the Châtelperronian. Reindeer and the woolly mammoth and arctic fox were still present during the Aurignacian levels. The original sampling of the teeth studied by this work was performed in the San Sebastian Heritage Collection headquarters, where the Guipuzcoa archaeological materials were deposited at that time.

Aitzbitarte III interior (Rentería, Guipúzcoa, País Vasco)

Aitzbitarte III is an archaeological site located within the Landarbaso karstic system comprising nine caves (43.270; -1.8905). The cave is situated 220 m.a.s.l. and is 10 km away from the present-day coastline. Initial archaeological interventions were carried out at the end of the 19th century by P.M. de Soraluce (Altuna, 2011). Recent excavations were initially conducted in the deep zone inside the cave between 1986 and 1993, where the studied tooth was recovered, and later focused on the cave entrance between 1994 and 2002, by J. Altuna, K. Mariezkurrena, and J. Ríos-Garaizar (Altuna et al., 2011; 2017).

While the cave's entrance area contains a sequence comprising possible Mousterian and Evolved Aurignacian and Gravettian levels (Altuna et al., 2011; 2013), the stratigraphy in the inner cave presents eight levels: level VIII (some tools with Mousterian features), VII (sterile), VIb, VIa and V (Middle Gravettian

1351 technocomplex with abundance of Noailles burins), IV-II (disturbed archaeological levels) and I (surface)
1352 (Altuna et al., 2017). Levels V have dates of 24,910 uncal BP (I-15208) and 23,230 uncal BP (Ua-2243);
1353 whereas level VI extends from 23,830 ± 345 uncal BP (Ua-2628) and 25,380± 430 uncal BP (Ua-2244)
1354 (Altuna, 1992; Altuna et al., 2017), with a possible outlier dated at 21,130 uncal BP (Ua-1917).

1355 The Gravettian occupation in the inner part of the cave was initially thought to be more recent than the one
1356 in the cave entrance. However, it was not easy to correlate the two excavation areas due to different
1357 sedimentation rates. The abundant human occupations took place during a singular cold phase in the Middle
1358 Gravettian with a specialized paleoeconomy focused on the hunting of *Bos primigenius* and *Bison priscus*
1359 (85% in level VI and 68% in level V), which is unusual in the Cantabrian region mostly focused on red deer
1360 and ibex. Other ungulates present are *Cervus elaphus* and *Rupicapra rupicapra*, and to a lesser extent
1361 *Capra pyrenaica, Capreolus capreolus, Rangifer tarandus*, and *Equus ferus* (Altuna et al., 2017; Altuna &
1362 Mariezkurrena, 2020). There is a scarce representation of carnivores. The tooth studied was sampled at the
1363 Gordailua Center for Heritage Collections of the Provincial Council of Gipuzkoa.

1364

1365 **El Otero (Secadura, Voto, Cantabria)**

1366 El Otero cave is located in Secadura (Voto) (43.3565; -3.5360), at 129 m.s.a.l and 12 km from the present-
1367 day coastline, near the Matienzo valley in a coastal plain environment covered by meadows and gentle hills.
1368 The discovery was made in 1908 by Lorenzo Sierra. The site was excavated in 1963 by J. Gonzalez
1369 Echegaray and M.A. García Guinea, in two different sectors (Sala I and Sala II) with an equivalent
1370 stratigraphic sequence (González Echegaray, 1966). Nine levels were identified in Sala I, from level IX to
1371 level I. Levels IX and VIII were initially related to the "Aurignacian-Mousterian, based on lithics assemblages
1372 with a combination of both technocomplex features. The overlying levels VI-IV were separated by a
1373 speleothem crust (level VII) and were initially related to Aurignacian, due to the presence of end-scrappers,
1374 bone points, blades, or burins on truncation (Freeman, 1964; Rios-Garaizar, 2013). Also, perforated deer,
1375 ibex, and fox teeth were found in levels V and IV. This site lacked chronological dating methods, until a
1376 selection of material from levels VI, V and IV revealed a difference in chrono-cultural attribution (Marín-
1377 Arroyo et al., 2018). Radiocarbon results yielded younger dates for such a cultural attribution and showed
1378 significant stratigraphic inconsistency. Level VI gave a result of 12,415±55 uncal BP (OxA-32585), two dates
1379 in Level V are 12,340±55 (OxA-32509) and 10,585±50 uncal BP (OxA-32510), and a date in Level IV is
1380 15,990±80 uncal BP (OxA-32508). All these results fall into the range of the Late Upper Paleolithic
1381 (Magdalenian-Azilian initially identified in levels III-I), eliminating attribution of these levels to the Aurignacian
1382 despite the presence of apparently characteristic artefacts. Further assessments of archaeological materials
1383 will be needed.

1384 Red deer dominate the assemblage, except for level IV where horses are more abundant. Wild boar, roe
1385 deer, and ibex are also present, but large bovids are relatively rare (González Echegaray, 1966). Level IV
1386 is the richest and most anthropogenic level, with evidence of butchering in red deer (captured in winter and
1387 early summer) and chamois (in autumn). The formation of this level involved humans and carnivores, and
1388 although certain data may suggest an anthropogenic predominance, the limited sample analyzed
1389 taphonomically and the pre-selection of preserved pieces do not allow for a definitive conclusion (Yravedra
1390 & Gómez-Castanedo, 2010). The material included in this work is curated at the Museo de Prehistoria y
1391 Arqueología de Cantabria (MUPAC, Santander).

1392

1393 **A2. Northeastern Iberia sites**

1394 **Terrasses de la Riera dels Canyars (Gavà, Barcelona, Cataluña)**

Terrasses de la Riera dels Canyars (henceforth, Canyars) is an open-air site located near Gavà (Barcelona) (41.2961;1.9797), at 28 m.s.a.l and 3 km straight from the present-day coastline. The site lies on a fluvial terrace at the confluence of Riera dels Canyars, a torrential stream between Garraf Massif, Llobregat delta and Riera de Can Llong (Daura et al., 2013). Archaeo-paleontological remains were discovered during quarries activities in 2005 and was complete excavated on 2007 by the *Grup de Recerca del Quaternari* (Daura and Sanz, 2006; Daura et al., 2013). This intervention determined nine lithological units. The paleontological and archaeological remains come exclusively from one unit, the middle luthitic unit (MLU), and specifically from layer I. The MLU is composed of coarse sandy clays and gravels, filling a paleochannel network named lower detrital unit (LDU) (Daura et al., 2013). Five radiocarbon dates were obtained on charcoals from layer I, which yield statistically consistent ages from 33,800 ±350 uncal BP to 34,900 ±340 uncal BP, which results in mean age of 39,710 cal BP (from 40,890 to 38,530 cal BP) (Daura et al., 2013; this work).

The layer I of the site has yielded a rich faunal assemblage, consisting of over 5,000 remains. Among the herbivores, the most common species found are *Equus ferus*, *Bos primigenius, Equus hydruntinus*, and *Cervus elaphus* (Daura et al., 2013; Sanz-Royo et al., 2020). *Capra* sp. and *Sus scrofa are* also present, although in lower frequencies. The carnivores found at the site are also noteworthy, with *Crocuta crocuta* and *Lynx pardinus* being the most frequent. Presence of cold-adapted fauna associated to stepped environments is recorded, such as cf. *Mammuthus* sp., *Coelodonta antiquitatis*, and *Equus hydruntinus*. Small mammal analysis, pollen, and use-wear analysis have provided further evidence that a steppe-dominated landscape surrounded the Canyars site, supporting a correlation with the Heinrich Stadial~~Event~~ 4, in coherence with the chronology obtained for the layer (López-García et al. 2013; 2023; Rivals et al., 2017). However, the presence of woodland is also attested by forest taxa within charcoal and pollen assemblages (Daura et al., 2013).

Taphonomic study is ongoing. But several evidences point that hyenas have played an important role in the accumulation of the faunal assemblage (Daura et al., 2013; Jimenez et al. 2019). However, sporadic human presence is documented by few human modifications found in faunal remains (cutmarks and fire alterations). Although the paucity of the lithic assemblage in the site, it shows a clear attribution to Upper Palaeolithic technocomplex, most likely the Early Aurignacian (Daura et al., 2013). Recently, it was documented a perforated bone fragment, which has been identified as a perforated board for leather production (Doyon et al., 2023). All teeth included in this work were sampled in *Laboratori de la Guixera* (Ajuntament de Casteldefels) where the material is stored.

References Appendix A

Altuna, J., Mariezkurrena, K., de la Peña, P., Rios-Garaizar, J. 2011. Ocupaciones Humanas En La Cueva de Aitzbitarte III (Renteria, País Vasco) Sector Entrada: 33.000-18.000 BP. Servicio Central de Publicaciones del Gobierno Vasco; EKOB: 11–21.

Altuna, J., Mariezkurrena, K., de la Peña, P., Rios-Garaizar, J. 2013. Los niveles gravetienses de la cueva de Aitzbitarte III (Gipuzkoa). Industrias y faunas asociadas, in: de las Heras, C., Lasheras, J.A., Arrizabalaga, Á., de la Rasilla, M. editors. Pensando El Gravetiense: Nuevos Datos Para La Región Cantábrica En Su Contexto Peninsular Y Pirenaico. Monografías Del Museo Nacional Y Centro de Investigación de Altamira, 23. Madrid: Ministerio de Educación, Cultura; pp. 184–204.

Altuna, J. & Mariezkurrena, K. 2020. Estrategias de caza en el Paleolítico superior de la Región Cantábrica. El caso de Aitzbitarte II (zona profunda de la cueva). Sagvntvm-Extra 21, Homenaje al Profesor Manuel Pérez Ripoll: 219-225.

Altuna, J., Mariezkurrena, K., Ríos Garaizar, J., & San Emeterio Gómez, A. 2017. Ocupaciones Humanas en Aitzbitarte III (País Vasco) 26.000 - 13.000 BP (zona profunda de la cueva). Servicio Central de Publicaciones del Gobierno Vasco. EKOB; 8: 348pp.

Arrizabalaga, A., 2000a. El yacimiento arqueológico de Labeko Koba (Arrasate, País Vasco). Entorno. Crónica de las investigaciones. Estratigrafía y estructuras. Cronología absoluta. In: Arrizabalaga, A., Altuna, J. (Eds.), Labeko Koba (País Vasco). Hienas y Humanos en los Albores del Paleolítico Superior, Munibe (Antropologia-Arkeologia) 52. Sociedad de Ciencias Aranzadi, San Sebastián-Donostia, pp. 15-72.

Arrizabalaga, A., 2000b. Los tecnocomplejos líticos del yacimiento arqueológico de Labeko Koba (Arrasate, País Vasco). In: Arrizabalaga, A., Altuna, J. (Eds.), Labeko Koba (País Vasco). Hienas y Humanos en los Albores del Paleolítico Superior, Munibe (Antropologia-Arkeologia) 52. Sociedad de Ciencias Aranzadi, San Sebastián-Donostia, pp. 193-343.

Arrizabalaga, A., Iriarte, E., Ríos-Garaizar, J., 2009. The Early Aurignacian in the Basque Country. Quaternary International, 207: 25–36.

Arrizabalaga, A., Iriarte, M.J. & Villaluenga, A. 2010. Labeko Koba y Lezetxiki (País Vasco). Dos yacimientos, una problemática común. Zona Arqueológica, 13: 322-334.

Barandiarán JM. 1980. Excavaciones en Axlor. 1967- 1974. En: Barandiarán, J. M.: Obras Completas. Tomo XVII; pp. 127-384.

Bernaldo de Quirós, F., Maíllo-Fernández, J.-M. 2009. Middle to Upper Palaeolithic at Cantabrian Spain. In: Camps M, Chauhan PR (eds) A sourcebook of Palaeolithic transitions: methods, theories and interpretations. Springer, New York, pp. 341–359.

Cabrera-Valdes, V. 1984. El Yacimiento de la cueva de «El Castillo» (Puente Viesgo, Santander). Bibliotheca Praehistorica Hispana 22, C.S.I.C., 485 p.

Cabrera-Valdes, V., Maillo-Fernandez, J.M., Lloret, M., Bernaldo De Quiros, F. 2001. La transition vers le Paléolithique supérieur dans la grotte du Castillo (Cantabrie, Espagne) la couche 18. L'Anthropologie 105, pp. 505–532.

Daura, J., Sanz, M. (2006). Informe de la troballa del jaciment arqueològic "Terrasses dels Canyars" (Castelldefels-Gavà). Notificació de la descoberta i propostes d'actuació. Grup de Recerca del Quaternari, SERP, UB. Servei d'Arqueologia i Paleontologia, Departament de Cultura i Mitjans de Comunicació, Generalitat de Catalunya. Unpublished Archaeological Report.

Daura, J., Sanz, M., García, N., Allué, E., Vaquero, M., Fierro, E., Carrión, J. S., López-García, J. M., Blain, H. A., Sánchez-Marco, A., Valls, C., Albert, R. M., Fornós, J. J., Julià, R., Fullola, J. M., Zilhão, J. 2013. Terrasses de la Riera dels Canyars (Gavà, Barcelona): The landscape of Heinrich stadial 4 north of the "Ebro frontier" and implications for modern human dispersal into Iberia. Quaternary Science Reviews, 60, 26–48.

Demuro, M., Arnold, L., González-Urquijo, J., Lazuen, T., Frochoso, M. 2023. Chronological constraint of Neanderthal cultural and environmental changes in southwestern Europe: MIS 5–MIS 3 dating of the Axlor site (Biscay, Spain). Journal of Quaternary Research

Doyon, L., Faure, T., Sanz, M., Daura, J., Cassard, L., D'Errico, F., 2023. A 39,600-year-old leather punch board from Canyars, Gavà, Spain. Scientific Advances, 9. https://doi.org/10.1126/sciadv.adg0834

Freeman, L.G. 1964. Mousterian Developments in Cantabrian Spain. Ph.D. thesis. Dept. of Anthropology, University of Chicago, Chicago.

Garralda, M.D. 2005. Los Neandertales en la Península Ibérica:The Neandertals from the Iberian Peninsula. Munibe (Antropologia-Arkeologia) 57, Homenaje a Jesús Altuna. pp. 289–314.

Garralda, M.D., Madrigal, T., Zapata, J., & Rosell, J. 2022. Neanderthal deciduous tooth crowns from the Early Upper Paleolithic at El Castillo Cave (Cantabria, Spain). Archaeological and Anthropological Sciences.

Gómez-Olivencia, A., Arceredillo, D., Álvarez-Lao, D.J., Garate, D., San Pedro, Z., Castaños, P., Rios-Garaizar, J., 2014. New evidence for the presence of reindeer (Rangifer tarandus) on the Iberian Peninsula in the Pleistocene: an archaeopalaeontological and chronological reassessment. Boreas 43, 286–308.

Gómez-Olivencia, A., Sala, N., Núñez-Lahuerta, C., Sanchis, A., Arlegi, M., Rios-Garaizar, J., 2018. First data of Neandertal bird and carnivore exploitation in the Cantabrian Region (Axlor; Barandiaran excavations; Dima, Biscay, Northern Iberian Peninsula). Scienti. Rep. 8, 10551.

González Echegaray, J.G. 1966. Cueva del Otero. Excavaciones Arqueológicas en España, 53. Madrid: Ministerio de Educación Nacional Dirección General de Bellas Artes Servicio Nacional de Excavaciones.

González-Urquijo, J.E., Ibáñez-Estévez, J.J. 2001. Abrigo de Axlor (Dima). Arkeoikuska: Investigación arqueológica 2001; 2002: 90–93.

González Urquijo, J.E., Ibáñez Estévez, J.J., Rios-Garaizar, J., Bourguignon, L., Castaños Ugarte, P., Tarriño Vinagre, A. 2005. Excavaciones recientes en Axlor. Movilidad y planificación de actividades en grupos de neandertales. In: Montes Barquín R, Lasheras Corruchaga JA, editors. Actas de La Reunión Científica: Neandertales Cantábricos. Estado de La Cuestión. Monografías Del Museo Nacional Y Centro de Investigación de Altamira No 20. Madrid: Ministerio de Cultura; 2005. pp. 527–539.

Jimenez, I. J., Sanz, M., Daura, J., Gaspar, I. D., García, N. 2019. Ontogenetic dental patterns in Pleistocene hyenas (Crocuta crocuta Erxleben, 1777) and their palaeobiological implications. International Journal of Osteoarchaeology, 29, 808–821.

Liberda, J.J., Thompson, J.W., Rink, W.J., Bernaldo de Quirós, F., Jayaraman, R., Selvaretinam, K., Chancellor-Maddison, K., Volterra, V., 2010. ESR dating of tooth enamel in Mousterian layer 20, El Castillo, Spain. Geoarchaeology n/a-n/a.

López-García, J.M., Blain, H.A., Fagoaga, A., Bandera, C.S., Sanz, M., Daura, J., 2022. Environment and climate during the Neanderthal-AMH presence in the Garraf Massif mountain range (northeastern Iberia) from the late Middle Pleistocene to Late Pleistocene inferred from small-vertebrate assemblages. Quaternary Science Reviews, 288.

López-García, J. M., Blain, H.-A., Bennàsar, M., Sanz, M., Daura, J. 2013. Heinrich event 4 characterized by terrestrial proxies in southwestern Europe. Climate of the Past, 9: 1053–1064.

Luret, M., Blasco, R., Arsuaga, J.L., Baquedano, E., Pérez-González, A., Sala, N., & Aranburu, A. 2020. A multi-proxy approach to the chronology of the earliest Aurignacian at the El Castillo Cave (Spain). Journal of Archaeological Science: Reports, 33: 102339.

Maroto, J., Vaquero, M., Arrizabalaga, Á., Baena, J., Baquedano, E., Jordá, J., Julià, R., Montes, R., Van Der Plicht, J., Rasines, P., Wood, R., 2012. Current issues in late Middle Palaeolithic chronology: New assessments from Northern Iberia. Quaternary International, 247: 15–25.

Marín-Arroyo, A.B., Rios-Garaizar, J., Straus, L.G., Jones, J.R., de la Rasilla, M., González Morales, M.R., Richards, M., Altuna, J., Mariezkurrena, K., Ocio, D., 2018. Chronological reassessment of the Middle to Upper Paleolithic transition and Early Upper Paleolithic cultures in Cantabrian Spain. PLoS One 13: 1–20.

Martín-Perea, D.M., Maíllo-Fernández, J., Marín, J., Arroyo, X., Asiaín, R., 2023. A step back to move forward: a geological re-evaluation of the El Castillo Cave Middle Palaeolithic lithostratigraphic units (Cantabria, northern Iberia). Journal of Quaternary Science, 38: 221–234.

Pederzani, S., Britton, K., Jones, J.R., Agudo Pérez, L., Geiling, J.M., Marín-Arroyo, A.B., 2023. Late Pleistocene Neanderthal exploitation of stable and mosaic ecosystems in northern Iberia shown by multi-isotope evidence. Quaternary Research: 1–25.

Rink, W.J., Schwarcz, H.P., Lee, H.K., Cabrera Valdés, V., Bernaldo de Quirós, F., Hoyos, M. 1997. ESR dating of Mousterian levels at El Castillo Cave, Cantabria, Spain. Journal of Archaeological Science, 24 (7): 593-600.

Rios-Garaizar J. 2012.Industria lítica y sociedad en la Transición del Paleolítico Medio al Superior en torno al Golfo de Bizkaia. Santander: PUbliCan - Ediciones de la Universidad de Cantabria.

Rios-Garaizar, J. 2017. A new chronological and technological synthesis for Late Middle Paleolithic of the Eastern Cantabrian Region. Quaternary International, 433: 50-63.

Rios-Garaizar, J., Arrizabalaga, A. & Villaluenga, A. 2012. Haltes de chasse du Châtelperronien de la Péninsule Ibérique: Labeko Koba et Ekain (Pays Basque Péninsulaire). L'Anthropologie, 116: 532–549.

Rios-Garaizar, J., de la Peña, P., Maillo-Fernández, J.M. 2013. El final del Auriñaciense y el comienzo del Gravetiense en la región cantábrica: una visión tecno-tipológica. In: de las Heras C., Lasheras J.A., Arrizabalaga Á., de la Rasilla M. (Eds.), Pensando El Gravetiense: Nuevos Datos Para La Región Cantábrica En Su Contexto Peninsular Y Pirenaico. Monografías Del Museo Nacional Y Centro de Investigación de Altamira, 23. Madrid: Ministerio de Educación, Cultura; pp. 369–382.

Rios-Garaizar, J., Iriarte, E., Arnold, L.J., Sánchez-Romero, L., Marín-Arroyo, A.B., San Emeterio, A., Gómez-Olivencia, A., Pérez-Garrido, C., Demuro, M., Campaña, I., Bourguignon, L., Benito-Calvo, A., Iriarte, M.J., Aranburu, A., Arranz-Otaegi, A., Garate, D., Silva-Gago, M., Lahaye, C., Ortega, I. 2022. The intrusive nature of the Châtelperronian in the Iberian Peninsula. PLoS One 17, e0265219.

Rivals, F., Uzunidis, A., Sanz, M., Daura, J., 2017. Faunal dietary response to the Heinrich Event 4 in southwestern Europe. Palaeogeogr. Palaeoclimatol. Palaeoecol. 473, 123–130.

Sanz-Royo, A., Sanz, M., Daura, J. (2020). Upper Pleistocene equids from Terrasses de la Riera dels Canyars (NE Iberian Peninsula): The presence of Equus ferus and Equus hydruntinus based on dental criteria and their implications for palaeontological identification and palaeoenvironmental reconstruction. Quaternary International, 566–567, 78–90.

Sanz-Royo, A., Terlato, G., Marín-Arroyo, A.B., 2024. Taphonomic data from the transitional Aurignacian of El Castillo cave (Spain) reveals the role of carnivores at the Aurignacian Delta level. Quaternary Science Advances, 13: 100147. https://doi.org/10.1016/j.qsa.2023.100147

Vidal-Cordasco, M., Ocio, D., Hickler, T., Marín-Arroyo, A.B., 2022. Ecosystem productivity affected the spatiotemporal disappearance of Neanderthals in Iberia. Nat. Ecol. Evol. 6, 1644–1657.

Villaluenga, A., Arrizabalaga, A. & Rios-Garaizar, J. 2012. Multidisciplinary approach to two Châtelperronian series: lower IX layer of Labeko Koba and X Level of Ekain (Basque country, Spain). Journal of Taphonomy, 10: 525–548.

Wood, R.E., Arrizabalaga, A., Camps, M., Fallon, S., Iriarte-Chiapusso, M.J., Jones, R., Maroto, J., De la Rasilla, M., Santamaría, D., Soler, J., Soler, N., Villaluenga, A., Higham, T.F.G. 2014. The chronology of the earliest Upper Palaeolithic in northern Iberia: New insights from L'Arbreda, Labeko Koba and La Viña. Journl of Human Evolution, 69: 91–109. https://doi.org/10.1016/j.jhevol.2013.12.017

Wood, R., Bernaldo de Quirós, F., Maíllo-Fernández, J.M., Tejero, J.M., Neira, A., Higham, T. 2018. El Castillo (Cantabria, northern Iberia) and the Transitional Aurignacian: Using radiocarbon dating to assess site taphonomy. Quaternary International, 474: 56–70.

Yravedra, J., & Gómez-Castanedo, A. 2010. Estudio zooarqueológico y tafonómico del yacimiento del Otero (Secadura, Voto, Cantabria). Espacio, Tiempo y Forma. Serie I, Nueva época. Prehistoria y Arqueología, 3: 21-38

Zilhao, J., DEerrico, F. 2003 The chronology of the Aurignacian and Transitional technocomplexes. Where do we stand? In Zilhão, J. et d'Errico, F. eds., The chronology of the Aurignacian and of the transitional technocomplexes Dating, stratigraphies, cultural implications Proceedings of Symposium 6.1 of the XIVth Congress of the UISPP, pp. 313–349.
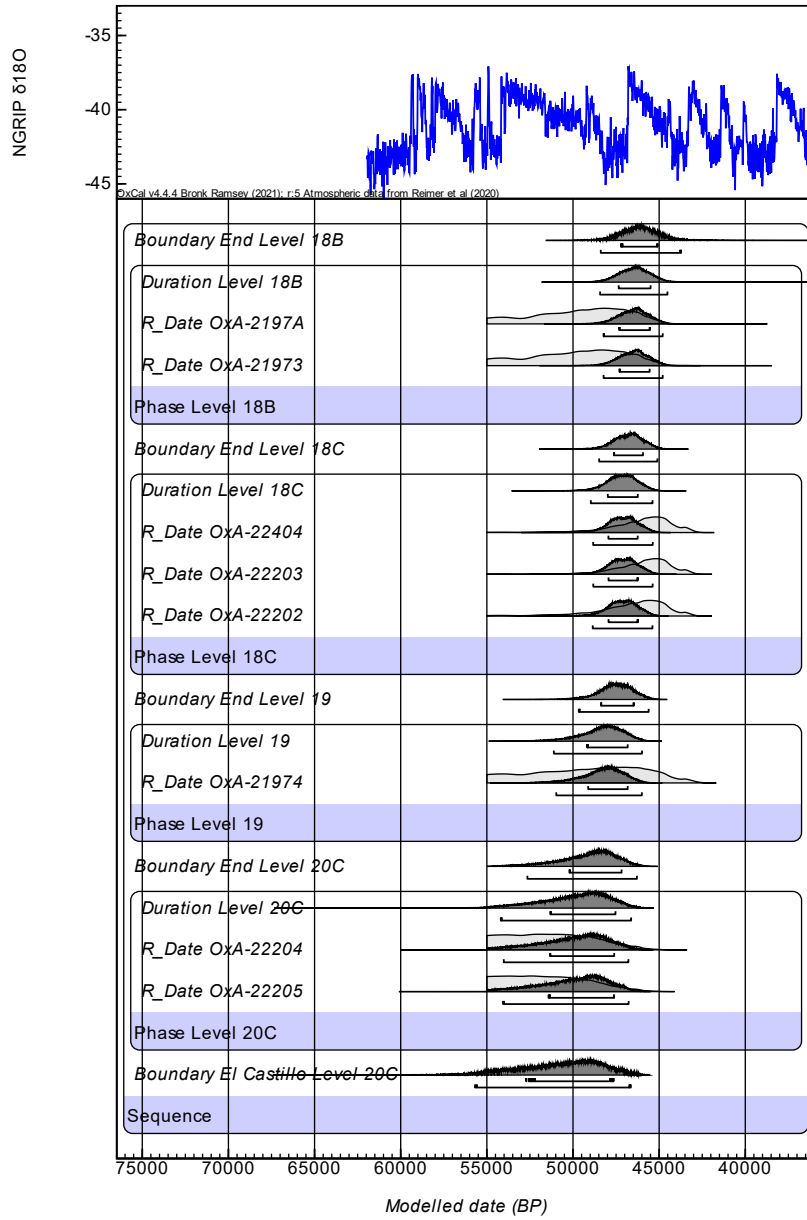
Appendix C - Individual Bayesian Models

1559

1560   **Figure C1.** Radiocarbon dates from El Castillo modelled in OxCal4.4 against INTCAL20.

1561

1562

OxCal v4.4.4 Bronk Ramsey (2021); r:20 Atmospheric data from Reimer et al (2020)
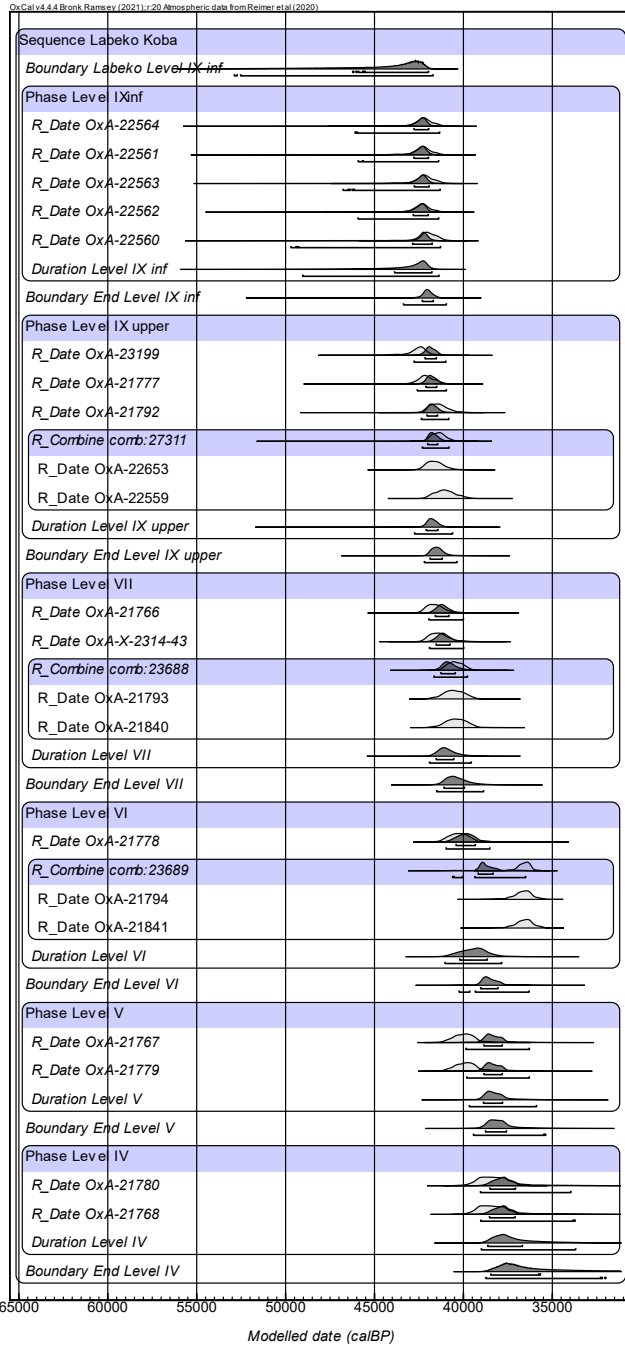
1563

Figure C2. Radiocarbon dates from Labeko Koba modelled in OxCal4.4 against INTCAL20.

Field Code Changed

1565
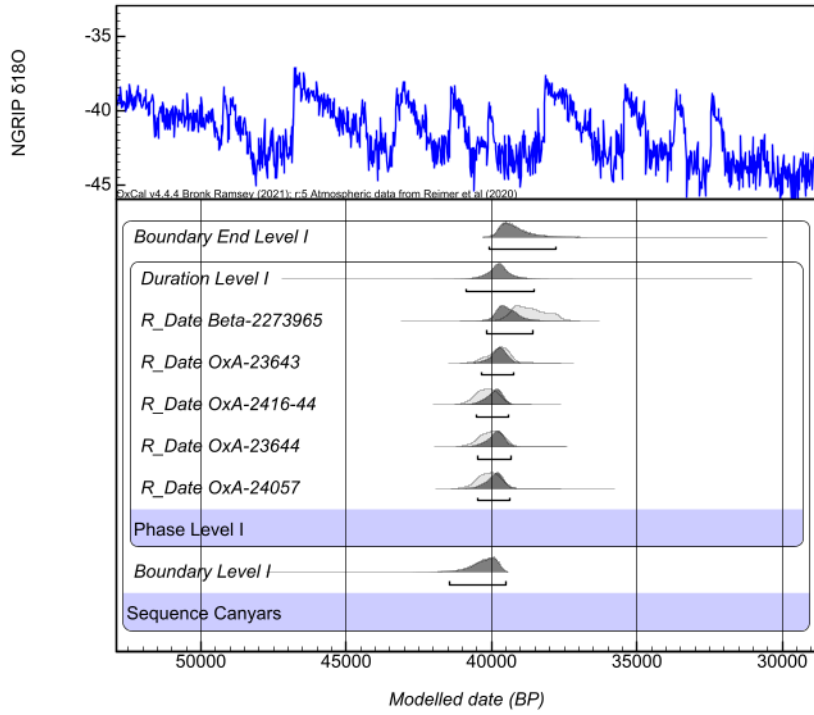
1566

1567   **Figure C3.** Radiocarbon dates from Canyars modelled in OxCal4.4 against INTCAL20.

1568
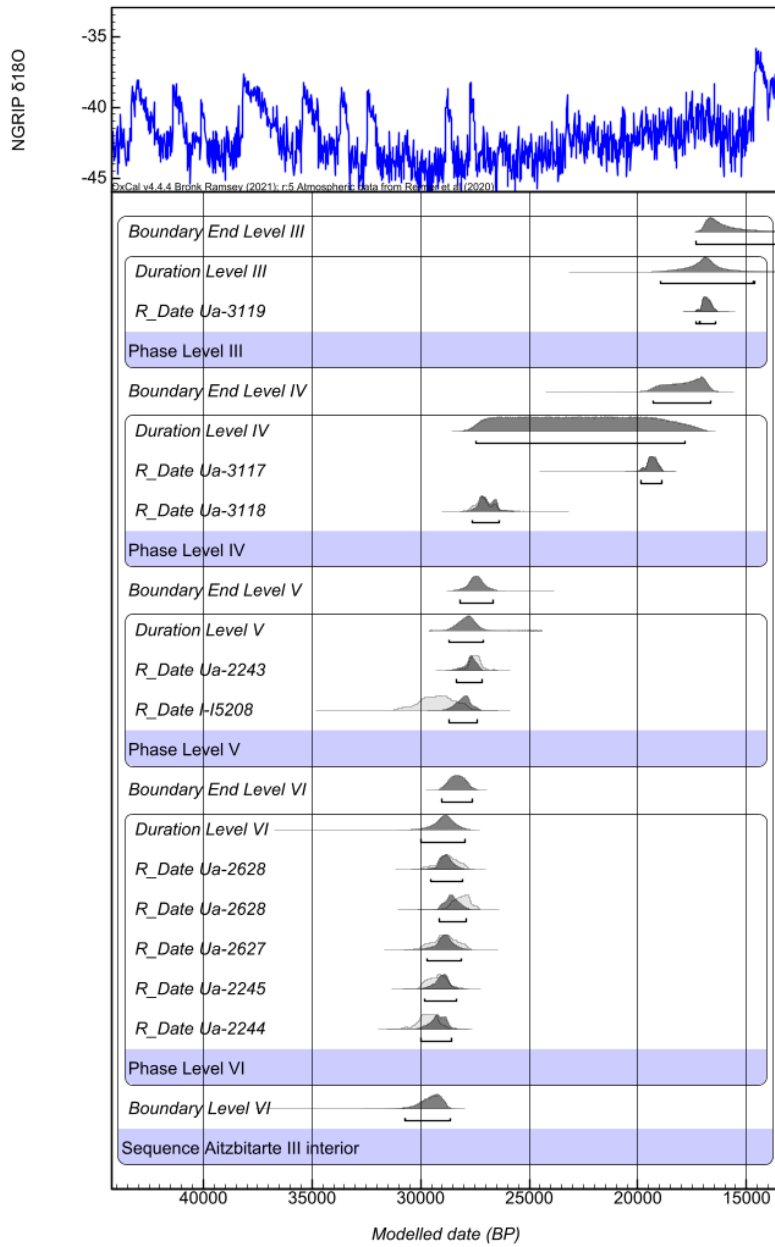
1569

Figure C4. Radiocarbon dates from Aitzbitarte III-interior modelled in OxCal4.4 against INTCAL20.

Field Code Changed

Results of Bayesian Models

El Castillo	Unmodelled (BP)			Modelled (BP)			Indices Amodel 78.8, Aoverall 82.4			
	from	to	%	from	to	%	A	L	P	C
Boundary End Level 18B				48383	43733	95.449.974				97.1
Duration Level 18B				**48438**	**44536**	**95.449.974**				**99.8**
R_Date OxA-2197A	...	45427	95.449.973	48235	44793	95.449.974	98.1		95.2	99.8
R_Date OxA-21973	...	45655	95.449.973	48240	44793	95.449.974	91.9		95.2	99.8
Phase Level 18B										
Boundary End Level 18C				48470	45117	95.449.974				99.8
Duration Level 18C				**48977**	**45382**	**95.449.974**				**99.9**
R_Date OxA-22404	49976	42918	95.449.974	48833	45383	95.449.974	82.2		95.3	99.8
R_Date OxA-22203	49451	42999	95.449.974	48819	45381	95.449.974	76.1		95.2	99.8
R_Date OxA-22202	51146	43039	95.449.974	48861	45386	95.449.974	101.2		95.4	99.8
Phase Level 18C										
Boundary End Level 19				49629	45623	95.449.974				99.7
Duration Level 19				51060	45997	95.449.974				99.7
R_Date OxA-21974	...	44367	95.449.974	50965	45998	95.449.974	120.2		95.3	99.8
Phase Level 19										
Boundary End Level 20C				52583	46286	95.449.974				99.5
Duration Level 20C				**54134**	**46593**	**95.449.974**				**99.3**
R_Date OxA-22204	...	47048	95.449.974	53958	46713	95.449.974	94		95.3	99.3
R_Date OxA-22205	...	47348	95.449.974	53965	46715	95.449.974	86.9		95.3	99.3
Phase Level 20C										
Boundary El Castillo Level 20C				55552	46609	95.449.974				95.3
Sequence										
U(0	68.268.949	3.99E-17	4	68.268.949	5.38E-17	3.776		100		
T(5)	-2.65	2.65	95.449.974							99.9
Outlier_Model General				-2684	2502	95.449.974				100

Table C1. Radiocarbon dates from El Castillo modelled in OxCal4.4 against INTCAL20.

Field Code Changed

Aitzbitarte III Interior	Unmodelled (BP)			Modelled (BP)			Indices Amodel 78.8, Aoverall 82.4			
	from	to	%	from	to	%	A	L	P	C
Boundary End Level III				17300	12910	9.544.997				98
Duration Level III				18960	14630	9.544.997				99.6
R_Date Ua-3119	17270	16390	9.544.997	17300	16430	9.544.997	100.8		95.8	99.8
Phase Level III										
Boundary End Level IV				19320	16640	9.544.997				99.3
Duration Level IV				27430	17820	9.544.997				98.9
R_Date Ua-3117	19830	18900	9.544.997	19840	18910	9.544.997	99.9		95.3	99.6
R_Date Ua-3118	27700	26430	9.544.997	27600	26360	9.544.997	98.1		95.2	99.5
Phase Level IV										
Boundary End Level V				28210	26680	9.544.997				99.7
Duration Level V				**28680**	**27130**	**9.544.997**				**99.9**
R_Date Ua-2243	28260	26610	9.544.997	28370	27190	9.544.997	88.8		95.4	99.8
R_Date I-I5208	30830	27760	9.544.997	28710	27370	9.544.997	57.7		94.8	99.8
Phase Level V										
Boundary End Level VI				29010	27630	9.544.997				99.7
Duration Level VI				29990	27930	9.544.997				99.8
R_Date Ua-2628	29760	27840	9.544.997	29570	28080	9.544.997	118.2		96	99.8
R_Date Ua-2628	28760	27360	9.544.997	29150	27920	9.544.997	67		94.3	99.8
R_Date Ua-2627	29920	27870	9.544.997	29680	28110	9.544.997	120.5		96	99.8
R_Date Ua-2245	30070	28280	9.544.997	29820	28360	9.544.997	108		95.9	99.8
R_Date Ua-2244	30720	28760	9.544.997	30010	28570	9.544.997	77.7		94.9	99.7
Phase Level VI										
Boundary Level VI				30730	28650	9.544.997				96
Sequence										
U(0,4)	3.99E-17	4	9.544.997	5.38E-17	3.772	9.544.997	100			99
T(5)	-2.65	2.65	9.544.997							95.5
Outlier_Model General				-1420	1280	9.544.997				99.9

Table C2. Radiocarbon dates from Labeko Koba modelled in OxCal4.4 against INTCAL20.

Field Code Changed

Canyars	Unmodelled (BP)			Modelled (BP)			Indices Amodel 78.8, Aoverall 82.4			
Boundary End Level I				40090	37770	95.45				95.3
Duration Level I				**40890**	**38530**	**95.45**				**99.7**
R_Date Beta-2273965	39630	37570	9.544.997	40190	38560	95.45	63.2		93.4	99.6
R_Date OxA-23643	40520	39140	9.544.997	40330	39240	95.45	114.2		96.1	99.8
R_Date OxA-2416-44	40880	39450	9.544.997	40540	39400	95.45	99.2		96	99.8
R_Date OxA-23644	40740	39300	9.544.997	40470	39340	95.45	110.5		96	99.8
R_Date OxA-24057	40790	39390	9.544.997	40490	39380	95.45	104.3		96	99.8
Phase Level I										
Boundary Level I				41450	39500	95.45				96.6
Sequence Canyars										
U(0,4)	3.99E-17	4	9.544.997	5.38E-17	3.82	95.45	100			100
T(5)	-2.65	2.65	9.544.997							99.4
Outlier_Model General				-800	1480	95.45				99.9

Table C3. Radiocarbon dates from Canyars modelled in OxCal4.4 against INTCAL20.

Labeko Koba	Unmodelled (BP)			Modelled (BP)			Indices Amodel 78.8, Aoverall 82.4			
	from	to	%	from	to	%	A	L	P	C
Boundary End Level IV				38710	32030	9.544.997				98.4
Duration Level IV				**39000**	**33710**	**9.544.997**				**99.8**
R_Date OxA-21768	39700	37030	9.544.997	39050	33820	9.544.997	75.5		80	99.8
R_Date OxA-21780	39780	36910	9.544.997	39050	33960	9.544.997	81.3		82.3	99.8
Phase Level IV										
Boundary End Level V				39470	35440	9.544.997				99.8
Duration Level V				**39730**	**35950**	**9.544.997**				**99.8**
R_Date OxA-21779	41170	38260	9.544.997	39830	36330	9.544.997	21		87.2	99.8
R_Date OxA-21767	41230	38500	9.544.997	39860	36340	9.544.997	15.5		85.5	99.8
Phase Level V										
Boundary End Level VI				40240	36360	9.544.997				99.8
Duration Level VI				**41030**	**37860**	**9.544.997**				**99.9**
R_Date OxA-21841	37710	35420	9.544.997							
R_Date OxA-21794	38040	35460	9.544.997							
R_Combine comb:23689	37350	35900	9.544.997	40620	36500	9.544.997	4.3			99.8
R_Date OxA-21778	41390	39190	9.544.997	40970	38550	9.544.997	90		94.4	99.9
Phase Level VI										
Boundary End Level VII				41490	38890	9.544.997				99.9
Duration Level VII				**41910**	**39570**	**9.544.997**				**99.9**
R_Date OxA-21840	41610	39250	9.544.997							
R_Date OxA-21793	41720	39390	9.544.997							
R_Combine comb:23688	41290	39570	9.544.997	41650	39780	9.544.997	87.3			99.9
R_Date OxA-X-2314-43	42350	40260	9.544.997	41900	40000	9.544.997	96.5		95.4	99.9
R_Date OxA-21766	42520	40530	9.544.997	41950	40020	9.544.997	80.3		94.6	99.9
Phase Level VII										
Boundary End Level IX upper				42190	40360	9.544.997				99.9
Duration Level IX upper				**42750**	**40580**	**9.544.997**				**99.9**
R_Date OxA-22559	42090	39850	9.544.997							
R_Date OxA-22653	42520	40530	9.544.997							
R_Combine comb:27311	42120	40600	9.544.997	42330	40800	9.544.997	95			99.9
R_Date OxA-21792	42370	40330	9.544.997	42380	40820	9.544.997	113.4		95.7	99.9
R_Date OxA-21777	43160	40960	9.544.997	42600	40950	9.544.997	99.5		95.6	99.9
R_Date OxA-23199	43980	41490	9.544.997	42800	40990	9.544.997	52.4		92.8	99.9
Phase Level IX upper										
Boundary End Level IX inf				43420	40970	9.544.997				99.9
Duration Level IX inf				**48940**	**41340**	**9.544.997**				**99.8**
R_Date OxA-22560	42780	40980	9.544.997	49670	41300	9.544.997	75.3		76	99.8
R_Date OxA-22562	43830	41220	9.544.997	45860	41380	9.544.997	102.8		90.9	99.8
R_Date OxA-22563	43250	41010	9.544.997	46280	41300	9.544.997	99.1		89.7	99.8
R_Date OxA-22561	43790	41130	9.544.997	45920	41340	9.544.997	102.3		90.7	99.8
R_Date OxA-22564	43370	41050	9.544.997	46060	41320	9.544.997	101		90.2	99.8
Phase Level IXinf										
Boundary Labeko Level IX inf				52660	41740	9.544.997				96.6
Sequence Labeko Koba										
N(0,2)	-4	4	9.544.997							99.4
Outlier_Model SSimple				...	840	9.544.997				97.5
U(0,4)	3.99E-17	4	9.544.997	5.38E-17	3.932	9.544.997	100			98.3
T(5)	-2.65	2.65	9.544.997							97.5
Outlier_Model General				-6130	9280	9.544.997				99.4

Table C4. Radiocarbon dates from Aitzbitarte III-interior modelled in OxCal4.4 against INTCAL20.

Appendix D. Intratooth curve plots

Original curves derived from enamel intratooth sampling on enamel carbonate. Provided by sites. In blue, oxygen stable isotope composition (δ18O), and, in brown, carbon stable isotope composition (δ13C). In the x-axis, the distance from Enamel Rooth Junction (ERJ). Notice that the y-axis can experience some variations between sites.
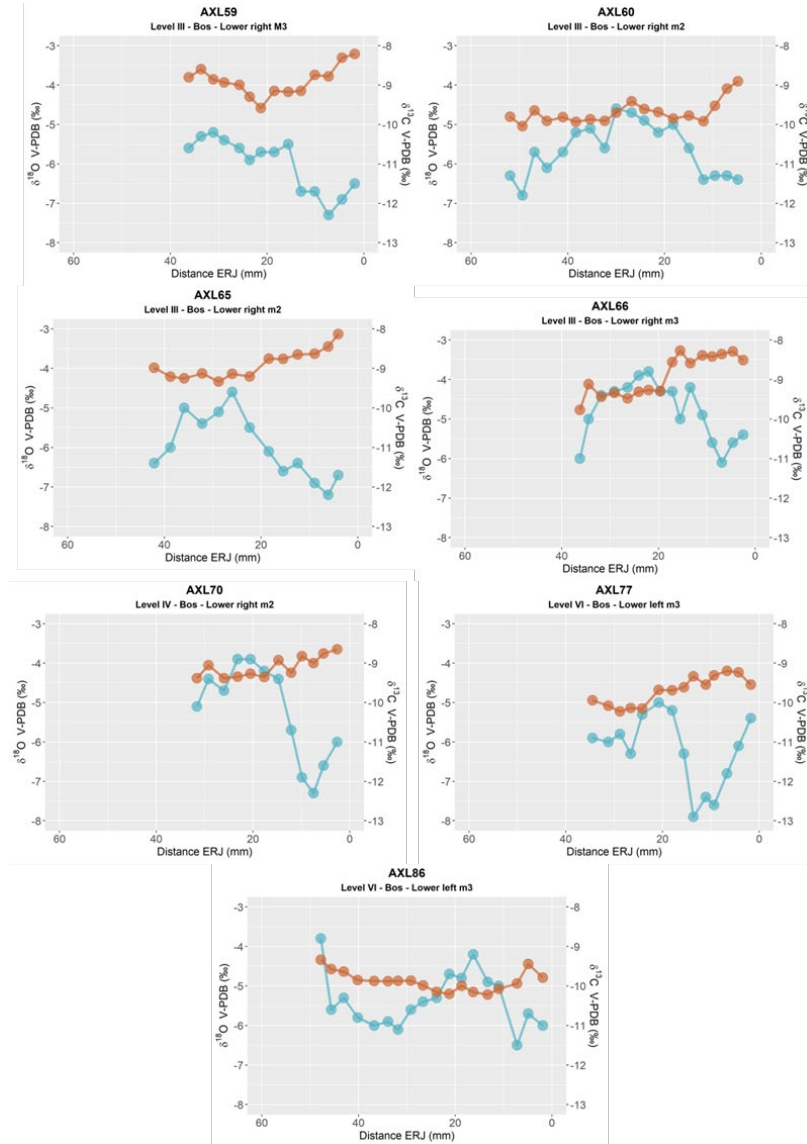
Figure D1. Intratooth plots of oxygen (δ18O) and carbon (δ13C) isotope composition from teeth from Axlor, considering distance from enamel root junction (ERC).
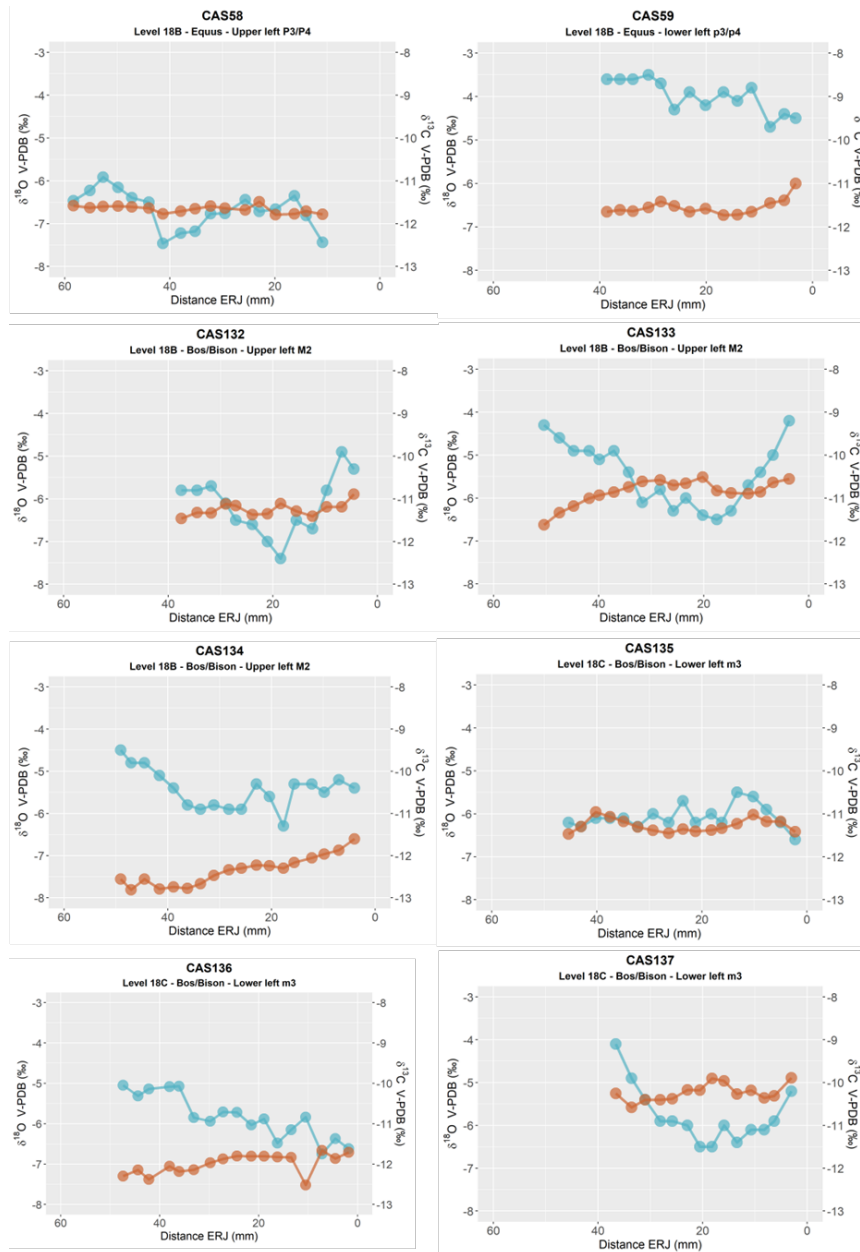
Figure D2. Intratooth plots of oxygen (δ^{18}O) and carbon (δ^{13}C) isotope composition from teeth from El Castillo, considering the sample's distance from the enamel root junction (ERC).
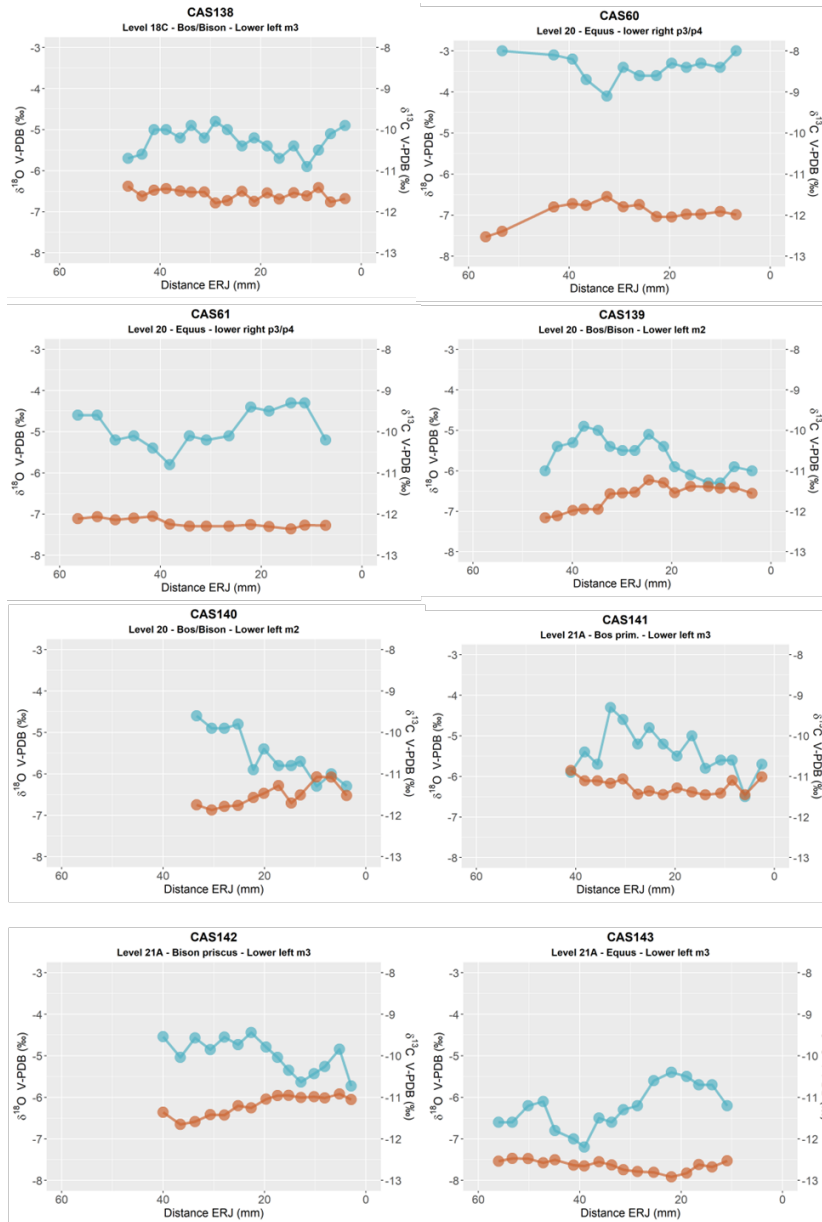
Figure D3. Intratooth plots of oxygen (δ¹⁸O) and carbon (δ¹³C) isotope composition from teeth from El Castillo, considering the sample's distance from the enamel root junction (ERC).
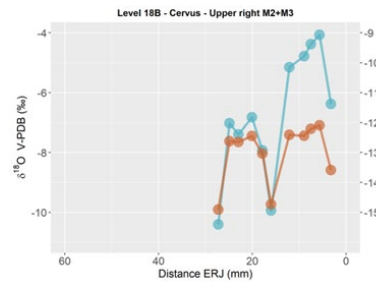
Figure D4. Intratooth plots of oxygen (δ¹⁸O) and carbon (δ¹³C) isotope composition from teeth from El Castillo, considering the sample's distance from the enamel root junction (ERC).
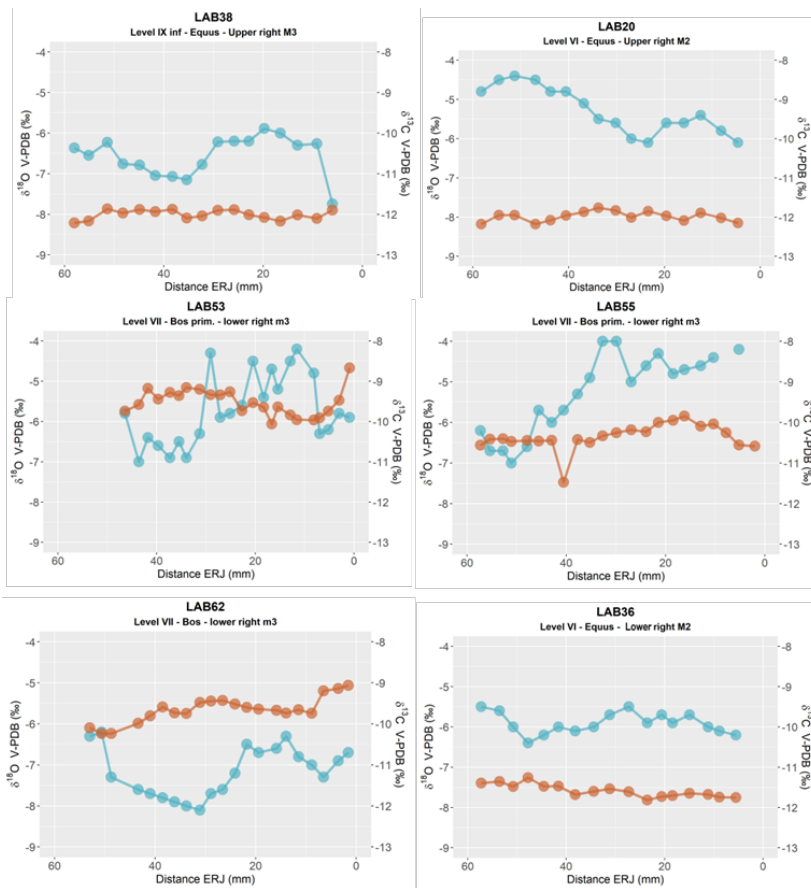
Figure D5. Intratooth plots of oxygen (δ¹⁸O) and carbon (δ¹³C) isotope composition from teeth from Labeko Koba, considering the sample's distance from the enamel root junction (ERC).
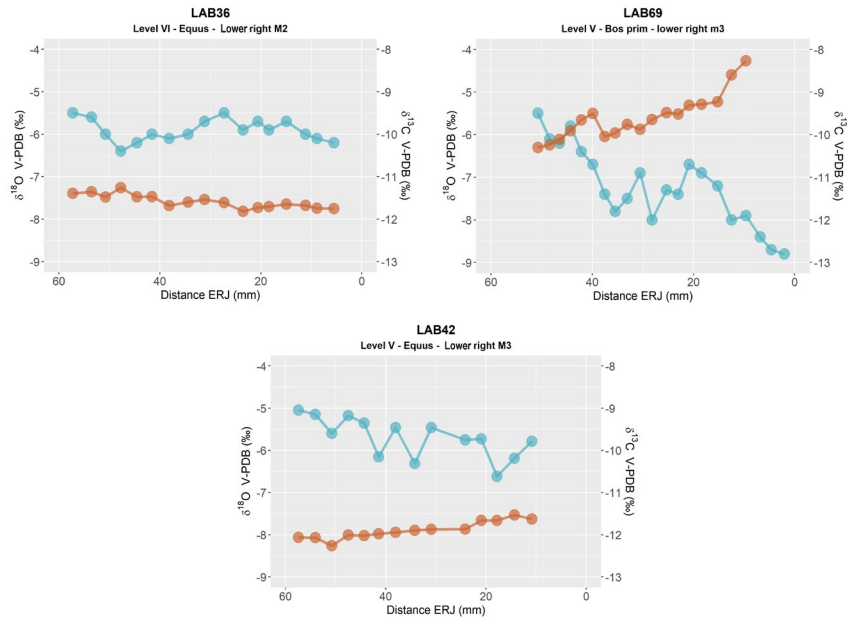
Figure D6. Intratooth plots of oxygen (δ^{18}O) and carbon (δ^{13}C) isotope composition from teeth from Labeko Koba, considering the sample's distance from the enamel root junction (ERC).
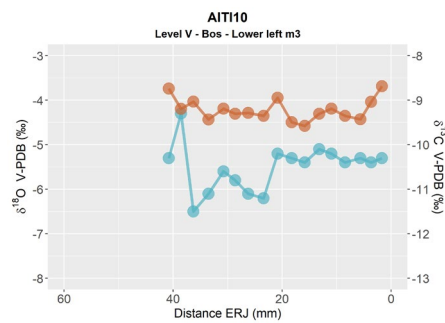
Figure D7. Intratooth plots of oxygen (δ^{18}O) and carbon (δ^{13}C) isotope composition from teeth from Aitzbitarte III interior, considering the sample's distance from the enamel root junction (ERC).
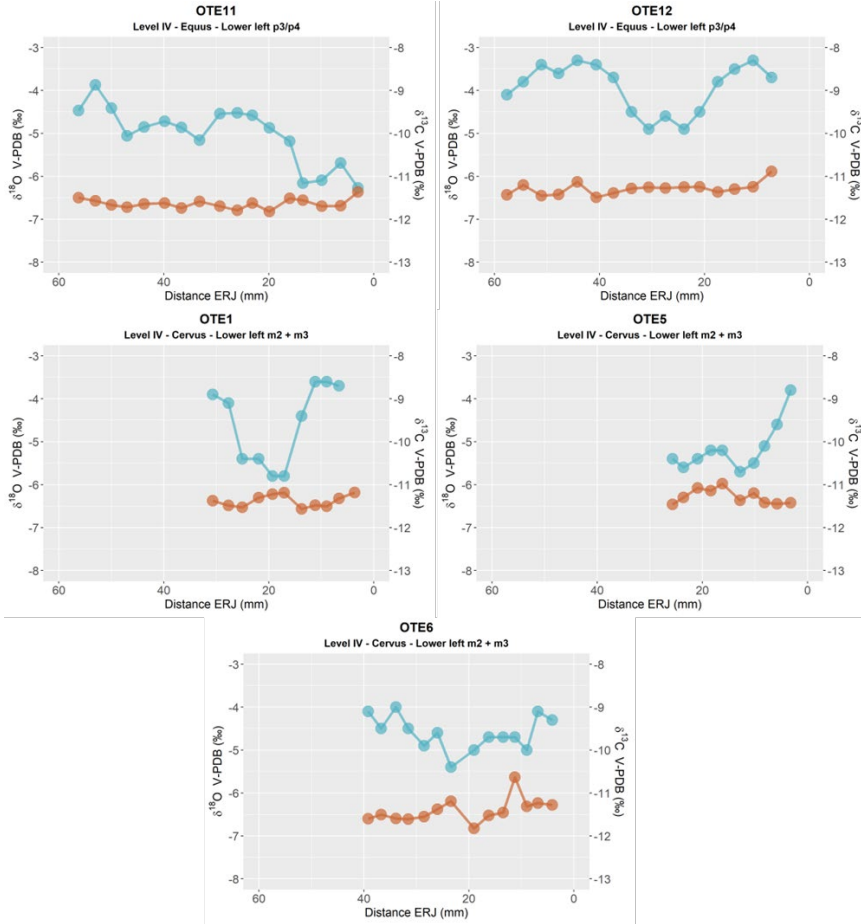
Figure D8. Intratooth plots of oxygen (δ18O) and carbon (δ13C) isotope composition from teeth from El Otero, considering the sample's distance from the enamel root junction (ERC).
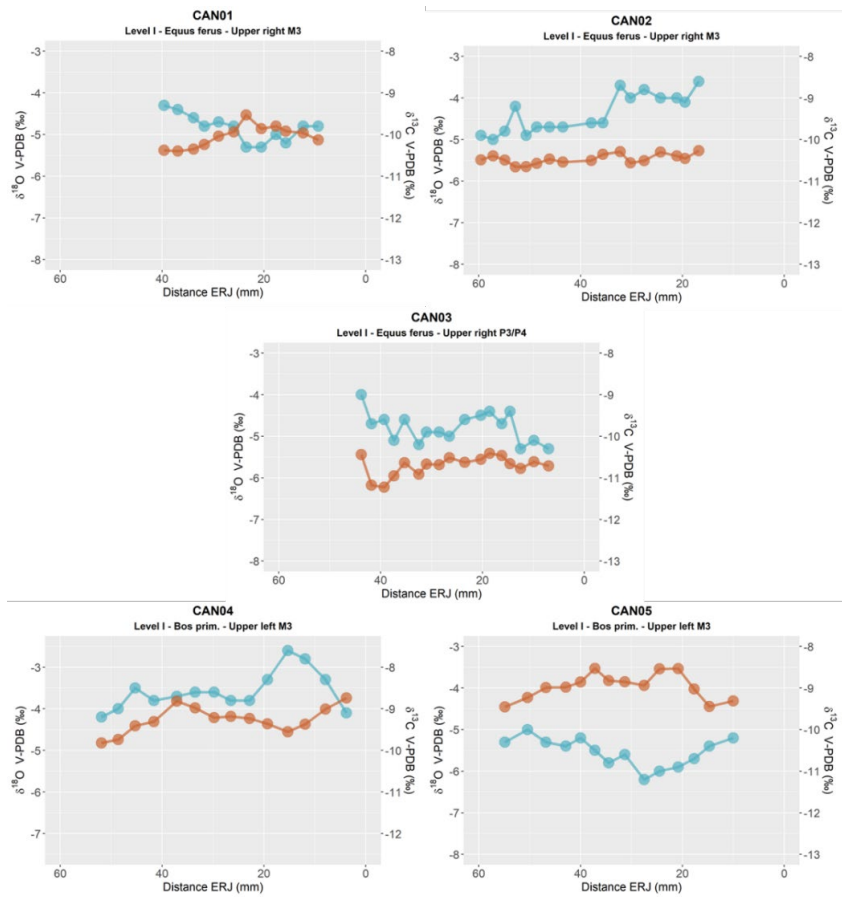
Figure D9. Intratooth plots of oxygen (δ¹⁸O) and carbon (δ¹³C) isotope composition from teeth from Canyars considering the sample's distance from the enamel root junction (ERC).

Appendix E. Inverse Modelling: Methodological Details and Models

The intratooth $\delta^{18}O$ profiles presented in this study were obtained through the application of inverse modelling, using an adapted version of the code published in reference (Passey et al., 2005b). This modeling approach allowed for the correction of the damping effect and the reconstruction of the original $\delta^{18}O$ input time series. The model reproduces the temporal delay between $\delta^{18}O$ changes in the animal's input and their manifestation in tooth enamel, exhibiting a consistent x-direction delay in the modelled $\delta^{18}O$ curve relative to the enamel $\delta^{18}O$ input time series. The model utilizes different species-specific parameters related to enamel formation, which vary between bovines and equids. These parameters have been established based on previous studies (Bendrey et al., 2015; Zazzo et al., 2012; Passey and Cerling, 2002; Kohn, 2004; Blumenthal et al., 2014). For *Bos/Bison* sp., the initial mineral content of enamel is fixed at 25%, the enamel appositional length is set at 1.5 mm, and the maturation length is 25 mm. For *Equus* sp., the initial mineral content of enamel is fixed at 22%, the enamel appositional length is set at 6 mm, and the maturation length is 28 mm.

In addition, the model requires other variables related to sampling geometry, as well as error estimates derived from mass spectrometer measurements. The distance between samples varies for each tooth, but as a general trend, the sampling depth on the tooth enamel surface in the samples of this study represents approximately 70% of the total enamel depth. The standard deviation of the measurements obtained from the mass spectrometer was typically set at 0.12‰, taking into account the uncertainty associated with the standards. Finally, the models require a damping factor that determines the cumulative damping along the isotopic profile by adjusting the measured error (Emeas) to the prediction error (Epred). In the teeth analysed in this study, the damping factor ranged from 0.001 to 0.1.

The most likely model solutions were selected, and summer and winter values were extracted from the $\delta^{18}O$ profiles, considering the original peaks and troughs identified in the unmodelled $\delta^{18}O$ profile. This approach was adopted to prevent the introduction of artificial peaks that the model may produce, particularly in teeth without a distinct sinusoidal shape. Flat and less sinusoidal profile are less suitable for the application of the model, given its inherent assumption of an approximately sinusoidal form. Non-sinusoidal curves can lead to complex interpretations in the model outcomes. Consequently, this methodology was not applied to analysed intratooth $\delta^{13}C$ profiles, as the examined individuals did not exhibit appreciable seasonal change.
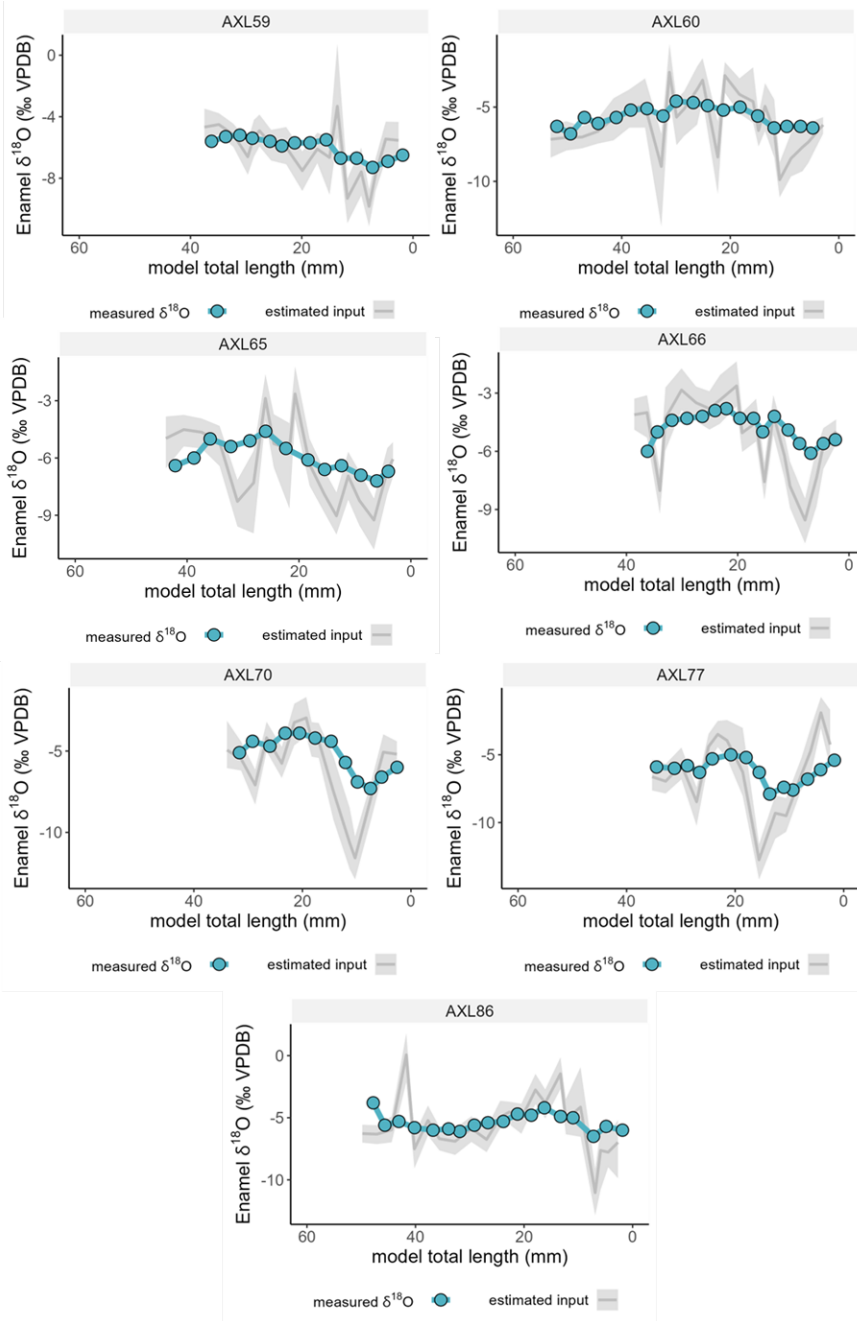
Figure E1. Inverse models for oxygen isotope composition ($\delta^{18}O$) from teeth from Axlor, considering distance from enamel root junction. The blue line and points correspond to original data and grey line the most likely model solution, with the 95% confidence interval shown in shaded areas.
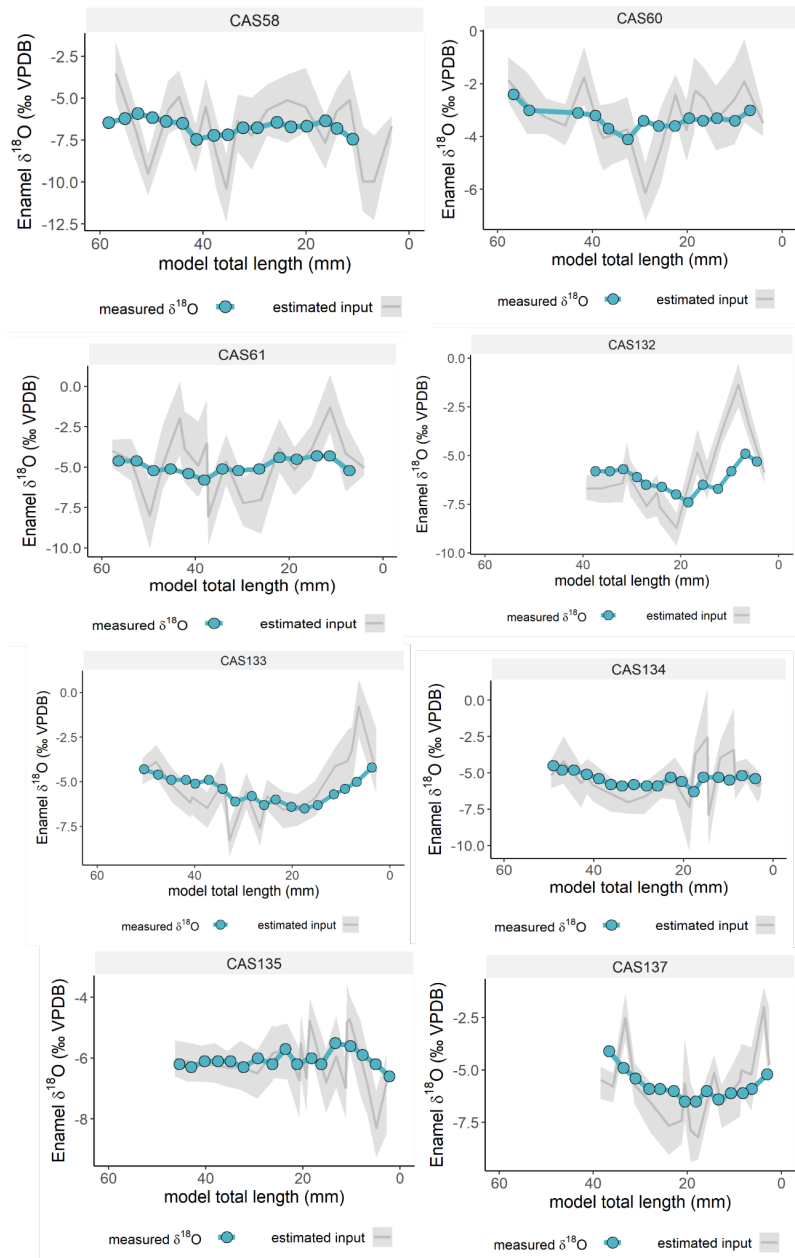
Figure E2. Inverse models for oxygen isotope composition (δ¹⁸O) from teeth from El Castillo, considering distance from enamel root junction. The blue line and points correspond to original data and grey line the most likely model solution, with the 95% confidence interval shown in shaded areas.
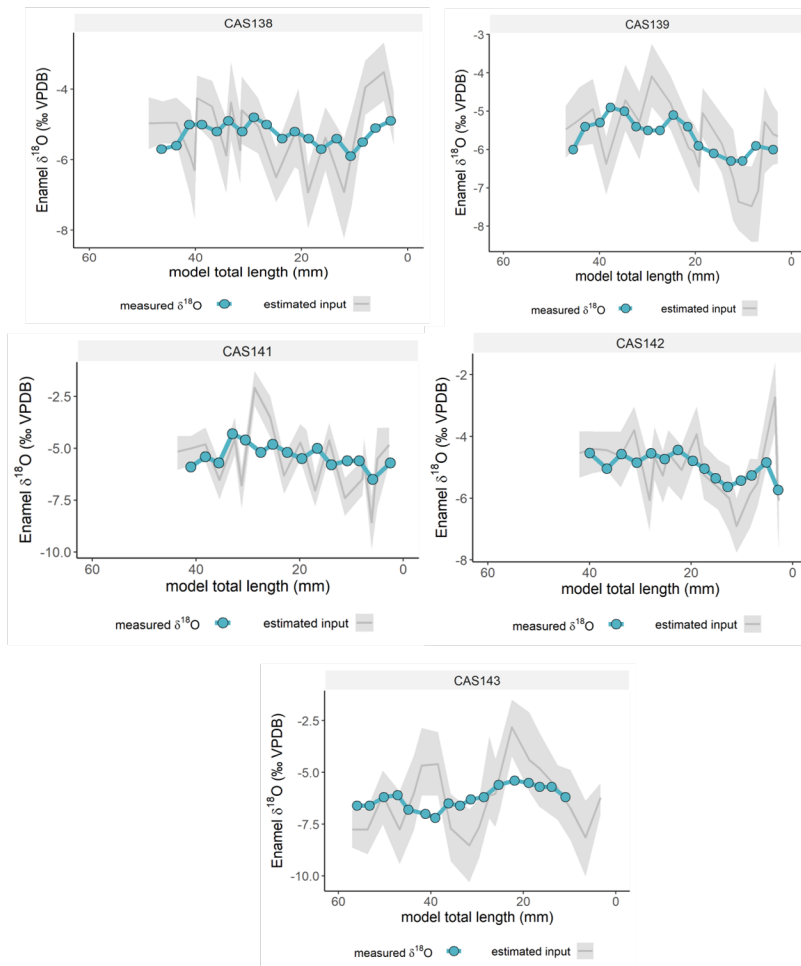
Figure E3. Inverse models for oxygen isotope composition (δ^{18}O) from teeth from El Castillo, considering distance from enamel root junction. The blue line and points correspond to original data and grey line the most likely model solution, with the 95% confidence interval shown in shaded areas.

Figure E4. Inverse models for oxygen isotope composition (δ18O) from teeth from Labeko Koba, considering distance from enamel root junction. The blue line and points correspond to original data and grey line the most likely model solution, with the 95% confidence interval shown in shaded areas.
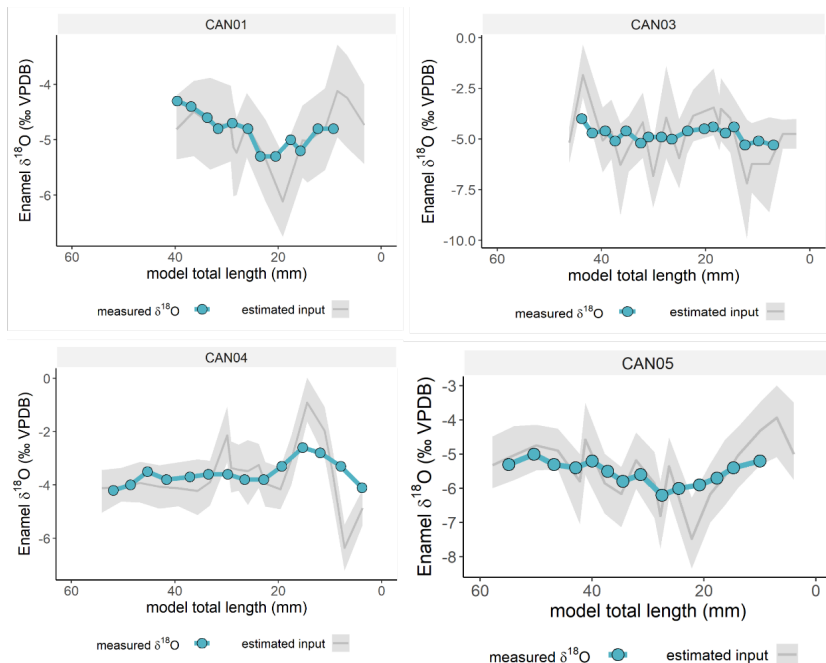
Figure E5. Inverse models for oxygen isotope composition (δ18O) from teeth from Canyars considering distance from enamel root junction. The blue line and points correspond to original data and grey line the most likely model solution, with the 95% confidence interval shown in shaded areas.
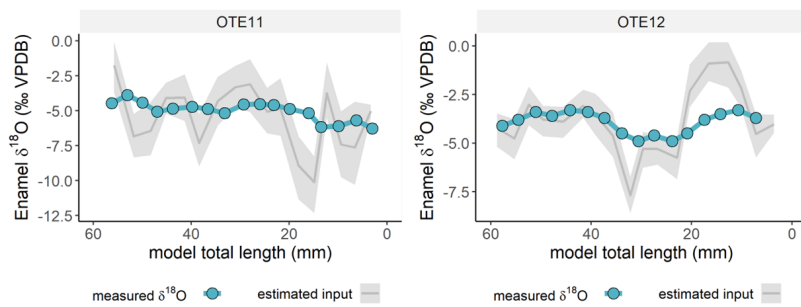
Figure E6. Inverse models for oxygen isotope composition (δ18O) from teeth from El Otero, considering distance from enamel root junction. The blue line and points correspond to original data and grey line the most likely model solution, with the 95% confidence interval shown in shaded areas.
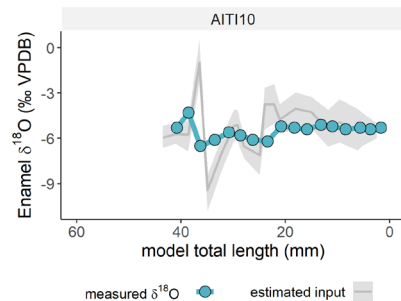
Figure E7. Inverse models for oxygen isotope composition (δ¹⁸O) from teeth from Aitzbitarte III interior, considering distance from enamel root junction. The blue line and points correspond to original data and grey line the most likely model solution, with the 95% confidence interval shown in shaded areas.

References Appendix E

Bendrey, R., Vella, D., Zazzo, A., Balasse, M., Lepetz, S., 2015. Exponentially decreasing tooth growth rate in horse teeth: implications for isotopic analyses. Archaeometry 57, 1104–1124. https://doi.org/10.1111/arcm.12151

Blumenthal, S.A., Cerling, T.E., Chritz, K.L., Bromage, T.G., Kozdon, R., Valley, J.W., 2014. Stable isotope time-series in mammalian teeth: In situ δ18O from the innermost enamel layer. Geochimica et Cosmochimica Acta 124, 223–236. https://doi.org/10.1016/j.gca.2013.09.032

Kohn, M.J., 2004. Comment: Tooth Enamel Mineralization in Ungulates: Implications for Recovering a Primary Isotopic Time-Series, by B. H. Passey and T. E. Cerling (2002). Geochimica et Cosmochimica Acta 68, 403–405. https://doi.org/10.1016/S0016-7037(03)00443-5

Passey, B.H., Cerling, T.E., 2002. Tooth enamel mineralization in ungulates: implications for recovering a primary isotopic time-series. Geochimica et Cosmochimica Acta 66, 3225–3234. https://doi.org/10.1016/S0016-7037(02)00933-X

Passey, B.H., Cerling, T.E., Schuster, G.T., Robinson, T.F., Roeder, B.L., Krueger, S.K., 2005. Inverse methods for estimating primary input signals from time-averaged isotope profiles. Geochimica et Cosmochimica Acta 69, 4101–4116. https://doi.org/10.1016/j.gca.2004.12.002

Zazzo, A., Bendrey, R., Vella, D., Moloney, A.P., Monahan, F.J., Schmidt, O., 2012. A refined sampling strategy for intra-tooth stable isotope analysis of mammalian enamel. Geochimica et Cosmochimica Acta 84, 1–13. https://doi.org/10.1016/j.gca.2012.01.012